TECHNISCHE UNIVERSITÄT WIEN

Diploma Thesis

Influence of the Gas Atmosphere on the Formation of Low-Friction Molybdenum- and Tungsten Diselenides

carried out for the purpose of obtaining the degree of Diplom-Ingenieur (Dipl.-Ing. or DI),

submitted at TU Wien
Faculty of Mechanical and Industrial Engineering

by

Daniel Erich Pölzlberger, BSc

Mat.No.: 11706028

under the supervision of
Univ.Prof. Dipl.-Ing. Dr.-Ing. Carsten Gachot
and
Dr.-Ing. Philipp Grützmacher, MSc
Institute of Engineering Design and Product Development,
E307-05-Research Unit of Tribology

Vienna, April 2024

Signature

Die approbierte gedruckte Originalversion dieser Diplomarbeit ist an der TU Wien Bibliothek verfügbar
The approved original version of this thesis is available in print at TU Wien Bibliothek.

Die approbierte gedruckte Originalversion dieser Diplomarbeit ist an der TU Wien Bibliothek verfügbar
The approved original version of this thesis is available in print at TU Wien Bibliothek.

I confirm, that the printing of this thesis requires the approval of the examination board.

Affidavit

I declare in lieu of oath, that I wrote this thesis and carried out the associated research myself, using only the literature cited in this volume. If text passages from sources are used literally, they are marked as such.

I confirm that this work is original and has not been submitted for examination elsewhere, nor is it currently under consideration for a thesis elsewhere.

I acknowledge that the submitted work will be checked electronically-technically using suitable and state-of-the-art means (plagiarism detection software). On the one hand, this ensures that the submitted work was prepared according to the high-quality standards within the applicable rules to ensure good scientific practice "Code of Conduct" at the TU Wien. On the other hand, a comparison with other student theses avoids violations of my personal copyright.

Vienna, April 2024

Signature

Die approbierte gedruckte Originalversion dieser Diplomarbeit ist an der TU Wien Bibliothek verfügbar
The approved original version of this thesis is available in print at TU Wien Bibliothek.
TU Bibliothek Your knowledge hub WIEN

Acknowledgement

In the journey of completing my diploma thesis, I want to thank a number of individuals whose support and guidance have been most important. Foremost, huge thanks to Univ.Prof. Dipl.-Ing. Dr.-Ing. Carsten Gachot and Dr.-Ing. Philipp Grützmacher, MSc for not only their expert mentorship, but also for introducing me to the fascinating world of 2D materials within the field of tribology. Their patience, knowledge, and encouragement has been essential to the success of the research.

To my family, friends, and people close to me, whose support has been my source of motivation and strength. Their presence during difficult times has been invaluable, significantly contributing to my personal and academic growth.

To all who have helped me along this journey, teachers, professors, colleagues, and fellow students, I am profoundly grateful.

Die approbierte gedruckte Originalversion dieser Diplomarbeit ist an der TU Wien Bibliothek verfügbar
The approved original version of this thesis is available in print at TU Wien Bibliothek.

Abstract

2D materials have been receiving a lot of attention in the field of tribology due to their exceptional potential to minimize friction and wear. Among these materials, Transition Metal Dichalcogenides (TMDs), especially MoS_2 and WS_2, have been greatly used in industrial applications due to their excellent tribological properties. However, selenides have demonstrated superior performance compared to sulfides under various conditions. Recent research developments include a novel method for synthesizing TMD layers on molybdenum or tungsten coatings using selenium powder in an in operando method.

This study explores how oxygen and humidity levels impact the friction and wear characteristics of TMD layers, with a focus on molybdenum and tungsten diselenides as solid lubricants. Using a ball-on-disc tribometer inside a custom built inert gas chamber, we assessed the tribological behavior of $MoSe_2$ and WSe_2 layers under ambient air, 10 % oxygen, nitrogen, and argon atmosphere. The methodology included several material characterization techniques such as Transmission Electron Microscopy (TEM), Energy-Dispersive X-ray (EDX), Confocal Laser Scanning Microscopy (CLSM), and Raman spectroscopy to carefully examine the tribofilms and wear tracks.

The results emphasized that $MoSe_2$ and WSe_2 layers maintain low Coefficients Of Friction (COFs) (below 0.1) and exhibit superb wear resistance, independent of the atmospheric conditions. Notably, the study highlights the influence of the gas atmosphere on the durability of these low-friction layers, as reduced oxygen and humidity levels significantly increased the wear life of the TMD layers due to their susceptibility to fast oxidation. This shows that in operando formed $MoSe_2$ and WSe_2 layers are effective solid lubricants, especially in extreme environments like space. The issue of reduced wear life and degradation of TMDs from environmental influences can be avoided through the simple yet effective method of repeated replenishment.

Die approbierte gedruckte Originalversion dieser Diplomarbeit ist an der TU Wien Bibliothek verfügbar
The approved original version of this thesis is available in print at TU Wien Bibliothek.

Kurzfassung

2D-Materialien haben aufgrund ihres großen Potenzials zur Reibungs- und Verschleißminimierung im Bereich der Tribologie große Beachtung gefunden. Unter diesen Materialien werden TMDs, insbesondere MoS_2 und WS_2, aufgrund ihrer reibungsmindernden Eigenschaften in der Industrie vielfältig eingesetzt. Selenide haben jedoch unter verschiedenen Bedingungen bessere Eigenschaften als MoS_2 gezeigt. Zu den jüngsten Fortschritten zählt eine neuartige Methode zur Synthese von TMD-Schichten auf Molybdän- oder Wolframbeschichtungen unter Verwendung von Selenpulver als in operando Methode.

In dieser Arbeit wird untersucht, wie sich der Sauerstoff- und Feuchtigkeitsgehalt auf die Reibungs- und Verschleißeigenschaften von TMD-Schichten auswirken, wobei der Schwerpunkt auf Molybdän- und Wolframseleniden als Festschmierstoffe lag. Mit Hilfe eines Kugel-Scheibe-Tribometers, das in einer selbstgebauten Inertgas-Kammer betrieben wurde, wurde das tribologische Verhalten von $MoSe_2$- und WSe_2-Schichten im Tribofilm unter Umgebungsluft, 10 % Sauerstoff, Stickstoff und Argon Atmosphäre untersucht. Die Methodik umfasste mehrere Materialcharakterisierungstechniken wie TEM, EDX, CLSM und Raman-Spektroskopie, um die Tribofilme und Verschleißspuren zu untersuchen.

Die Ergebnisse unterstreichen, dass $MoSe_2$- und WSe_2-Schichten, unabhängig von den atmosphärischen Bedingungen, niedrige Reibungswerte (unter 0.1) beibehalten und eine sehr gute Verschleißfestigkeit aufweisen. Insbesondere wird in der Studie der Einfluss der Gasatmosphäre auf die Haltbarkeit dieser reibungsarmen Schichten hervorgehoben, wobei ein geringerer Sauerstoff- und Feuchtigkeitsgehalt die Lebensdauer der TMD-Schichten aufgrund ihrer Anfälligkeit für eine schnelle Oxidation deutlich erhöhte. Das verdeutlicht die Wirksamkeit von $MoSe_2$ und WSe_2 als in operando gebildete Festschmierstoffe, insbesondere in extremen Umgebungen wie dem Weltraum. Das Problem der verminderten Lebensdauer und der Oxidation von TMDs durch Umwelteinflüsse kann durch die einfache, aber effektive Methode der wiederholten Nachfüllung vermieden werden.

Die approbierte gedruckte Originalversion dieser Diplomarbeit ist an der TU Wien Bibliothek verfügbar
The approved original version of this thesis is available in print at TU Wien Bibliothek.
TU Bibliothek Your knowledge hub WIEN

Table of Contents

Die approbierte gedruckte Originalversion dieser Diplomarbeit ist an der TU Wien Bibliothek verfügbar
The approved original version of this thesis is available in print at TU Wien Bibliothek.
TU Bibliothek Your knowledge hub WIEN

Die approbierte gedruckte Originalversion dieser Diplomarbeit ist an der TU Wien Bibliothek verfügbar
The approved original version of this thesis is available in print at TU Wien Bibliothek.
TU Bibliothek Your knowledge hub WIEN

List of Abbreviations

ALS	Asymmetric Least Squares
BP	Black Phosphorous
CLSM	Confocal Laser Scanning Microscopy
COF	Coefficient Of Friction
CVD	Chemical Vapor Deposition
EDX	Energy-Dispersive X-ray
FIB	Focussed Ion Beam
MBE	Molecular Beam Epitaxy
PVD	Physical Vapor Deposition
RH	Relative Humidity
ROI	Region Of Interest
SAED	Selected Area Electron Diffraction
SEM	Scanning Electron Microscopy
STEM	Scanning Transmission Electron Microscopy
TEM	Transmission Electron Microscopy
TMCC	Transition Metal Carbo-Chalcogenide
TMD	Transition Metal Dichalcogenide

Die approbierte gedruckte Originalversion dieser Diplomarbeit ist an der TU Wien Bibliothek verfügbar
The approved original version of this thesis is available in print at TU Wien Bibliothek.

List of Figures

Die approbierte gedruckte Originalversion dieser Diplomarbeit ist an der TU Wien Bibliothek verfügbar
The approved original version of this thesis is available in print at TU Wien Bibliothek.
TU Bibliothek Your knowledge hub WIEN

Die approbierte gedruckte Originalversion dieser Diplomarbeit ist an der TU Wien Bibliothek verfügbar
The approved original version of this thesis is available in print at TU Wien Bibliothek.
TU Bibliothek Your knowledge hub WIEN

Die approbierte gedruckte Originalversion dieser Diplomarbeit ist an der TU Wien Bibliothek verfügbar
The approved original version of this thesis is available in print at TU Wien Bibliothek.
TU Bibliothek Your knowledge hub WIEN

Die approbierte gedruckte Originalversion dieser Diplomarbeit ist an der TU Wien Bibliothek verfügbar
The approved original version of this thesis is available in print at TU Wien Bibliothek.
TU Bibliothek Your knowledge hub WIEN

Die approbierte gedruckte Originalversion dieser Diplomarbeit ist an der TU Wien Bibliothek verfügbar
The approved original version of this thesis is available in print at TU Wien Bibliothek.
TU Bibliothek Your knowledge hub WIEN

List of Tables

Die approbierte gedruckte Originalversion dieser Diplomarbeit ist an der TU Wien Bibliothek verfügbar
The approved original version of this thesis is available in print at TU Wien Bibliothek.

Die approbierte gedruckte Originalversion dieser Diplomarbeit ist an der TU Wien Bibliothek verfügbar
The approved original version of this thesis is available in print at TU Wien Bibliothek.

1 Motivation and State of the Art

Tribology is the study of interacting surfaces in relative motion, including wear, friction, and lubrication. The energy losses related to tribological contacts are one of the major factors for energy consumption, material loss, and machine reliability [1, 2]. It has been estimated that around 23 % of the global energy consumption can be attributed to tribological contacts, with 20 % being expended to overcome friction and the remaining 3 % associated with losses due to wear-related failures. Consequently, advances in lubrication technology have the potential to significantly reduce energy losses from friction and wear by up to 40 % over the long term [3]. Improved tribological performance of materials can be achieved mainly by surface engineering and lubrication or a combination of them, contributing to more energy efficient processes [2, 4]. The main way of surface engineering is to alter the surface topography, whereas lubrication consists of using liquid, semi-solid, or solid lubricants to reduce friction and wear [2, 5]. This thesis focuses mainly on the usage of solid lubrication. Solid lubricants greatly outperform liquid lubricants in extreme conditions, like high or cryogenic temperatures, high vacuum and radiation. They also excel when exposed to corrosion, contact pressure and contamination risk are high, weight limitations are present, and complicated maintenance work is required beyond the limitations of liquid and semi-solid lubricants. However, solid lubricants are not among the best performers in transferring heat and providing damping [4–6]. Nevertheless the lubrication process of solid lubricants is similar to other lubricants, providing a stable protective layer between the contact surfaces reducing friction and wear. The performance is influenced by the type of solid lubricant, the environment, counteracting components, applied load, and operational speed, among others [5]. Materials that have been considered for solid lubrication purposes are layered structure materials (e.g., hexagonal boron nitride, Transition Metal Dichalcogenides (TMDs), graphite, MXenes), soft metals (e.g., silver, gold, copper), binary or ternary metal oxides and sulfates (e.g., PbO, Magnéli phases, TiO_2, Ag_2MoO_4) [7], alkaline earth fluorides, dimanond-like carbons, polymers (e.g., polytetrafluoroethylene), and one-dimensional materials, or a blend of these [5, 6, 8, 9]. These materials

Die approbierte gedruckte Originalversion dieser Diplomarbeit ist an der TU Wien Bibliothek verfügbar
The approved original version of this thesis is available in print at TU Wien Bibliothek.
TU Bibliothek Your knowledge hub WIEN

are widely used in industries, such as automotive, aerospace, and other high tech fields [8, 10]. A solid lubricant can be applied on the substrate in different ways, such as spin coating, drop coating, or plasma preparation techniques, like plasma chemical heat treatment, Physical Vapor Deposition (PVD), or plasma electrolytic oxidation [10].

In recent years TMDs have aroused great interest from scientists and industries not only due to their semiconducting properties, but also their excellent tribological behavior [11, 12]. These 2D materials can reduce the Coefficient Of Friction (COF) to around 0.05 - 0.2, but also values below 0.01, in the region of superlubricity, have been reported in perfect conditions [13, 14]. This property is attributed to the weak interlayer interaction and therefore easy sliding between adjacent atomic layers [15]. TMDs consist of a layer of transition metal atoms between two layers of chalcogen atoms forming a material with semiconducting character. Of this material family, MoS_2 is the most studied and has been extensively used in industry applications as a solid lubricant due to its robustness [16], even though selenides and tellurides have shown more promising tribological properties in an ambient air atmosphere [17, 18]. In general TMDs are highly impacted by environmental influences, such as temperature, humidity, and oxygen, causing more friction and wear due to oxidation of the metal atom and the harder metal oxides increasing third body wear [11]. Nevertheless, molybdenum and tungsten selenides demonstrate little influence of humidity on the COF compared to MoS_2 [17, 19, 20]. This might be explained by spontaneous surface transfer doping phenomena under ambient air [17]. Still they are prone to fast lubricity degradation by environmental influences, thus impairing the range of applications [11].

Considering the importance of extending the wear life of a TMD containing tribofilm, it is necessary to find methods for its replenishment. A great way can be observed in human joints, where lubrication is thought to be generated by shear forces in an in operando manner, directly at the point of contact. This process involves the biosynthesis and replenishment of biomolecules that act as natural lubricants, theoretically extending the wear life for as long as the necessary precursors are provided to form the lubricant [11]. Inspired by this natural mechanism, several methods have been proposed to synthesize lubricants tribochemically triggered by shear, flash heating, or high contact pressure [11, 21–24]. A novel in operando method to convert selenium nanopowders into molybdenum and tungsten selenides was proposed by Grützmacher et al. [11], effectively facilitating the replenishment of the solid lubricant by sprinkling nanopowder on the substrate. Due to tribochemical reactions, the nanopowder reacts with the molybdenum or tungsten in the contact

Die approbierte gedruckte Originalversion dieser Diplomarbeit ist an der TU Wien Bibliothek verfügbar
The approved original version of this thesis is available in print at TU Wien Bibliothek.
TU Bibliothek Your knowledge hub WIEN

point to form the respective TMD right where it is needed. The experiments were conducted in an air atmosphere, resulting in superb values of COF, presenting a possibility to be used in space applications. Thus, our study under nitrogen or argon atmosphere investigates the behavior of the TMD materials with little oxygen and humidity influence. Resulting in the scientific question of this thesis:

- Scientific Question: What is the influence of oxygen and humidity on the tribological behavior of in operando formed molybdenum- and tungsten diselenides as solid lubricants?

Die approbierte gedruckte Originalversion dieser Diplomarbeit ist an der TU Wien Bibliothek verfügbar
The approved original version of this thesis is available in print at TU Wien Bibliothek.
TU Bibliothek Your knowledge hub WIEN

2 Theoretical Background

2.1 Tribological Fundamentals

2.1.1 Friction

A fundamental understanding of friction was formulated by Guillaume Amontons in 1699 [25], but can also be contributed to Leonardo Da Vinci, who actually described it 200 years earlier in 1493. The friction force is proportional to the normal force exerted, and remains unaffected by the apparent contact surface area. In 1785, Coulomb added the concept that the friction force does not vary with the sliding speed [26]. These three statements are not reliable for all materials, but provide a good approximation and can be expressed in Equation (2.1), where F_R represents the frictional force, μ the COF, and F_N the normal load [27].

$$F_R = \mu \cdot F_N \tag{2.1}$$

Bowden and Tabor [28] theorized an adhesion based model where when one surface is put over another, contact occurs only at isolated parts within the nominal area, specifically at the rigid asperities. Only at the actual contact area forces are applied between the two bodies. Consequently, friction arises from the shear resistance between contacting surfaces, known as adhesion, and from the resistance caused by surface asperities as they plough through the contact surface [27, 29].

2.1.2 Wear

The material removal due to the interaction of two solids is referred to as wear and is one of the leading factors for machines to lose their durability and reliability. Research has shown that there is no obvious correlation between friction and wear and wear cannot be ascribed as a material property, but rather as a system response. Wear is influenced by dynamic, environmental, and material parameters and even a small change of these parameters can change the wear notably [30].

Die approbierte gedruckte Originalversion dieser Diplomarbeit ist an der TU Wien Bibliothek verfügbar
The approved original version of this thesis is available in print at TU Wien Bibliothek.
TU Bibliothek Your knowledge hub WIEN

In general four wear mechanisms can be identified, as depicted in Figure 2.1. Adhesive wear, shown in Figure 2.1a, occurs when two solids under plastic contact have enough adhesive bonding at the interface that large deformation result in the transfer of a wear particle. Figure 2.1b describes abrasive wear, the removal of material due to ploughing, as the two surfaces interlock in a contact [30]. This can be distinguished into two-body abrasive wear, which is caused by hard particles attached to it, and three-body abrasion, where the hard particles are free to roll and slide between two sliding surfaces [27]. Fatigue wear (Figure 2.1c) is caused due to repetitive stresses, resulting in cracks after more than one contact, whereas adhesive and abrasive wear can occur at the first contact [27, 30]. In corrosive environments, the formation of surface layers through chemical or electrochemical interactions often lead to a significant change in the material's wear characteristics. Mechanical abrasion removes the newly formed surface layers, making the surface prone to more corrosion, resulting in more wear, called corrosive wear, as depicted in Figure 2.1d [30].

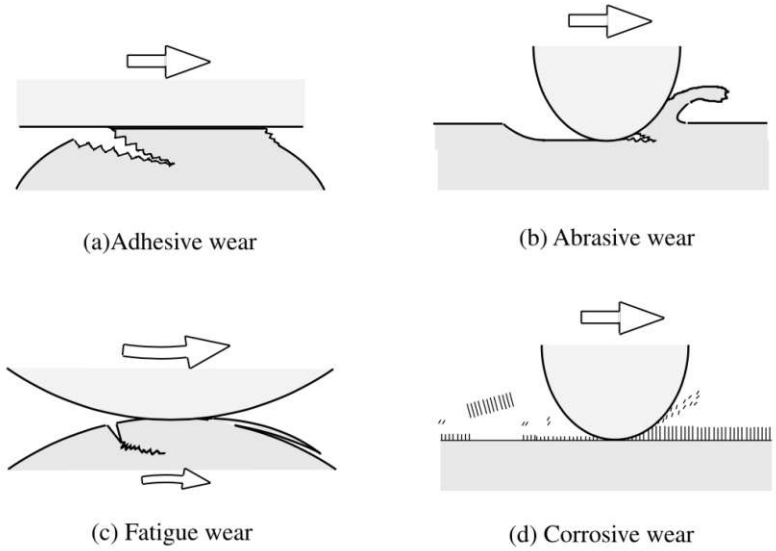

Figure 2.1: Illustration of (a) adhesive, (b) abrasive, (c) fatigue, and (d) corrosive wear mechanisms. Reprinted from [30]. Copyright 2000, CRC Press LLC.

To quantify the material loss, Equation (2.2) is used to calculate a wear coefficient, which gives the probability to eject wear particles [31]. K is the wear coefficient expressed in ${}^{mm^3}/_{Nm}$, W_V represents the wear volume in mm^3, F_N denotes the normal force in N, and s signifies the sliding distance in m [32].

$$K = \frac{W_V}{F_N \cdot s} \tag{2.2}$$

Die approbierte gedruckte Originalversion dieser Diplomarbeit ist an der TU Wien Bibliothek verfügbar
The approved original version of this thesis is available in print at TU Wien Bibliothek.
TU Bibliothek Your knowledge hub WIEN

2.1.3 Hertzian Contact

In 1881, Heinrich Hertz [33] pioneered the study of contact mechanics by examining the behavior of two elastic bodies in contact. His work laid the foundation for understanding the stresses involved in point loads, spherical contacts, or cubical indentations. This principle is crucial in tribological testing, where understanding the contact mechanics between a ball and a plane surface is essential for analyzing wear, friction, and lubrication effects. Contact mechanics describes the deformation of solid bodies touching each other at one or more points. The interactions can be categorized into two types: Conformal contact, where the solid bodies make contact across an area and non-conformal contact either along a line or a point [32], which is described by the Hertzian Theory [33]. In this thesis the ball-plane contact scenario is the most important, where a spherical object is pressed against a flat surface, as illustrated in Figure 2.2.

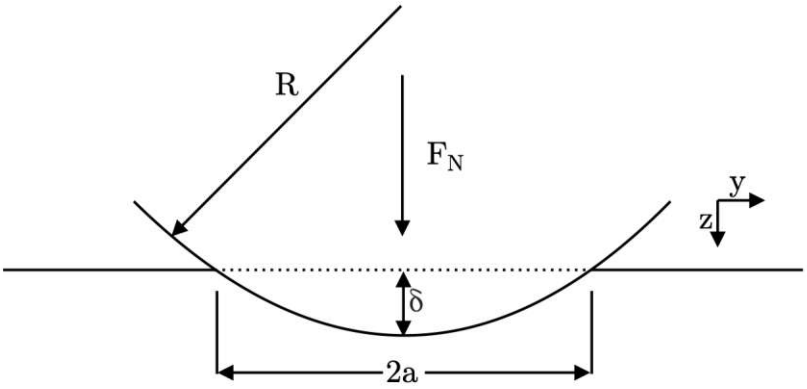

Figure 2.2: Hertzian contact mechanics of a spherical object pressing against a flat surface. Adapted from [32].

Ball-plane contact scenarios with elastic deformations form a circular contact area under a force F_N. This setup is governed by specific equations, such as Equation (2.3) representing the maximum contact pressure p_0.

$$p_0 = \frac{3F_N}{2\pi a^2} \tag{2.3}$$

R represents the radius of the sphere and a the radius of the projected contact area. a is calculated using Equation (2.4).

$$a = \left(\frac{1.5F_N R}{E'}\right)^{1/3} \tag{2.4}$$

The reduced Young's modulus E' is described in Equation (2.5), with E_1 denoting

Die approbierte gedruckte Originalversion dieser Diplomarbeit ist an der TU Wien Bibliothek verfügbar
The approved original version of this thesis is available in print at TU Wien Bibliothek.

the Young's modulus and ν_1 the Poisson's ratio of the sphere and E_2 the Young's modulus and ν_2 the Poisson's ratio of the surface.

$$\frac{1}{E'} = 0.5 \left[\frac{1-\nu_1^2}{E_1} + \frac{1-\nu_2^2}{E_2} \right] \tag{2.5}$$

The penetration depth δ follows with the radius of the contact area a and the radius of the sphere R (Equation (2.6)) [32].

$$\delta = \frac{a^2}{R} \tag{2.6}$$

In Table 2.1 the Young's modulus E and the Poisson's ratio ν for each material, that is used in the tribological experiments, are stated. The values of the hardness and the Young's modulus for the Mo and W coating were determined by colleagues [11] with a nanoindentater at 4 mN load and 40 indents. The Al_2O_3 data were obtained from the datasheet provided by the manufacturer Kugel Pompel®. With the given mechanical properties and F_N of 1 N, the maximum Hertzian contact pressure calculated for Mo is 0.887 GPa and for W 0.966 GPa. The penetration depth reaches 0.179 µm for Mo and 0.165 µm for W. This is significantly less than 10 % of the molybdenum and tungsten coating's thickness, so that there is negligible influence on the measurements from the steel substrate on the tribological behavior of the transition metal coating, according to Fischer-Cripps [34].

Table 2.1: Mechanical properties of the arc evaporated molybdenum and tungsten coatings, alongside those of the Al_2O_3 ball.

	Mo	**W**	**Al_2O_3**
Young's modulus	310 GPa	405 GPa	365 GPa
Hardness	7.1 GPa	12.6 GPa	1250 - 1700 HV
Poisson's ratio	0.3	0.28	0.22

2.2 Lubrication

The major role of lubricating the solid surface contact is to decrease the normal and shear stresses by interposing a layer of lubricant in between to separate the solid bodies [1, 35]. These layers are usually very thin from 1 μm to 100 μm, but they can be even much thinner or thicker as well [36]. Lubricants are most commonly categorized into either inert fluids (gases and liquids), greases, or solids, these will be further discussed in this thesis [35]. The type of lubricant that is chosen for a specific application depends on various factors, such as temperature, atmosphere,

Die approbierte gedruckte Originalversion dieser Diplomarbeit ist an der TU Wien Bibliothek verfügbar
The approved original version of this thesis is available in print at TU Wien Bibliothek.
TU Bibliothek Your knowledge hub WIEN

and ambient pressure [1]. Greases can provide a simple design with low speed, solid lubricants can withstand high temperature and contact pressures, and liquid lubricants excel in high speed, damping, and cooling [1, 35].

2.2.1 Liquid Lubrication

Stribeck Curve

The Stribeck curve, first introduced by Richard Stribeck [37] in 1901, describes the relationship of the COF and a dimensionless lubrication parameter, called Hersey number [1]. Figure 2.3 illustrates schematically the progress of the lubrication regimes. At very low speeds the friction is high, as surfaces rub directly each other without any lubricant film, this regime is called solid friction. With increasing velocity and decreasing load the regime changes into boundary, where protective monolayers, oil, or lubricous molecules form and adhere at the surface that are thinner than the asperities of the opposing solid, which are supporting most of the load, resulting in high friction and wear. With an increasing Hersey number, mixed lubrication occurs. Both surface interactions and the developing lubricant film supports the load, decreasing friction. When the surfaces are completely separated by the lubricant film the hydrodynamic regime is reached with low friction. Friction is solely determined by the rheology of the lubricant and viscous forces, that increase with higher speeds, viscosity, and lower loads [1, 27, 32, 35]. Figure 2.3 also shows the lubrication regimes on a logarithmic scale. Boundary lubrication occurs at $\lambda < 1$, followed with mixed lubrication for $1 < \lambda < 3$. With $\lambda > 3$ hydrodynamic lubrication dominates [27, 38].

Die approbierte gedruckte Originalversion dieser Diplomarbeit ist an der TU Wien Bibliothek verfügbar
The approved original version of this thesis is available in print at TU Wien Bibliothek.
TU Bibliothek Your knowledge hub WIEN

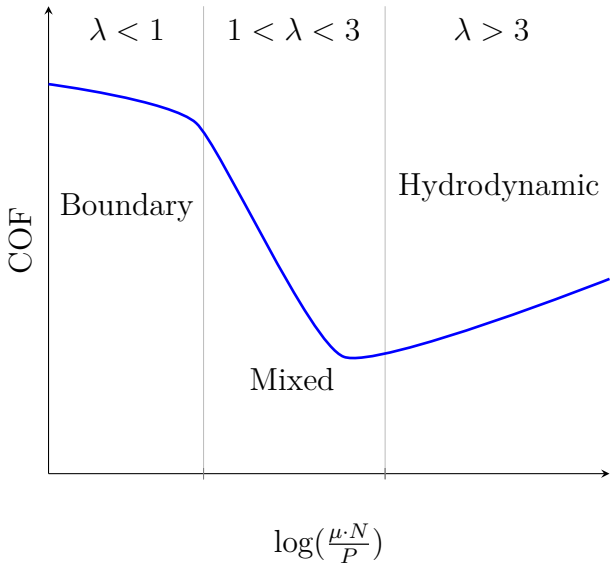

Figure 2.3: Schematic stribeck curve illustrating the coefficient of friction as a function of the Hersey number including the respective lubrication regimes, where viscosity (μ), velocity (N), and load (P). Adapted from [27, 32].

The lubrication regimes are classified with the lambda ratio (λ), which is a snapshot of the current state and changes constantly, as defined in Equation (2.7) [27].

$$\lambda = \frac{h_c}{\sigma} \tag{2.7}$$

h_c represents the central film thickness for point contacts postulated by Hamrock and Dowson [39] and σ the root mean square roughness of the two surfaces, shown in Equation (2.8).

$$\sigma^2 = R_{q1}^2 + R_{q2}^2 \tag{2.8}$$

Types of Liquid Lubricants

The most commonly used liquid lubricant are oils. Conventional lubricants have evolved from being derived from crude oil and formulated with mineral oils, to synthetic hydrocarbon oil [1]. The search for environmentally friendly liquid lubricants has drawn attention towards alternatives like glycerol, ionic liquids, and water, among others, as replacements for traditional oils. These substitutes show significant potential both with and without the addition of additives [40–42].

Die approbierte gedruckte Originalversion dieser Diplomarbeit ist an der TU Wien Bibliothek verfügbar
The approved original version of this thesis is available in print at TU Wien Bibliothek.
TU Bibliothek Your knowledge hub WIEN

2.2.2 Grease Lubrication

Grease is a semi-solid mixture of an oil, called oleogel, including 5 - 20 wt.-% of a thickening agent, and optionally additives. Mostly mineral oils are incorporated, but in special applications also synthetic oils, such as silicone greases for very high or low temperatures are used. As thickening agent many times a soap (e.g., calcium or lithium based) or a clay mineral is used. The additives used are similar to those in liquid lubricants, like molybdenum disulfide or graphite. Greases are less likely to be displaced compared to oils, form a very good squeeze film, and seal well against contamination. However, they are poor in transferring frictional heat away from the surface contact and due to higher viscous forces usually have a higher COF [27, 43].

2.2.3 Solid Lubrication

The mechanism of solid lubrication to decrease the COF is similar to liquid or semi-solid lubrication. Materials with a lamellar structure align themselves parallel to the direction of relative motion and can achieve low friction values under certain conditions [1, 15]. Several other substances, such as soft metals, polytetrafluoroethylene, polyimide, specific oxides, rare-earth fluorides, diamond and diamond-like carbons, and fullerenes, can offer lubrication despite lacking a layered crystal structure. However, they will not be further elaborated upon as the materials examined in this thesis have a layered structure [1].

The interaction between two surfaces coated with a solid lubricant typically results in the transfer of a thin layer of material from the coating surface to the opposing surface, a phenomenon traditionally referred to as tribofilm formation (third bodies) [15, 44]. Surfaces experiencing wear may display different chemical compositions, microstructures, and crystallographic textures compared to the bulk coating. This arises from the surface interactions with the ambient surroundings. Consequently, solid lubricant coatings that perform great in one environment may not exhibit the same friction reduction behavior in another setting [44]. This effect of ambient pressure on friction is depicted in Figure 2.4a exemplary with two of the most common and most studied solid lubricants graphite and molybdenum disulfide (MoS_2). The graphite's COF is fairly high in vacuum or dry nitrogen at 0.5, but with increasing pressure at around 1 torr (≈1.333 mbar) the COF drops to ≈0.2. In contrast MoS_2, whose structure is illustrated in Figure 2.4b, shows similar friction values at atmospheric pressure, but with decreasing pressure the friction performance improves even further to 0.04 [45]. Graphite, an allotrope of carbon, and molybdenum disulfide exhibit a layered hexagonal crystal structure, contributing to their strong

Die approbierte gedruckte Originalversion dieser Diplomarbeit ist an der TU Wien Bibliothek verfügbar
The approved original version of this thesis is available in print at TU Wien Bibliothek.
TU Bibliothek Your knowledge hub WIEN

anisotropy in mechanical and physical properties. The bonding of carbon atoms within each plane is covalent and relatively strong, yet the interplanar bonding is weak consisting primarily of van der Waals forces and a weak covalent bond from interactions between the π orbitals of the carbon atoms. This results in low shear resistance and relatively easy sliding of the planes. Still without contaminants, in principal oxygen, water, or other hydrocarbons, graphite does not lubricate, as described in Figure 2.4a. Consequently, the intercalation of certain molecules is necessary for graphite to exhibit low friction values [27, 32, 45].

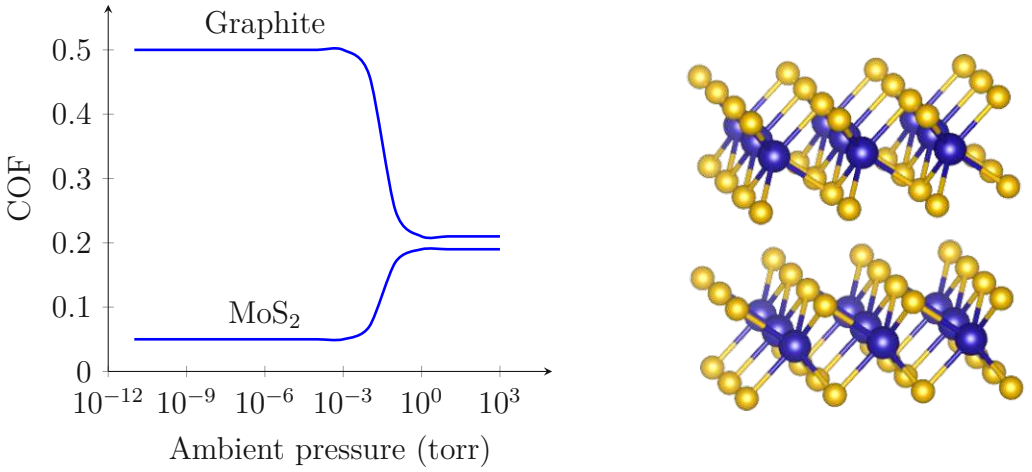

Figure 2.4: (a) Friction behavior of graphite and MoS_2 from low to high ambient pressure. Adapted from [45]. (b) Crystal structure of MoS_2, where blue denotes the transition metal atoms and yellow the chalcogen atoms. Data retrieved from the Materials Project for MoS_2 (mp-1018809) from database version v2023.11.1. [46]. Visualized using VESTA [47].

Molybdenum disulfide's interplanar bonding is due only to short-ranged van der Waals forces and its spacing between adjacent sulphur layers exceeds the thickness of the layers themselves, contributing to the easy sliding [27, 45]. It does not depend on the intercalation of molecules to reduce friction and performs even better without them [32]. Thus, the lubricating properties of graphite and molybdenum disulfide and consequently all solid lubricants depend on their environment and not all materials with similar structures demonstrate low friction. Great friction performance cannot be ascribed to having weak interplanar forces alone, as for instance mica and calcium hydroxide do not exhibit low friction values, although they have lamellar structures [27, 45]. Solid lubricants demonstrate differing responses to variations in sliding speed or load. For instance, graphite exhibits an increase in friction values with an increase in sliding speed and load, while molybdenum disulfide exhibits a

Die approbierte gedruckte Originalversion dieser Diplomarbeit ist an der TU Wien Bibliothek verfügbar
The approved original version of this thesis is available in print at TU Wien Bibliothek.
TU Bibliothek Your knowledge hub WIEN

decrease of the COF with both factors [45]. However, the wear of solid lubricants typically increases with rising load and speed, resulting in a corresponding decrease in lifespan associated with both stress factors [32].

The function of a solid lubricant's transfer film serves two primary purposes. Initially, the transfer film covers the contact area, averting direct contact between the sliding surfaces. Secondly, the low friction and extended wear life relies on the transfer film's ability to maintain low shear resistance at or near the sliding interface. If the transfer film diminishes, the COF increases, leading to a degradation of the contacting surfaces, unless, the transfer film is replenished [15]. Thus, self-lubricating and self-replenishing lubrication films are of great interest for industrial applications [1].

2.3 2D Materials as Solid Lubricants

2D materials are crystal layered structures only one or up to ten layers thick and present a spectrum of promising properties [48]. Among the more well known examples are graphene, hexagonal-boron nitride, molybdenum disulfide, MXenes, black phosphorus, and TMDs, some of which will be briefly discussed with specific focus on TMDs. The potential application fields for these materials are vast, including photonics, energy harvesting, electronics, and sensing, establishing them as a significant area of research [12, 15]. Several 2D materials demonstrate great tribological performance due to the easy sliding between adjacent layers, much like playing cards effortlessly moving across when shuffling them on a table [15, 44]. However, the reduced friction can be further attributed to a misalignment of atomic layers, which significantly decreases the kinetic friction force [49]. These materials are characterized by low friction coefficients and minimal wear rates. They showcase high deformability, great chemical inertness, thermal stability, and excellent mechanical strength, making them an efficient solution for lubrication in various extreme environmental conditions [15]. In addition to the materials' low shear resistance, it is theorized in literature that their unique electrical and thermal properties may have an impact on their tribological performance, as kinetic energy is dissipated either electronically or phononically [15, 50, 51].

2.3.1 MXenes

MXenes, a new class of 2D materials, first discovered by Gogotsi's and Barsoum's groups in 2011 [52], have gained significant scientific attention in various applications, especially for energy storage and as catalysts. Due to their low shear resistance

Die approbierte gedruckte Originalversion dieser Diplomarbeit ist an der TU Wien Bibliothek verfügbar
The approved original version of this thesis is available in print at TU Wien Bibliothek.
TU Bibliothek Your knowledge hub WIEN

and the ability to modify their surface termination groups, MXenes demonstrate low friction and wear. MXenes can be employed as lubricant additives, solid lubricants, or as reinforcement phases, making them a possible novel lubricant solution in various industries, such as automotive, aerospace, and machining [53]. MXenes are the result of selectively etching the A part of a MAX phase, for instance with hydrofluoric acid, revealing its layered 2D structure [54]. The M, A, X stand for a transition metal, an element of the 13th or 14th group in the periodic table, and carbon or nitrogen, respectively [54]. Recent research has tested $Ti_3C_2T_x$ MXenes to be used as additives in ionic liquids [55], as multilayer coating [56], or nanosheets [57], endorsing their potential as solid lubricant.

2.3.2 Black phosphorous

Another promising 2D material with a layered structure is Black Phosphorous (BP), showing great tribological properties as a lubricant additive [58, 59]. The preparation can be as simple as, milling red phosphorus and subsequently exfoliating it in liquid N-methyl pyrolidone solvent, resulting in BP nanosheets [58]. As a consequence of its initially poor air stability, measures need to be taken to encapsulate the BP, to extend its friction and wear reducing properties as a lubrication additive [59, 60]. The material is also interesting for nanoelectronic and optoelectronic devices, due to its adjustable bandgap, high thermal resistance, distinctive anisotropy, and weak interlayer interaction [61].

2.3.3 Transition Metal Carbo-Chalcogenides

As an extension to the MXene family, a new material family called Transition Metal Carbo-Chalcogenides (TMCCs) have been published by Majed et al. [62] to bridge the gap between MXenes and TMDs, consisting of TM_2X_2C, TM representing a transition metal, X a chalcogen, and C a carbon atom. Due to the similar van der Waals heterostructure at the atomic level, and the reported 50 % higher elastic moduli compared to TMDs, TMCCs are thought to have great tribological properties, yet further research is required to confirm this [62].

2.4 Transition Metal Dichalcogenides (TMDs)

The structure of TMDs was first discovered by Pauling in 1923 [63], with the first material being MoS_2 from the naturally occurring mineral molybdenite. In 1963, Frindt [64] was the first to obtain ultrathin MoS_2 layers using an adhesive tape and by 1986 Joensen et al. [65] achieved the first production of MoS_2 monolayer suspen-

Die approbierte gedruckte Originalversion dieser Diplomarbeit ist an der TU Wien Bibliothek verfügbar
The approved original version of this thesis is available in print at TU Wien Bibliothek.
TU Bibliothek Your knowledge hub WIEN

sions [16]. When in 2004 for the first time the group of Geim and Novoselov [66] produced atomically thin graphene films, the development of techniques for working with 2D materials with semiconducting properties surged. With the discovery of strong photoluminescence in $MoSe_2$ monolayers in 2010 [67, 68] and the demonstration of the first TMD transistor in 2011 [69], the study of ultrathin TMDs has seen a substantial increase [16]. TMDs are three atom layers thick, offer great electronic and mechanical properties, and a direct bandgap, making them suitable for applications in high-end electronics, spintronics, energy harvesting, DNA sequencing, and personalized medicine [16].

2.4.1 Structure of Transition Metal Dichalcogenides

TMDs or also (TMDCs) constitute a family of materials with semiconductor character of the type MX_2, where M represents a transition metal and X a chalcogen. Referring to Figure 2.5, all the transition metal elements highlighted in blue can serve as the M component and one of the elements from the chalcogen group, denoted by the yellow color, as the X constituent for the TMD [16].

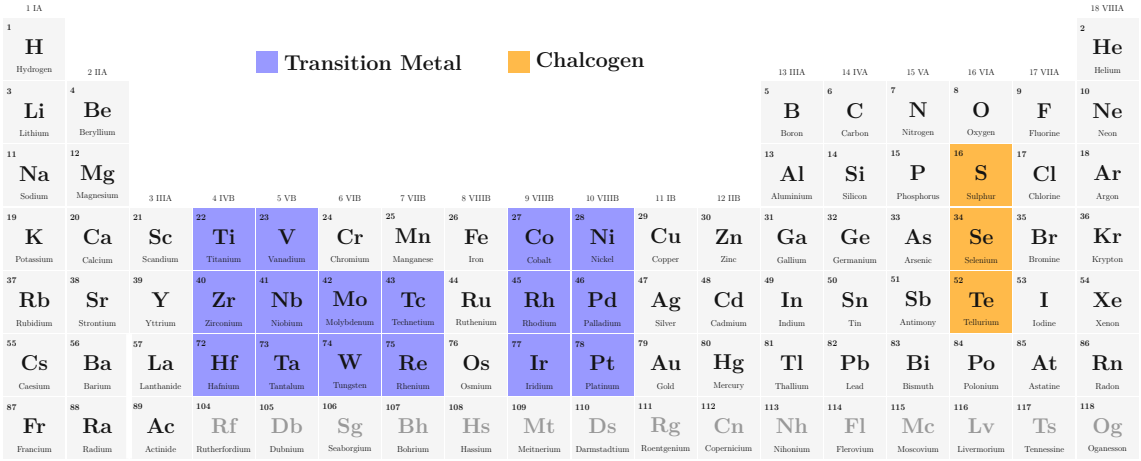

Figure 2.5: Periodic table illustrating the transition metal (blue) and chalcogen (yellow) elements used as a component of TMDs. Adapted from [70, 71].

The two most common structural phases of TMDs are characterized by a trigonal prismatic (2H) and octahedral (1T) coordination of the transition metal atoms [16]. The different structural phases of these materials correspond to a specific stacking order of their three atomic planes (X-M-X). The 2H phases exhibit an ABA stacking where the chalcogen atoms align vertically across layers, while the 1T phases demonstrate an ABC stacking, indicating a shift of the chalcogen atoms [16]. The thermodynamically stable phase, either 2H or 1T, is determined by the specific combination of transition metal and chalcogen elements, however the other can be

Die approbierte gedruckte Originalversion dieser Diplomarbeit ist an der TU Wien Bibliothek verfügbar
The approved original version of this thesis is available in print at TU Wien Bibliothek.
TU Bibliothek Your knowledge hub WIEN

a metastable phase [16]. TMDs composed of group VI transition metals (Mo or W) and chalcogens (S, Se, or Te) are thermodynamically stable in the 2H phase, with the exception of WTe_2 having a stable orthorhombic (1Td) phase [16]. Figure 2.6a demonstrates the stable trigonal prismatic structure of $MoSe_2$, while Figure 2.6b shows the structure for WSe_2. Hence, highlighting their identical three atom layered structure, with the transition metal atoms in the middle and the chalcogen atoms above and below.

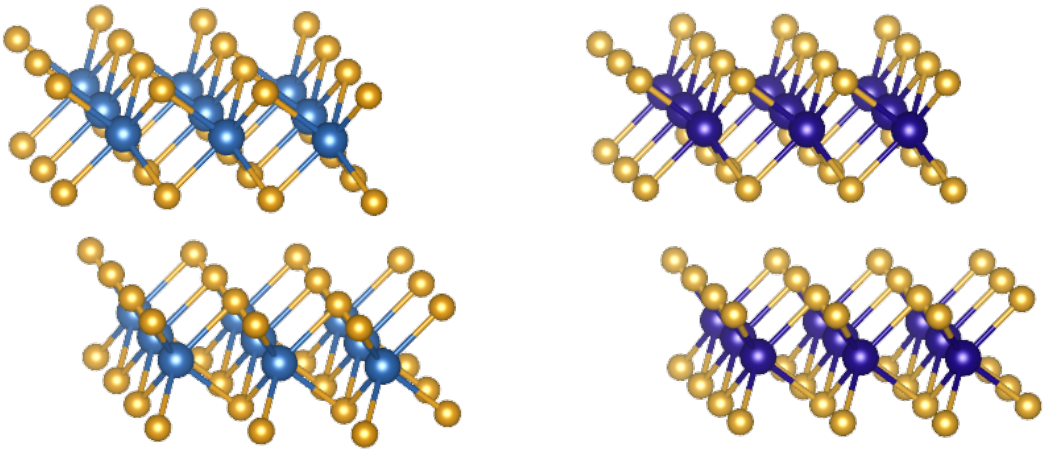

(a) (b)

Figure 2.6: Depiction of the crystal structures of (a) $MoSe_2$ and (b) WSe_2, highlighting their atomic arrangements. Blue denotes the transition metal atoms and yellow the chalcogen atoms. Data retrieved from the Materials Project for $MoSe_2$ (mp-1634) and WSe_2 (mp-1821) from database version v2023.11.1. [72]. Visualized using VESTA [47].

2.4.2 Synthesis of Transition Metal Dichalcogenides

Utilizing the favorable properties of TMDs necessitates reliable production quality. In principle there are two approaches, the top-down method and the bottom-up method, for synthesizing TMDs, as illustrated in Figure 2.7. Top-down methods include mechanical- or chemical exfoliation, and Molecular Beam Epitaxy (MBE). The 2D layers are obtained from their bulk form by using external energy to overcome the interlayer van der Waal forces. Bottom-up methods encompass Chemical Vapor Deposition (CVD), chemical synthesis, electrodeposition, and atomic layer deposition, which create the TMDs using elemental precursors [73, 74].

Die approbierte gedruckte Originalversion dieser Diplomarbeit ist an der TU Wien Bibliothek verfügbar
The approved original version of this thesis is available in print at TU Wien Bibliothek.
TU Bibliothek Your knowledge hub WIEN

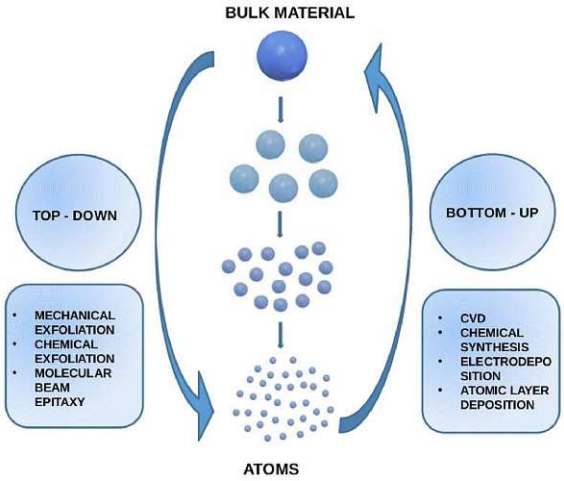

Figure 2.7: Top-down and bottom-up synthesis methods for TMDs. Reprinted from [73]. Copyright 2023, Elsevier.

Mechanical Exfoliation

Very thin layers of TMDs can be obtained by peeling them off their bulk crystals using a simple adhesive tape [16, 73, 74]. The samples produced are of high quality with high purity and cleanliness and can be placed on SiO_2/Si substrates for further fabrication of devices and characterization [16, 73, 74]. However, this method is not scalable, has a poor production yield, and uniform reproducibility is hard. Thus, this method is usually only used for rapid prototyping, for instance as shown by Li et al. [75] as MoS_2 field-effect transistors for sensing nitrous oxide [16, 73, 74].

Chemical Exfoliation

Exfoliating the layers of a bulk crystal includes ultrasonication in water and adding intercalating agents between its layers. Typically, organometallic compounds, such as butyl lithium, naphthyl, and sodium [76], are utilized for this intercalation step. A common process involves immersing TMD powder in a lithium-based compound, such as n-butyllithium for more than a day to allow lithium ions to intercalate between the layers. Following this, the material with intercalated lithium is exposed to water, causing a reaction with the lithium ions to produce hydrogen gas, which helps in separating the layers. Chemical exfoliation production yield higher amounts than mechanical exfoliation and result in a controllable thickness. The first production of $MoSe_2$ monolayers using lithium for chemical exfoliation was reported in 1986 by Joensen et al. [65] and until today, many more methods have been investigated. However, the use of ultrasonication might lead to more structural defects and smaller flake sizes, which can restrict its use in large-scale integrated circuits and electronic gadgets. Lithium intercalation of MoS_2 was reported to induce a phase transition

Die approbierte gedruckte Originalversion dieser Diplomarbeit ist an der TU Wien Bibliothek verfügbar
The approved original version of this thesis is available in print at TU Wien Bibliothek.
TU Bibliothek Your knowledge hub WIEN

from trigonal prismatic to octahedral losing its semiconducting character, but annealing at 300 °C can cause a reverse phase change, restoring the semiconducting bandgap [77]. A more rapid and controllable approach for lithiation, reported by Zeng et al. [78, 79], employs an electrochemical cell featuring a lithium foil anode and a cathode containing TMDs, offering improved speed and control. However, the flammability requires an inert gas atmosphere and lithium is expensive, incentivicing finding an alternative as intercalator [16, 73, 74].

An alternative offers solvent-based exfoliation by ultrasonicating in appropriate liquids, such as aqueous surfactant solutions, organic solvents, or solutions of polymers in solvents. Ultrasonication typically exfoliates the layered crystals mechanically and the resulting nanosheets are kept from recombining by solvation or by repulsion forces, stemming from molecule adsorption [16, 73, 74].

Molecular Beam Epitaxy

In recent years the method of MBE has gained significant research interest to directly grow TMD flakes ususally smaller than 200 nm. It excels in producing high purity flakes and in controlling the composition, structural phases, thickness, and other properties of TMDs, making them a great method for exploring novel applications. In an ultrahigh vacuum chamber various high purity elemental source materials, such as gallium and selenium, generate molecular beams. The deposition occurs on a preheated substrate, where the thickness of the material and the crystalline quality of the substrate are being tracked using reflection high-energy electron diffraction and low energy electron diffraction techniques. Exploiting the weak van der Waals forces enables epitaxial growth, where the lattice structure of the substrate is used for alignment of the overlayer's orientation. Hence, MBE serves as a valuable method for exploring the basics of 2D materials and their mixtures [16, 73].

Chemical Vapour Deposition

CVD is one of the most effective approaches to construct the TMD based on direct chemical reactions with precursor materials. The method does not require ultrahigh vacuum chambers, making it a relatively cheap and simple process [16, 73, 74, 80]. The first synthesis of MoS_2 on a SiO_2 substrate using CVD has been reported in 2011 by Zhan et al. [81]. However, controlling the thickness and hence producing MoS_2 monolayers was first achieved by Zande et al. [82] and Najmaei et al. [83] simultaneously in 2013 [16]. Typically different solid precursors, with the required transition metals and chalcogen atoms (e.g., sulphur powder and MoO_3 powder),

Die approbierte gedruckte Originalversion dieser Diplomarbeit ist an der TU Wien Bibliothek verfügbar
The approved original version of this thesis is available in print at TU Wien Bibliothek.
TU Bibliothek Your knowledge hub WIEN

are exposed to the substrate at high temperature and pressure forming a atomically thin TMD film [16, 73, 74]. Alternatively, a thin layer of molybdenum metal can be deposited onto a heated wafer in the presence of solid sulfur or also substrates are dip-coated in a solution of $(NH_4)_2MoS_4$ and then heated in an atmosphere of sulfur gas [74]. Using atomic layer deposition a special case of CVD Song et al. [84] demonstrated the production of WS_2 layers by depositing powdered WO_3 and sulphur on SiO_2 substrates. CVD techniques produce high-quality, thin TMD layers characterized by controlled crystallinity, morphology, and defect levels, essential for effective device applications [74].

2.4.3 Tribological Behavior of Transition Metal Dichalcogenides

A main research focus on TMDs is contributed to electronic applications due to the suitable band gap that enables TMDs to be used as semiconductors [16]. Nevertheless, the tribological characteristics appear to be highly advantageous, exhibiting low COF in both dry and vacuum conditions across a wide temperature range and demonstrating significant stability in radiative environments, thus presenting a great solid lubricant [15, 85]. There are several reports of TMDs reducing the COF down to 0.05 - 0.2. Moreover, increasing the applied load typically leads to a decrease in the friction coefficient for TMDs [86]. However, in some conditions even a COF of under 0.01 could be achieved, such as sliding a tungsten disulfide monolayer on epitaxial graphene [13] or on h-BN [14], therefore reaching the regime of superlubricity. Especially MoS_2 has been extensively studied and acknowledged as a solid lubricant, however selenides and tellurides have shown superior tribological behavior [17, 18]. A meta-analysis from Chakrapani [17] collected several friction data of TMDs comparing each in air and dry nitrogen atmosphere, shown in Table 2.2.

Table 2.2: Friction coefficient comparison of MoS_2, WS_2, $MoSe_2$, and WSe_2 against different kinds of steel in air and dry nitrogen atmospheres [17].

Atmosphere	**MoS_2**	**WS_2**	**$MoSe_2$**	**WSe_2**
Air	0.19	0.2 - 0.3	0.06	0.07
Dry nitrogen	0.05	0.03	0.08	0.03

Sulfides and selenides exhibit similar friction values in a dry nitrogen atmosphere at around 0.05. However, whereas the influence of oxygen and humidity on molybdenum and tungsten selenides is negligible, sulfides perform poorly in air with the COF rising to 0.2 and more [17, 20]. The reason for the huge difference in atmospheric behavior has not yet been fully clarified, but might be related to spontaneous

Die approbierte gedruckte Originalversion dieser Diplomarbeit ist an der TU Wien Bibliothek verfügbar
The approved original version of this thesis is available in print at TU Wien Bibliothek.
TU Bibliothek Your knowledge hub WIEN

surface transfer doping phenomena under ambient air [17]. However molybdenum and tungsten selenides are still very much prone to lubricity degradation by environmental influences [11]. Tungsten disulfides and diselenides are preferred for high-temperature applications, because of their superior thermal stability and resistance to oxidation, maintaining lubrication up to 600 °C. MoS_2 loses its lubricity at around 300 °C due to oxidation [85].

Die approbierte gedruckte Originalversion dieser Diplomarbeit ist an der TU Wien Bibliothek verfügbar
The approved original version of this thesis is available in print at TU Wien Bibliothek.
TU Bibliothek Your knowledge hub WIEN

3 Materials and Methods

3.1 Ball-on-Disc Tribometry

3.1.1 Working Principle and Test Setup

The working principle of a tribometer can be found in Figure 3.1, which is described in the ASTM Standard G99-17 [87]. F_N describes a normal force on the pin and thus on the disc, d is the diameter of the ball, D is the diameter of the disc, R is the radius of the wear track, and w is the rotational speed.

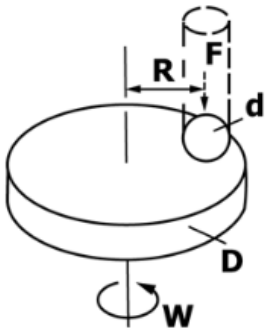

Figure 3.1: Working principle of a ball-on-disc tribometer, with a rotating disc and a static counterbody. Reprinted from [87]. Copyright 2020, ASTM International.

The pin could not move during the test, and only the specimen rotated clockwise at a certain rotational speed. Therefore, the ball left a circular wear track. For the measurement of the COF, the ball-on-disc tribometer MFT2000A from Rtec-Instruments was used. Inside the tribometer a force transducer was employed to measure the frictional force between the ball and the specimen. Additionally, the tribometer was equipped with sensors that recorded the applied force and the number of rotations. The COF, shown in Equation (3.1) was obtained and plotted using the tribometer's software, where μ describes the COF, F_R the frictional force, and F_N the normal force.

$$\mu = \frac{F_R}{F_N} \tag{3.1}$$

Die approbierte gedruckte Originalversion dieser Diplomarbeit ist an der TU Wien Bibliothek verfügbar
The approved original version of this thesis is available in print at TU Wien Bibliothek.
TU Bibliothek Your knowledge hub WIEN

An Al_2O_3 ball with a diameter of 6 mm was fixed into the tribometer's ball holder so that it could not move. The tribometer was set up to press onto the specimen with a specific normal force of 1 N and leave a wear track with a radius of 2 mm at a linear speed of 1000 $^{mm}/_{\text{min}}$. Two distinct types of tests were conducted, at room temperature, and each test was repeated three times for consistency. The initial set of tests concluded after 750 revolutions, while the extended tests continued until a COF threshold of 0.2 was reached.

To conduct the tribometer tests inside an inert gas atmosphere, an atmospheric chamber was constructed. This square chamber was built with aluminum profiles outlining its edges and acrylic glass panels filling the spaces in between. The chamber was bottomless, so that it can be easily positioned over the tribometer, facilitating seamless testing conditions.

3.1.2 3D Model of the Inert Gas Chamber

To construct the inert gas chamber, the initial step involved creating a comprehensive 3D model with the Autodesk Inventor software [88] that incorporated all desired functionalities. Key features included ensuring the tribometer's free movement, incorporating a tribometer connection inside, providing an inlet for the inert gas and an outlet for a vacuum pump, integrating a hole for an oxygen sensor, a door as access to the tribometer, sufficient internal space, and allowing for easy removal of the chamber for maintenance or repairs. Detailed 3D model images are illustrated in Figure 3.2, where Figure 3.2a shows a realistic illustration of the inert gas chamber from the east view and Figure 3.2c from the west view. Further Figure 3.2b showcases a more technical view, highlighting the edges of the chamber. A technical drawing for the assembly of the chamber is provided in the Appendix A, which was also created using the Autodesk Inventor software [88].

The primary structural framework of the chamber was made of 40x40 mm aluminum profiles with a groove size of 8 mm from Item Industrietechnik GmbH. These profiles offered robust support, and their compatibility with various additional items from the manufacturer made them versatile. The connection was realized using an Automatic-Fastening Set, size 8 mm, from Item Industrietechnik GmbH, which proved effective given the moderate forces acting on the structure. To ensure effective sealing of the chamber, silicone was applied to all edges and openings, providing a reliable barrier against gas leakage.

Die approbierte gedruckte Originalversion dieser Diplomarbeit ist an der TU Wien Bibliothek verfügbar
The approved original version of this thesis is available in print at TU Wien Bibliothek.
TU Bibliothek Your knowledge hub WIEN

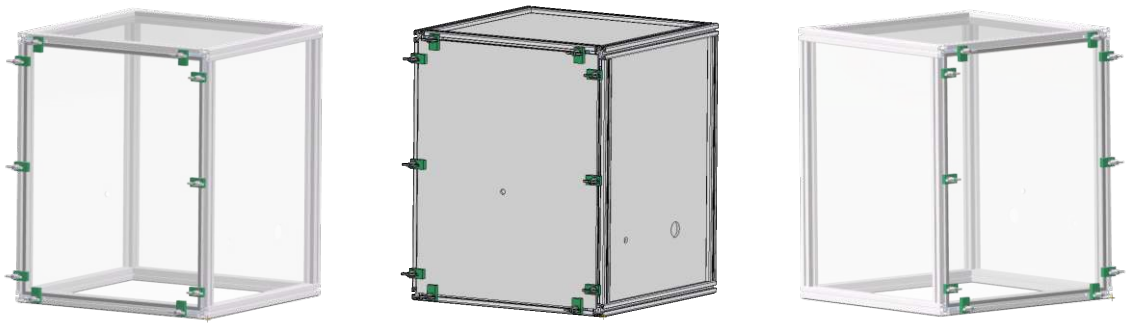

(a) (b) (c)

Figure 3.2: 3D model of the inert gas chamber depicted in realistic views from (a) the east and (c) the west, and (b) a high-contrast technical illustration. Visualized using Autodesk Inventor [88].

3.1.3 Leakage Testing

To assess the amount of gas leaking from the chamber, a leakage test was conducted, as seen in Figure 3.3. The chamber was filled with ≥99.999 vol.-% pure nitrogen to displace the air until the O_2 sensor (Greisinger GMH 3692 oxygen meter and Greisinger GGO 370 gas sensor) read a value of 0.1 % oxygen. Initially, a sharp decline in oxygen was observed, gradually flattening as oxygen levels decreased. The average time to reach 0.1 % oxygen was around 22 minutes (red curve) and a little less then one quarter of the 200 bar and 50 l flask was consumed. Subsequently, the inlet was shut (blue line) for 60 minutes and values were recorded every 5 minutes. Eventually, a slow increase to 0.5 % O_2 indicated efficient sealing of the chamber for the testing purposes. Measurements of the absolute pressure inside the chamber revealed to be consistent and equal to the outside ambient air pressure, indicating that the pressure induced by nitrogen inletting could be rapidly equalized and posed no issues for the comparative experiments. Further humidity declined drastically to around 8 %.

In an attempt to reduce the nitrogen consumption and the time that was required to reach the desired oxygen level, a Pfeiffer Vacuum pump with a pumping speed of 0.7 m^3/h was used, but no improvement was observed, as seen in Figure 3.3 (orange curve). This could be due to the pump's low power. Given the satisfactory results without the pump, further investigation in this regard was not pursued.

Furthermore, for some tests the tribometer operated in an argon environment, where the chamber was filled with ≥99.999 vol.-% pure argon gas. Notably, in comparison to nitrogen, the more expensive argon proved to be significantly more volatile in our setup. The total consumption for two tests depleted the entire 200 bar and 50 l

Die approbierte gedruckte Originalversion dieser Diplomarbeit ist an der TU Wien Bibliothek verfügbar
The approved original version of this thesis is available in print at TU Wien Bibliothek.
TU Bibliothek Your knowledge hub WIEN

flask. During the test run, a substantial amount of gas was necessary to maintain the nearly 100 % argon environment.

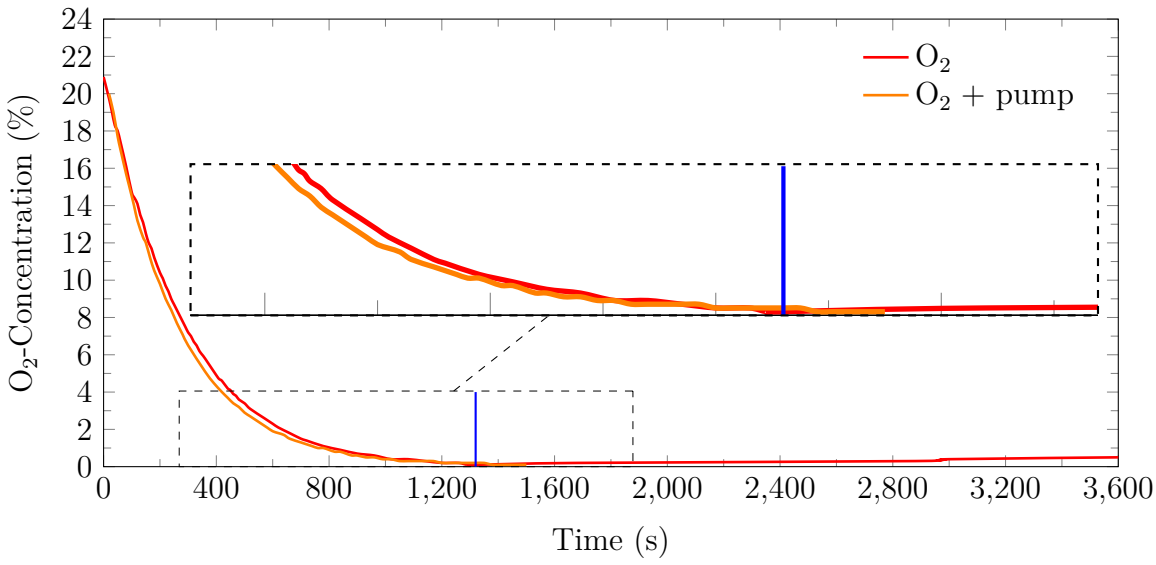

Figure 3.3: Leakage test conducted on the inert gas chamber, illustrating the variation in oxygen concentration over time with and without the integration of a pump.

3.2 Test Execution

The Mo and W PVD coated specimen were glued with a copper tape and then clamped onto the rotational module of the tribometer. The pin was positioned over the metal specimen and the two components were cleaned first with ethanol and than with isopropanol as they might have been touched with gloves or a tweezer. After the evaporation of the solvents and employing a dry air bottle, 10 mg of the selenium nanoparticles were sprinkled with a spatula on the metal plate directly beneath the Al_2O_3 ball. The counterbody was lowered into the selenium powder pile to touch it, and then moved back up so that some of the powder was still on the ball, ensuring there would be powder at the contact spot.

Tests in air atmosphere could be started from that moment on. For nitrogen tests the atmospheric chamber was closed, the oxygen sensor connected, and then the nitrogen was let in the chamber until the oxygen sensor read 0.0 %. Thus, indicating that the oxygen level was lower than 0.05 %, as the sensor displayed values in increments of tenths. Then also the nitrogen tests could be started. To keep the oxygen level below 0.05 %, the nitrogen valve was continuously left open with a very low flow rate that was constantly monitored and adjusted, to remove the air. Humidity was controlled by the inlet of dry nitrogen and reached a value of 8 ± 2 % RH when the

Die approbierte gedruckte Originalversion dieser Diplomarbeit ist an der TU Wien Bibliothek verfügbar
The approved original version of this thesis is available in print at TU Wien Bibliothek.
TU Bibliothek Your knowledge hub WIEN

oxygen sensor showed 0.0 %, 20 ± 2 % RH at 10 ± 0.5 % oxygen, and for a normal air atmosphere 30 ± 2 % RH.

To simplify future references on the various experiments and their corresponding samples, Table 3.1 presents a comprehensive list of of the measurement matrix.

Table 3.1: Measurement matrix for the experiments and their respective samples, facilitating easier reference in subsequent discussions.

Denotation	Material	Powder	Atmosphere	Revolutions
Mo1	Molybdenum	Selenium	Air	750
Mo2	Molybdenum	Selenium	Air	Until Failure
Mo3	Molybdenum	Selenium	Nitrogen	750
Mo4	Molybdenum	Selenium	Nitrogen	Until Failure
Mo5	Molybdenum	-	Air	750
Mo6	Molybdenum	-	Nitrogen	750
W1	Tungsten	Selenium	Air	750
W2	Tungsten	Selenium	Air	Until Failure
W3	Tungsten	Selenium	Nitrogen	750
W4	Tungsten	Selenium	Nitrogen	Until Failure
W5	Tungsten	Tellurium	Air	750
W6	Tungsten	Tellurium	Nitrogen	750
W7	Tungsten	Selenium	Argon	Until Failure
W8	Tungsten	-	Air	750
W9	Tungsten	-	Nitrogen	750

3.3 Software

To enhance data analysis and visualization, custom Python scripts and TikZ (LaTeX) codes were developed. For the visualization and modification of microscopy images and molecular structures the ImageJ [89], ReciprOgraph [90], and VESTA [47] softwares were utilized. Additionally, sketches were produced using Apple's FreeForms application. Autodesk Inventor [88] played a crucial role in the creation of 3D models and design visualizations of the inert gas chamber.

Throughout the course of this thesis, tools such as ChatGPT and DeepL were utilized exclusively for the purposes of grammar, spelling, and syntax refinement. These tools did not contribute to the research content or information generation.

Die approbierte gedruckte Originalversion dieser Diplomarbeit ist an der TU Wien Bibliothek verfügbar
The approved original version of this thesis is available in print at TU Wien Bibliothek.
TU Bibliothek Your knowledge hub WIEN

3.4 Characterization Methods

3.4.1 Transmission Electron Microscopy (TEM)

A Transmission Electron Microscopy (TEM) is one of the most versatile scientific instrument for material characterization at a high analytical and spatial resolution, allowing for accurately determining the thickness of the tribofilm and its structure [91]. Many additional analytical instruments can be added to a TEM, e.g., Energy-Dispersive X-ray (EDX) and SAED that were also employed in this thesis. The first TEM was developed by Ernst Ruska in 1933, based on the development of electric lenses to focus the electrons, using the principle of the wave like properties of electrons. The underlying technique of a TEM is a beam of high energy electrons that are transmitted through a solid in high vacuum to obtain an image of the internal structure. This is achieved by recording the electron flux after passing through a thin specimen, which can be schematically seen in Figure 3.4.

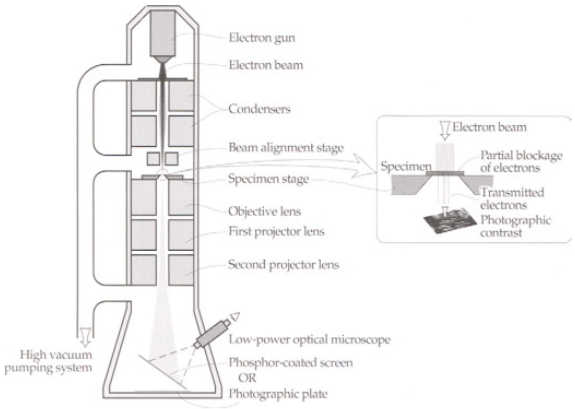

Figure 3.4: Working principle of a TEM. Reprinted from [92]. Copyright 2004, Elsevier.

The electron beam, generated by an electron gun, is directed and focused onto the specimen. Subsequently, the electrons that pass through hit a screen recording the image. The resolution is determined by the wavelength, whereby the wavelength of the electron flow is inversely proportional to the square root of the electron voltage. The preparation of the specimen can be extensive, as the material has to be thinner than 100 nm. This is achieved by the Focussed Ion Beam (FIB) technique, where ions bombard the specimen thinning it down, further explained in Section 3.6 [92]. For the material characterization a TECNAI F20 ”60-200” from the USTEM department at TU Wien with an accelerating voltage of 200 kV, a lattice resolution of 0.14 nm, and a point resolution of 0.24 nm was utilized. For some uses the TEM was put in STEM mode, the Gatan DigiSTEM II with HAADF, with a point resolution

Die approbierte gedruckte Originalversion dieser Diplomarbeit ist an der TU Wien Bibliothek verfügbar
The approved original version of this thesis is available in print at TU Wien Bibliothek.
TU Bibliothek Your knowledge hub WIEN

of 0.15 nm. This mode is similar to the basic TEM, but like a Scanning Electron Microscopy (SEM) the electron beam is focussed on precise points and scanning along a grid, to produce the image assembling it one after another [93].

3.4.2 Energy Dispersive X-Ray Spectroscopy (EDX)

For the examination of the specimen an EDAX-AMETEK Apollo XLTW SDD spectrometer, in combination with the TEM from the USTEM department at TU Wien, was used. To use the EDX mode, a STEM image is first obtained in the region of interest and then the analysis can be performed. The EDX spectrometer uses a silicon semiconductor detector which is sensitive enough to identify elements above lithium in the periodic table. Charge pulses, that are converted to a voltage, are generated by the detector proportional to the energies of the incident X-rays. Thus, with data processing, elements can be quantitatively assigned simultaneously to peaks on a spectrum according to their energy, with the energy in keV on the x-axis and the intensity count on the y-axis. Further the elements can be displayed on a profile or map along a line or area [91, 94].

It is a widely used, fast, precise, and reliable method for investigating the elemental composition of a sample with a depth of analysis of up to 2 µm [95, 96]. The principle of EDX detection is based on the emission of characteristic X-rays due to the excitation of the inner shell by incident electrons. When an electron from an inner shell, e.g., the K or L shell, gets excited and ejected from its shell, an electron from a higher energy level fills the hole and may emit a characteristic X-ray with the energy between these two energy levels. The transition of an electron from the L to the K shell is denoted by $K\alpha$, the transition from the M to the L shell by $L\alpha$. If an electron gets excited, an auger electron may be emitted instead of the characteristic X-ray, the probability for that decreases with the increase in atomic number. Thus, EDX spectrometry is especially advantageous for heavier elements and small element contents [95].

3.4.3 Confocal Laser Scanning Microscopy

A VK-X1000 Confocal Laser Scanning Microscopy (CLSM) by Keyence was employed to examine the wear track as well as obtain the roughness and wear rate. In a CLSM, a laser is directed onto scanning mirrors that sweep over the sample, the emitted fluorescence is then detected. By changing the focal point, it is possible to generate a 3D image of the sample [97]. This allows for precise structural surface information, e.g., to obtain the surface roughness [98]. The resolution is limited by

Die approbierte gedruckte Originalversion dieser Diplomarbeit ist an der TU Wien Bibliothek verfügbar
The approved original version of this thesis is available in print at TU Wien Bibliothek.
TU Bibliothek Your knowledge hub WIEN

the numerical aperture of the objective lens, the refractive index of the sample, and the wavelength of the light [99]. A conventional light microscope is used to find the area of interest before scanning in confocal mode [97]. Furthermore images in optical mode can be made, so that the tribofilm on the wear track can be examined with high magnification.

3.4.4 Raman Spectroscopy

For our wear track analyses a Micro-Raman spectrometer LabRam ARAMIS-UV Vis from Horiba Yvon, which is located in Wiener Neustadt at the Centre for Electrochemical Surface Technology (CEST), was employed. Raman spectroscopy is based on the process of Raman scattering. It is often used to obtain information about chemical structures, not just the elemental composition of a sample, and to identify and quantify the amount of a substance. The sample can be in a wide range of states of matter and the Raman spectrometers are easy to use. When light interacts with matter, the photons may be absorbed, scattered or not interact with the material at all. In Raman spectroscopy, the detection of scattered radiation provides information about the vibrational states of the molecules and is usually interpreted using the wavenumber ω [100]. The intensity in a Raman spectrum is then plotted as a function of the wavenumber ω, expressed in cm^{-1} [101]. If the sample is irradiated with a monochromatic source, the light can be scattered elastically, which is called Rayleigh scattering, where the frequency is the same as that of the incident photon. However, every 10^6th to 10^8th photon is scattered inelastically, which is called Raman scattering [100]. As shown in Figure 3.5, the wavenumber ω of the Raman scattered photons is either higher or lower than that of the incident radiation. If the difference between the wavenumbers and the incident radiation is positive, this is called Stokes scattering and if the difference is negative, it is called anti-Stokes scattering; both are usually in the range of $10^4\,\mathrm{cm}^{-1}$ to $10^2\,\mathrm{cm}^{-1}$ [101, 102].

Die approbierte gedruckte Originalversion dieser Diplomarbeit ist an der TU Wien Bibliothek verfügbar
The approved original version of this thesis is available in print at TU Wien Bibliothek.
TU Bibliothek Your knowledge hub WIEN

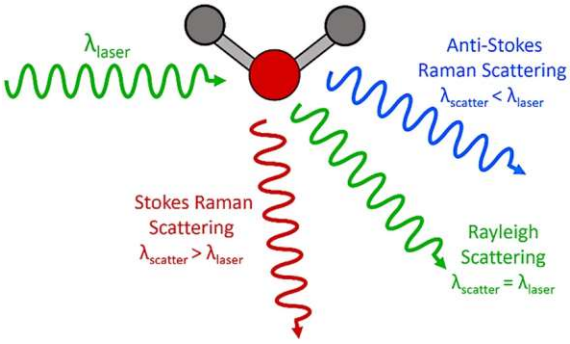

Figure 3.5: Principle of Raman scattering used in Raman spectroscopy. Reprinted from [103]. Copyright 2023, Springer Nature BV.

3.5 Selenium Nanoparticles

The selenium nanoparticle powder, with the CAS number 7782-49-2, was ordered from NANOSHEL UK Ltd. The product had a specified purity level of 99.9 % and an average particle size of <80 nm, as indicated by the provided specification sheet. Noteworthy properties included a molecular weight of 78.96 g/mol, a density of 4.81 g/mol, a melting point at 217 °C, a boiling point at 684.9 °C, and a Young's modulus of 10 GPa. The color of the selenium was characterized as Gray to Black [104].

3.5.1 TEM and EDX Investigation of Selenium

The selenium powder was examined using a TEM in collaboration with the USTEM department at TU Wien. Figure 3.6a shows the selenium nanoparticles as they were piled up on the carbon grid that was used as the specimen holder. The measured particles were smaller than 80 nm, as stated in the datasheet. Yet in Figure 3.6b a selenium nanoparticle powder was bundled into an agglomerate that was larger than 2 µm, indicating there will be some larger particles. This might have happened due to the long storage time of the selenium, but enough nanoparticles were identifiable. Figure 3.6c shows the location of the EDX line scan analysis on the selenium powder.

Die approbierte gedruckte Originalversion dieser Diplomarbeit ist an der TU Wien Bibliothek verfügbar
The approved original version of this thesis is available in print at TU Wien Bibliothek.
TU Bibliothek Your knowledge hub WIEN

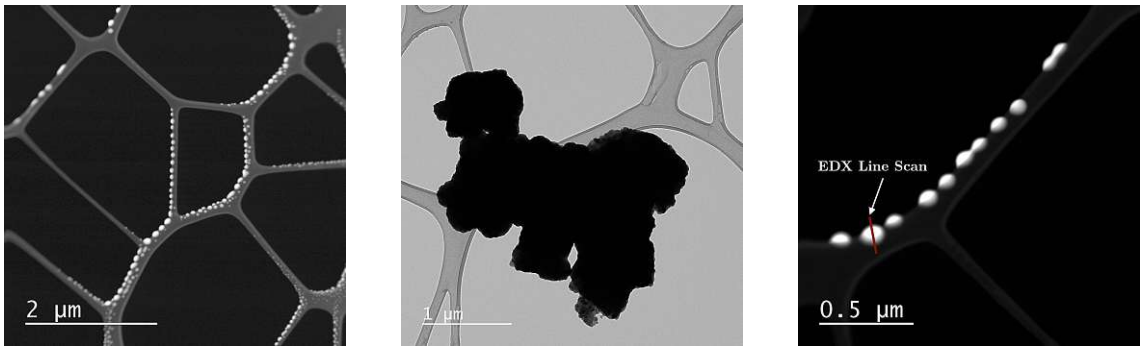

(a) (b) (c)

Figure 3.6: STEM image (a) showing selenium nanoparticles piled up on the carbon specimen holder, TEM image (b) depicting a selenium agglomerate, and (c) an illustration detailing the EDX line scan trajectory across a selenium nanoparticle.

The results depicted in Figure 3.7 revealed a significant carbon presence, attributable to the carbon fiber composition of the specimen holder. Notably, there was a pronounced concentration of selenium and a negligible presence of oxygen in the analyzed region. This was similar to high-quality selenium nanoparticles literature results of Safaei et al. [105] and Avendaño et al. [106], investigating selenium nanoparticles, except in our study even less oxygen was noticable. The agglomerate was also examined to rule out contamination, and it was confirmed to be pure selenium.

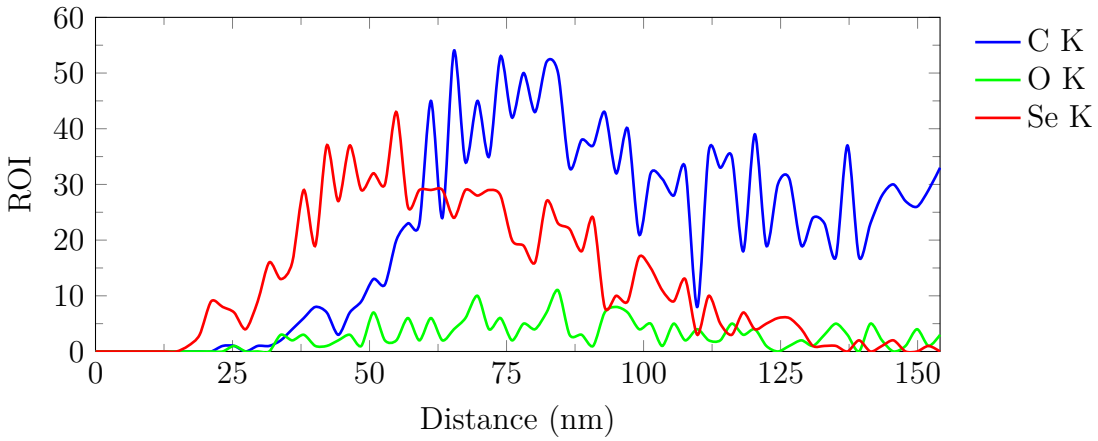

Figure 3.7: ROI values of the EDX line scan across the selenium particle.

3.5.2 Selenium Diffraction Patterns

With the TEM analysis a SAED pattern was also obducted to confirm the expected trigonal crystallographic pattern of selenium. The diffraction pattern can be seen in Figure 3.8a. The inspected rings and spots were compared to the literature

Die approbierte gedruckte Originalversion dieser Diplomarbeit ist an der TU Wien Bibliothek verfügbar
The approved original version of this thesis is available in print at TU Wien Bibliothek.
TU Bibliothek Your knowledge hub WIEN

(lit.) and theoretical (th.) d-spacing values for several crystallographic planes, as seen in Table 3.2. The values matched well with the experimental values, thus confirming the one-dimensional alpha selenium ribbon structure that is illustrated in Figure 3.8b.

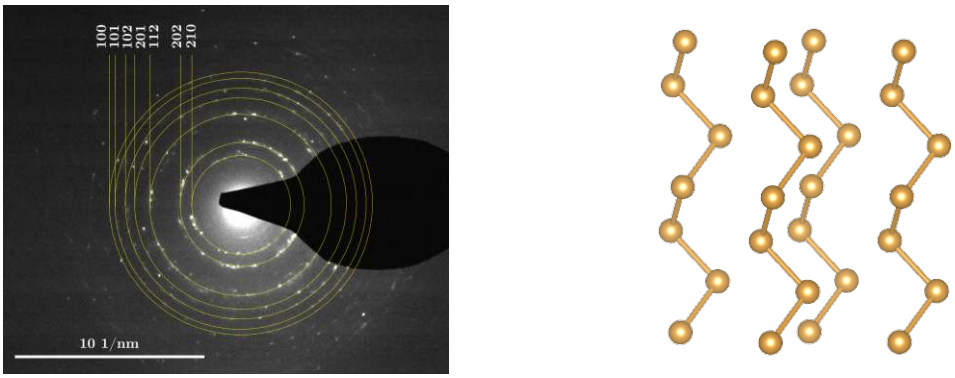

(a) (b)

Figure 3.8: (a) SAED patterns of selenium representing various crystallographic planes and (b) representing the trigonal crystal structure of selenium. Data retrieved from the Materials Project for Se (mp-14) from database version v2023.11.1. [46]. Visualized using VESTA [47].

A Se atom is bonded to two equivalent Se atoms in a water-like geometry, with a bond length of 2.40 Å [46]. The literature values in Table 3.2 for the d-spacing of the selenium SAED pattern were provided by the USTEM department at TU Wien and theoretical values were obtained using the ReciprOgraph applet from Schoeni and Chapuis [90].

Table 3.2: Comparison of d-spacings measured in angstroms (Å), derived from the SAED pattern of selenium, with both literature and theoretical values.

d (Å)	**d (Å)** lit.	**d (Å)** th.	**hkl**
3.83	3.78	3.90	100
3.06	3.01	3.07	101
2.09	2.07	2.10	102
1.79	1.77	1.82	201
1.64	1.64	1.67	112
1.51	1.50	1.54	202
1.44	1.43	1.47	210

Concluding the investigation into selenium nanoparticles, the observed quality aligned with comparable literature results and our expectations, with the majority of detectable particles being smaller than 80 nm. Little oxidation was identified, and the crystal structure conformed to the trigonal form. This powder was consistent with

Die approbierte gedruckte Originalversion dieser Diplomarbeit ist an der TU Wien Bibliothek verfügbar
The approved original version of this thesis is available in print at TU Wien Bibliothek.
TU Bibliothek Your knowledge hub WIEN

that used by our colleagues in their experiments, as documented in Grützmacher et al. [11].

3.6 FIB Preparation for TEM Analysis

The sample preparation for the TEM analysis involved the usage of a FIB at the USTEM department of TU Wien. The process involved sculpting a lamella from the sample. Therefore gallium ions were employed to precisely mill the bulk material and extract a thin section, achieving a final thickness of less than 100 nm, which is an essential criterion for effective TEM examination.

3.6.1 Preparation of the Molybdenum Sample

Figure 3.9a displays the wear track, highlighting the presence of Se nanoparticles predominantly next to the wear track. This distribution suggests that the Se particles were either displaced by the counterbody or were integrated into the tribofilm. Close to the wear track, the surface appeared free from Se nanoparticles, while a considerable amount of loose powder was evident further away. Figure 3.9b illustrates the location of the extracted cutout and the applied protective tungsten layer. After milling, the extracted section was then finely thinned to meet the requirements for the TEM analysis, as depicted in Figure 3.9c. The finished specimen included the steel substrate as the darker lower area, with the PVD-coated Mo layer above and the protective tungsten layer on top. The tribofilm, while not distinctly visible due to its thinness, was situated between these layers.

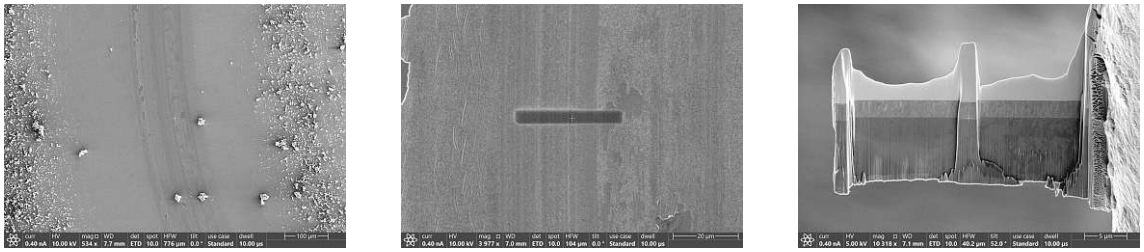

(a) (b) (c)

Figure 3.9: FIB preparation of the molybdenum sample depicting (a) the wear track, (b) the location of the lamella extraction including the protective layer, and (c) the different layers of the specimen.

3.6.2 Preparation of the Tungsten Sample

The preparation process for the tungsten sample was identical to that of the molybdenum sample. Initially, a SEM was utilized to identify an optimal location

Die approbierte gedruckte Originalversion dieser Diplomarbeit ist an der TU Wien Bibliothek verfügbar
The approved original version of this thesis is available in print at TU Wien Bibliothek.
TU Bibliothek Your knowledge hub WIEN

showcasing a visible formation of the tribofilm. Figure 3.10a shows the placement of the protective tungsten layer directly across the wear track, where the tribofilm was prominently visible. Following the milling operation, Figure 3.10b presents the finished specimen. This image distinctly displays the layered arrangement comprising the steel substrate, tungsten PVD coating, tribofilm, and the protective layer, illustrating the fine preparation and structure of the sample. Additionally, Figure 3.10c presents the carrier with both specimens affixed during the FIB procedure. The W sample was indicated by the circle on the left, while the Mo sample was marked by the diamond on the right.

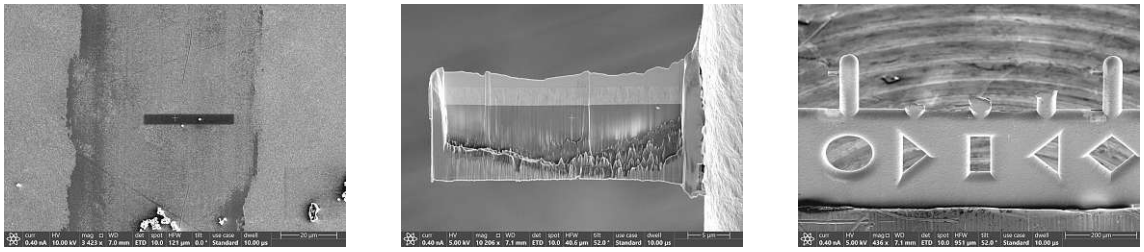

(a) (b) (c)

Figure 3.10: FIB preparation of the tungsten sample depicting (a) the location of the lamella extraction including the protective layer, (b) the layers of the specimen, and (c) the final carrier for both samples.

Die approbierte gedruckte Originalversion dieser Diplomarbeit ist an der TU Wien Bibliothek verfügbar
The approved original version of this thesis is available in print at TU Wien Bibliothek.
TU Bibliothek Your knowledge hub WIEN

4 Results and Discussion

After carefully studying both the chemical composition and the structural characteristics of the selenium particles, we performed a series of tribological experiments. These tests were designed to explore the potential for the formation of $MoSe_2$ as well as WSe_2 layers through tribochemical reactions occurring between molybdenum or tungsten surfaces and the selenium particles. A key aspect of this investigation was to understand how varying atmospheric conditions during these experiments could influence the outcomes of the tribochemical reactions and the subsequent formation of $MoSe_2$ and WSe_2 layers. This focus on atmospheric conditions stemmed from the hypothesis that the environment in which these reactions occur could significantly affect the efficiency and the mechanism of the layer formation process.

4.1 Molybdenum Diselenide

4.1.1 Reference Measurements for Molybdenum

We conducted the initial reference measurements for molybdenum without lubrication in both ambient air and a nitrogen atmosphere, as illustrated in Figure 4.1. The COF starts in air at 0.2 and in nitrogen at 0.15 and quickly increased to 0.35 (air) and 0.25 (nitrogen). This increase in friction is attributed to the growth of the actual contact area, along with the elimination of contaminants and thin native oxide layers, which leads to greater adhesion [11]. After running-in the COF eventually stabilized at 0.35 in both atmospheric conditions [107].Similar values have been reported in previous studies [108–110], although none matched our exact testing conditions. The study by Grützmacher et al. [11], under similar testing conditions in an air atmosphere, reported higher friction values of approximately 0.6, but with considerable variance. While friction values initially appeared lower in a nitrogen atmosphere, with a RH of 8 %, they eventually converged with those in ambient air. The lack of oxygen limits the formation of harder, more abrasive metal oxides by reducing molybdenum's reaction with oxygen, typically leading to increased friction

Die approbierte gedruckte Originalversion dieser Diplomarbeit ist an der TU Wien Bibliothek verfügbar
The approved original version of this thesis is available in print at TU Wien Bibliothek.
TU Bibliothek Your knowledge hub WIEN

[27]. Conversely, humidity in air may reduce friction as water molecules can serve as a liquid lubricant [111].

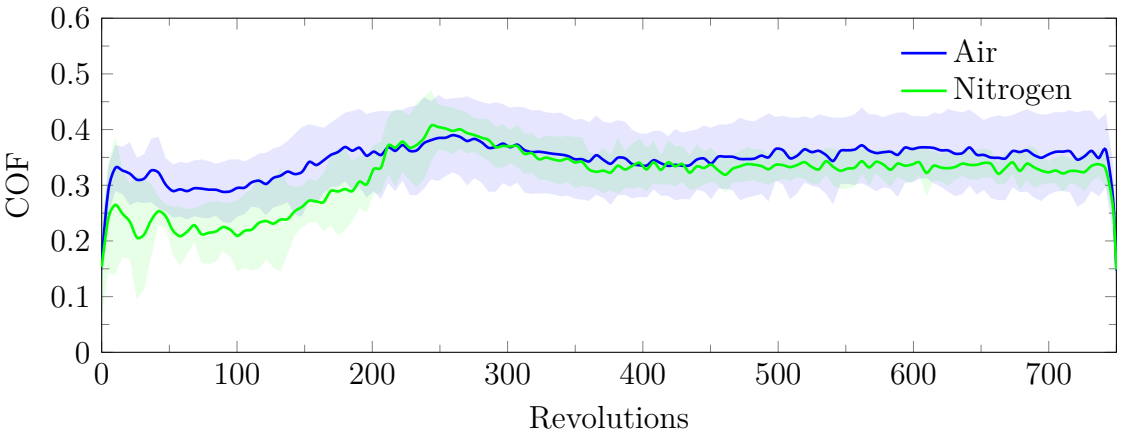

Figure 4.1: Reference measurements of Mo without lubrication, subjected to a 1 N load and a linear speed of 1000 $^{mm}/_{\text{min}}$, conducted in air with 30 % RH (blue curve) and in a nitrogen atmosphere with 8 % RH (green curve).

4.1.2 Initial Formation and Behavior of $MoSe_2$ Layers

We explored the formation of $MoSe_2$ layers under three different conditions: ambient air, 10 % oxygen, and nitrogen atmosphere. This was done by adding Se powder to the contact zone before initiating the tests. Figure 4.2 illustrates the COF over the first 750 cycles. Initially, the COF was around 0.15 attributed to breaking the hard, thin oxide layer and evolution of the real contact area. However, it significantly decreased to below 0.1 after the running-in period, highlighting the effectiveness of the $MoSe_2$ TMD layer formation in reducing friction across all tested atmospheres [11, 107]. Compared to the higher friction values and higher variance seen in Grützmacher et al. [11], in our study a lower starting COF was observed, potentially due to a different selenium powder application technique, although this was not replicable. Notably, the COF ended up at 0.07 in air, 0.03 in 10 % oxygen, and 0.06 in nitrogen, showing no significant difference between different atmospheric conditions, as the error bars overlap. These findings align with Chakrapani [17], Kubart et al. [19], and Domínguez-Meister et al. [20] that oxygen levels have no significant influence on the friction reducing characteristics of $MoSe_2$.

Die approbierte gedruckte Originalversion dieser Diplomarbeit ist an der TU Wien Bibliothek verfügbar
The approved original version of this thesis is available in print at TU Wien Bibliothek.
TU Bibliothek Your knowledge hub WIEN

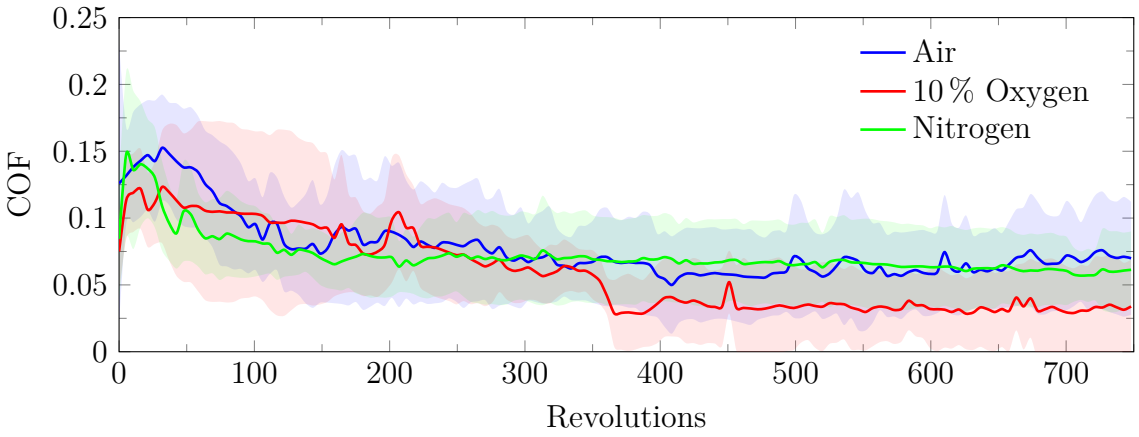

Figure 4.2: COF performance for Mo with Se powder addition under a 1 N load and a linear speed of 1000 $^{mm}/_{\text{min}}$, conducted in air with 30 % RH (blue curve), in 10 % oxygen with 20 % RH (red curve), and in nitrogen atmosphere with 8 % RH (green curve). In all atmospheric conditions friction reduction is similar, indicating no significant atmospheric influence on performance.

The interaction between surface oxygen and the Mo coating results in MoO_2 and MoO_3 layers, which initially cover the samples. For $MoSe_2$ to form, these oxide layers must first be removed through wear in the ball-on-disc setup, a conclusion supported by Grützmacher et al. [11]. The mechanical stress from the test facilitates the transformation of Se powder into crystalline $MoSe_2$ layers, incorporating defects and debris from the worn Mo surface. While oxide debris does not directly lead to the TMD layer's formation, it plays a role in increasing wear as a third body, which, in turn, aids the formation and efficiency of the $MoSe_2$ tribofilm by introducing surface defects and extracting metal atoms [11].

4.1.3 Extended Durability Testing of $MoSe_2$ Layers

Thereafter, the experiment was extended until a noticeable increase in the COF was observed, following its initial reduction. As illustrated in Figure 4.3, the COF was monitored until it reached a threshold value of 0.2, indicating a substantial deterioration of the $MoSe_2$ TMD tribofilm, as this is close to the lowest friction values for the Mo reference measurements without lubrication.

The tests were again carried out in the different atmospheric conditions. The results clearly showed that oxygen concentration significantly influences the tribofilm's durability and lower oxygen levels reduce degradation. Remarkably, the longest test run in a nitrogen atmosphere lasted more than 200 % longer (over 30 000 cycles) than the longest one with atmospheric air (under 10 000). When comparing our findings

Die approbierte gedruckte Originalversion dieser Diplomarbeit ist an der TU Wien Bibliothek verfügbar
The approved original version of this thesis is available in print at TU Wien Bibliothek.
TU Bibliothek Your knowledge hub WIEN

with those of Grützmacher et al. [11], we observed that the friction-reducing effect of the $MoSe_2$ layers often lasted significantly longer across numerous measurements. However, in some instances, we also noticed the COF increased relatively quickly, similar to the observations from their study.

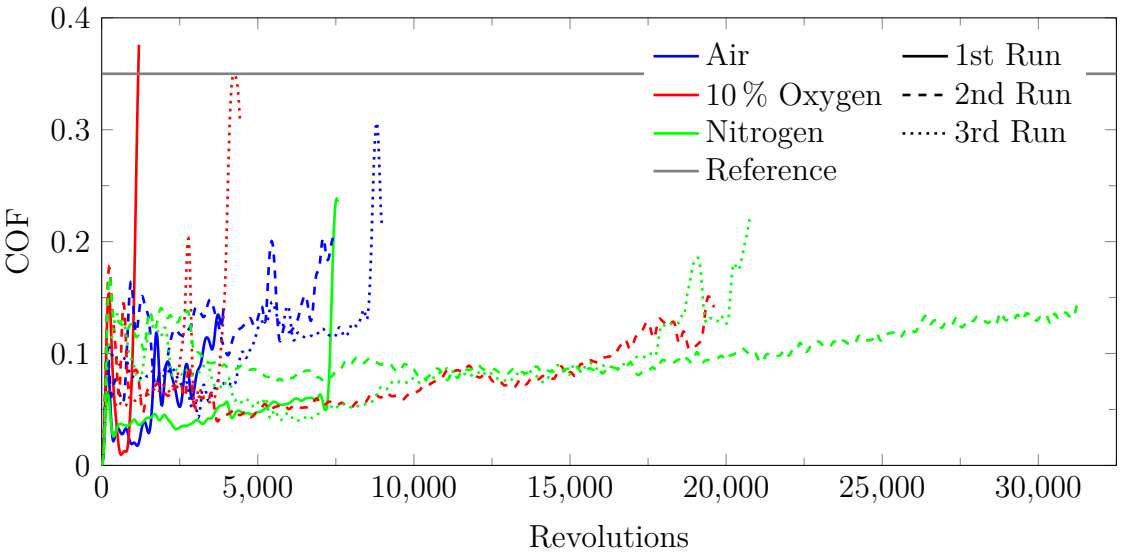

Figure 4.3: Durability performance of $MoSe_2$ under a 1 N load and a linear speed of 1000 $^{mm}/_{\text{min}}$, conducted in air with 30 % RH (blue curve), in 10 % oxygen with 20 % RH (red curve), and in nitrogen atmosphere with 8 % RH (green curve). The average reference value is illustrated in gray. Decreasing oxygen levels increase the duration of friction reducing properties of the TMD.

The presence of lower oxygen levels reduces the rate at which metal oxides form, these oxides typically reduce the effective formation of the $MoSe_2$ layers [112]. Thus, at lower oxygen levels more Mo atoms are available to form a TMD with the Se powder. The same conclusion is true for humidity, which in general reduces oxidation at lower levels [113].

Moreover, $MoSe_2$ and other TMDs are susceptible to oxidation, which is reduced by lower levels of oxygen and humidity. The thickness of TMD layers makes them particularly vulnerable to environmental degradation, especially given their high surface-to-volume ratio, making them sensitive to oxygen and humidity [16, 80]. While perfect monolayers of TMDs are somewhat resistant to oxygen due to weak physical adsorption, oxygen atoms can chemically bind to the TMD at single vacancies of chalcogen, a common defect in TMDs [114].

Die approbierte gedruckte Originalversion dieser Diplomarbeit ist an der TU Wien Bibliothek verfügbar
The approved original version of this thesis is available in print at TU Wien Bibliothek.
TU Bibliothek Your knowledge hub WIEN

4.2 Tungsten Diselenide

4.2.1 Reference Measurement for Tungsten

Following the approach used with molybdenum, we conducted identical tests using tungsten as the substrate under the same conditions. Starting with reference tests without lubrication to assess the interaction between pure metal and the ceramic ball in both air and nitrogen environments. Figure 4.4 presents the results for W, where initial COF values were low, around 0.1, across all conditions. During the running-in phase, the COF quickly escalated to 0.3 in air, but in nitrogen, the increase was more gradual, maintaining a value of 0.1 for 400 cycles before rising to 0.25 [107]. These observations are typical for metal-ceramic contacts with similar results in literature [115], though Grützmacher et al. [11] noted a higher COF of 0.4, but with significant variance. The increase in friction is primarily caused by enhanced adhesion due to the increase of contact area and the removal of the oxide layer [11].

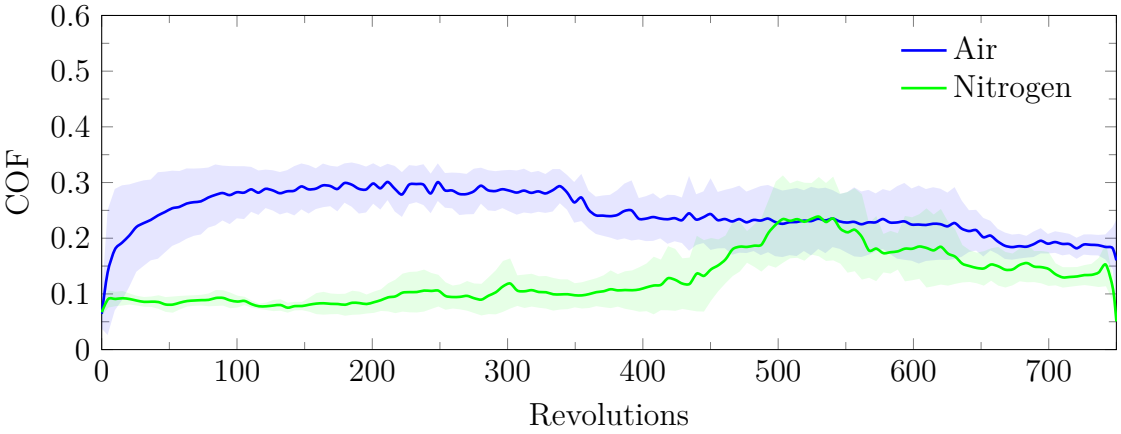

Figure 4.4: Reference measurements of W without lubrication, subjected to a 1 N load and a linear speed of 1000 $^{mm}/_{\text{min}}$, conducted in air with 30 % RH (blue curve) and in a nitrogen atmosphere with 8 % RH (green curve).

Similar to the molybdenum experiments, an atmosphere low in oxygen leads to the formation of fewer and harder tungsten oxides [27]. While increased humidity can introduce water vapor to the surface, which tends to reduce friction, it also promotes oxidation [111]. The presence of more tungsten oxides, known for increasing friction due to their amorphous nature and lack of lubricating properties, could explain the higher friction [116].

Tungsten's COF is notably lower than molybdenum's, stemming from its higher hardness that results in a smaller real contact area and less disturbance to the

Die approbierte gedruckte Originalversion dieser Diplomarbeit ist an der TU Wien Bibliothek verfügbar
The approved original version of this thesis is available in print at TU Wien Bibliothek.

native oxide film, thereby reducing friction [11, 117].

4.2.2 Initial Formation and Behavior of WSe_2 Layers

Similar to the molybdenum experiments, we investigated the formation of WSe_2 layers through a tribochemical reaction under various atmospheric conditions. Figure 4.5 shows the change in the COF over the initial 750 cycles. The COF started at 0.2, but it decreased after running-in to steady-state values of 0.06 in air, 0.09 in 10 % oxygen, and 0.08 in a nitrogen atmosphere, with the differences not being statistically significant due to overlapping error margins. Thus, the atmospheric conditions did not seem to affect the friction outcomes significantly, which aligned with findings from the literature on WSe_2 under similar conditions [17, 19, 20]. Our results show a lower initial friction value, but similar final COF compared to Grützmacher et al. [11].

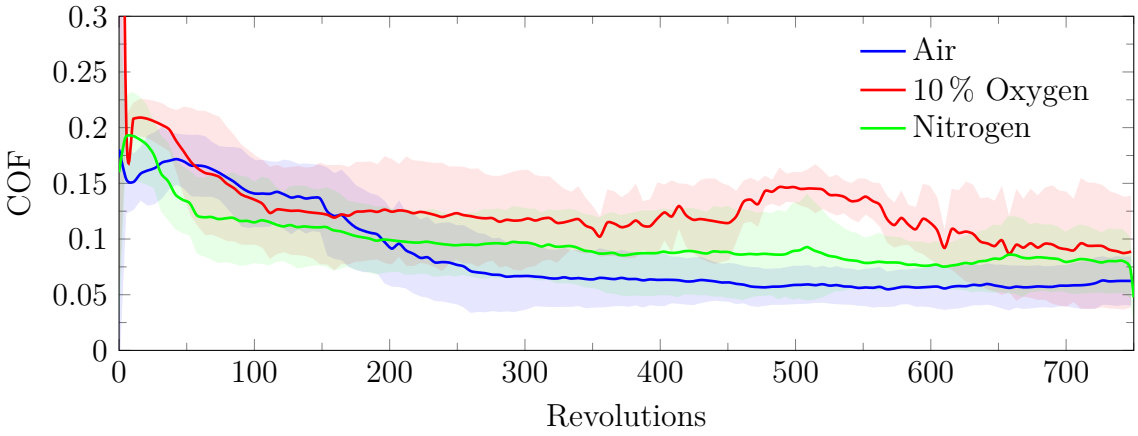

Figure 4.5: COF performance for W with Se powder addition under a 1 N load and a linear speed of 1000 $^{mm}/_{\text{min}}$, conducted in air with 30 % RH (blue curve), in 10 % oxygen with 20 % RH (red curve), and in nitrogen atmosphere with 8 % RH (green curve). In all atmospheric conditions friction reduction is similar, indicating no significant atmospheric influence on performance.

The process behind the WSe_2 layer's formation is similar to that of $MoSe_2$. The initial step involves wearing away the tungsten oxide (WO_3) layer through friction, enabling selenium to react with the exposed tungsten surface. Mechanical stress converts selenium powder into WSe_2 layers, making use of defects and debris from the tungsten surface. These metal oxides facilitate the increase in surface defects and the extraction of tungsten atoms, contributing to the tribofilm formation [11].

Die approbierte gedruckte Originalversion dieser Diplomarbeit ist an der TU Wien Bibliothek verfügbar
The approved original version of this thesis is available in print at TU Wien Bibliothek.
TU Bibliothek Your knowledge hub WIEN

4.2.3 Extended Durability Testing of WSe_2 Layers

We extended the tungsten experiments until the COF reached a threshold of 0.2, as depicted in Figure 4.6. This threshold is close to the steady-state COF of the tungsten reference measurements. The findings highlight the role of oxygen in determining the durability of the WSe_2 containing tribofilm. The shortest tribofilm lifespan was observed in air (blue), while in nitrogen (green) the friction reduction lasted the longest, of up to 10 000 cycles, almost a 150 % increase compared to the average wear life in air. The 10 % oxygen environment (red) showed values in between these two. This demonstrates how elevated oxygen levels accelerate the TMD degradation process.

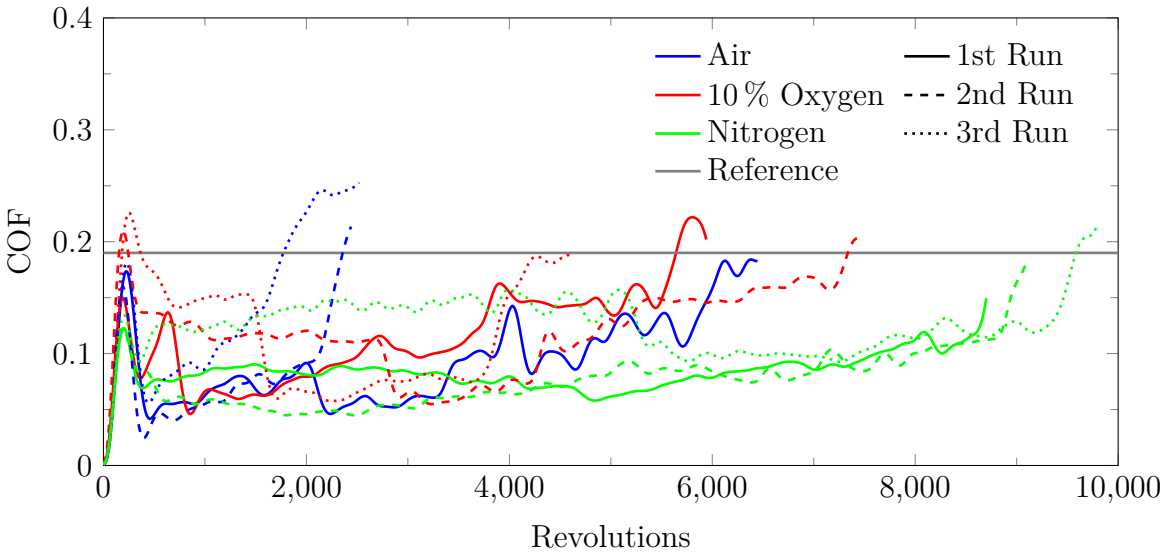

Figure 4.6: Durability performance of WSe_2 under a 1 N load and a linear speed of 1000 $^{mm}/_{\text{min}}$, conducted in air with 30 % RH (blue curve), in 10 % oxygen with 20 % RH (red curve), and in nitrogen atmosphere with 8 % RH (green curve). The average reference value is illustrated in gray. Decreasing oxygen levels increase the duration of friction reducing properties of the TMD.

Prasad et al. [118] found that also tungsten disulfides exhibit a markedly longer wear life in dry nitrogen environments, highlighting the effect of reduced oxidation for TMDs in conditions with low oxygen levels. Compared to molybdenum, the tungsten tribofilm's longevity is shorter. This is attributed to tungsten's higher hardness, which results in fewer wear particles that promote the formation of WSe_2 layers. Our observations also showed longer tribofilm lifespans and, on average, lower friction values compared to those reported by Grützmacher et al. [11], aligning with our molybdenum experiment outcomes. Lower levels of oxygen and humidity contribute to a decrease in tungsten oxide formation [112, 113]. Like $MoSe_2$, WSe_2

Die approbierte gedruckte Originalversion dieser Diplomarbeit ist an der TU Wien Bibliothek verfügbar
The approved original version of this thesis is available in print at TU Wien Bibliothek.
TU Bibliothek Your knowledge hub WIEN

significantly degrades when exposed to oxygen and humidity, especially thin layers are more vulnerable [16, 80, 114].

4.2.4 WSe_2 Tribofilm Behavior after Failure

To investigate how tribofilms with in operando formed TMD layers behave after losing their friction-reducing capabilities, we continued testing beyond the threshold of 0.2. Figure 4.7 illustrates this test conducted in a 10 % oxygen atmosphere. The COF remained low for an extended period of time, until rising to over 0.2 at around 6000 cycles. Interestingly, the dynamics of the test setup and the loose Se powder, occasionally led to the tribofilm's reformation reducing the COF to under 0.1. However, the friction coefficient gradually rose again, reaching a value of 0.2 after another 5000 cycles.

This suggested that, beyond deliberately adding Se powder into the contact zone as Grützmacher et al. [11] recommended, a self-lubricating effect could arise from random occurrences. Such replenishment, while unpredictable, indicated that excess Se powder spontaneously contributed to the TMD formation, enhancing the tribological performance even after the initial tribofilm has worn away.

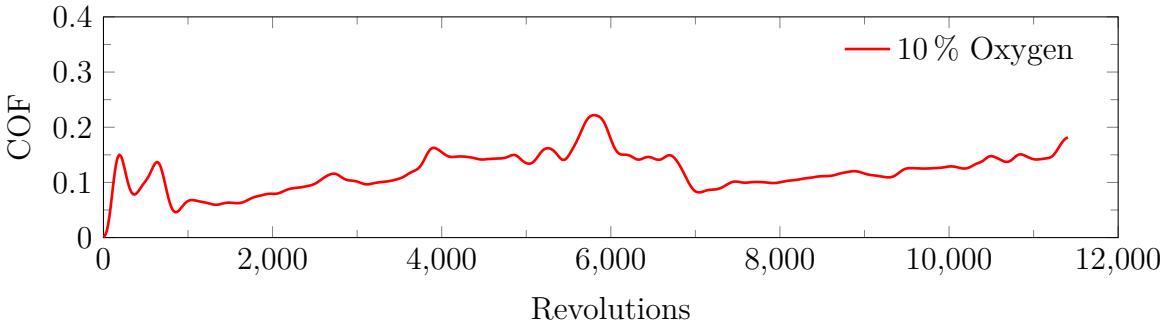

Figure 4.7: Extended test with tungsten and selenium in a 10 % oxygen atmosphere continued after an initial rise of friction coefficient above 0.2. Resulting in a reestablishment of the tribofilm containing WSe_2 layers due to loose Se powder.

4.2.5 Formation and Behavior of WSe_2 Layers in Argon

As a further step, we replaced the air in the inert gas chamber with argon instead of nitrogen, to study the formation of the TMD layers in a noble gas atmosphere. This stemmed on the theory that nitrogen's presence does not affect the tribochemical reactions or the degradation of the TMD layers, as nitrogen is non-reactive at the operating conditions [119, 120]. The experiments conducted in an argon atmosphere, as shown in Figure 4.8, confirmed our expectation that there would be no

Die approbierte gedruckte Originalversion dieser Diplomarbeit ist an der TU Wien Bibliothek verfügbar
The approved original version of this thesis is available in print at TU Wien Bibliothek.
TU Bibliothek Your knowledge hub WIEN

significant difference in the behavior of the COF during the first 750 cycles compared to those in a nitrogen atmosphere. The friction coefficient initially was 0.15 in both environments, then quickly dropped to a steady value of 0.08 in nitrogen and 0.06 in argon, with these differences falling within the margin of error.

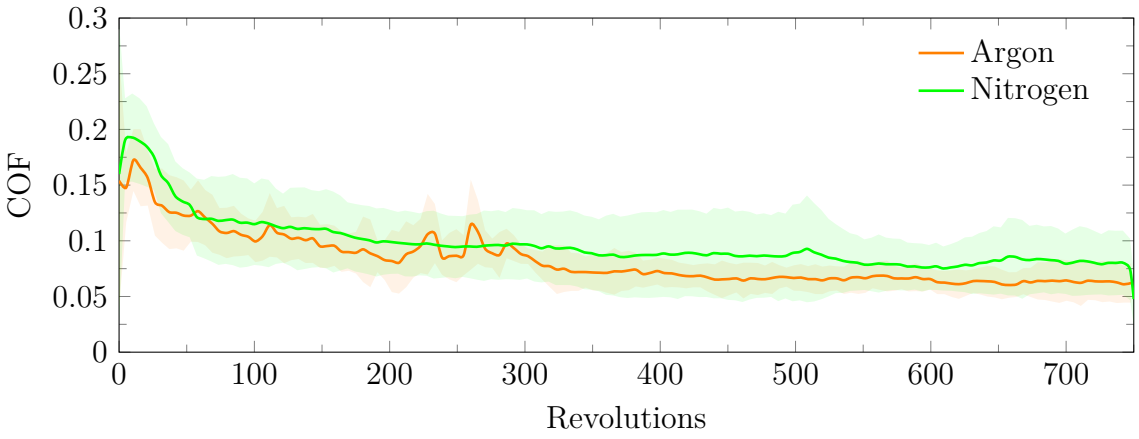

Figure 4.8: COF performance for W with Se powder addition under a 1 N load and a linear speed of 1000 $^{mm}/_{\text{min}}$ in argon (orange curve), compared to in nitrogen (green curve) both with 8 % RH. In both atmospheric conditions friction reduction is similar, due to the low oxygen and humidity levels.

The test in argon again lasted until the tribofilm noticeably degraded and the COF had a value of more than 0.2. The COF behavior over an extended period, depicted in Figure 4.9, was similar to that in nitrogen tests, significantly increasing the wear life compared to in air, with one test surpassing 19 000 cycles. The TMD tribofilm lasted significantly longer in the absence of oxygen and humidity, as this is one of the major degradation factors of TMDs.

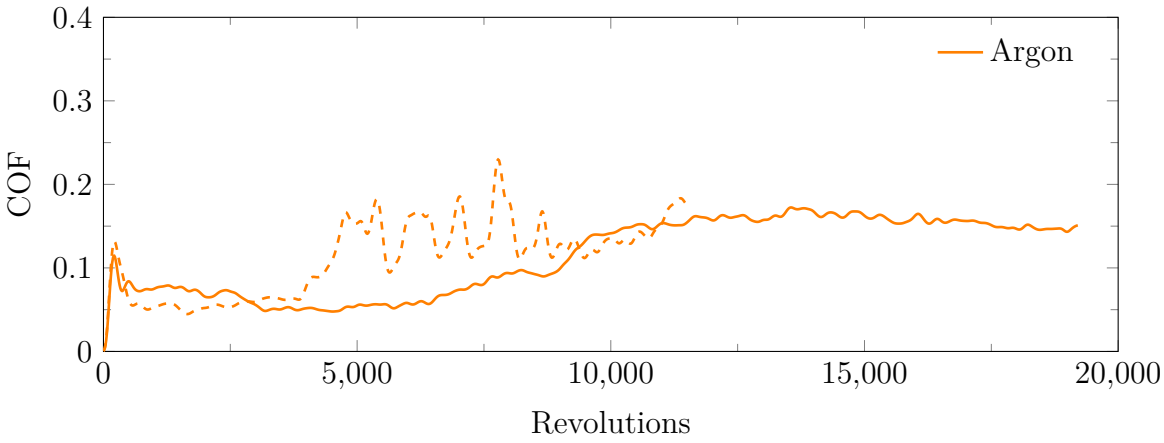

Figure 4.9: Durability performance of WSe_2 under a 1 N load and a linear speed of 1000 $^{mm}/_{\text{min}}$, conducted in argon atmosphere with 8 % RH (orange curve).

Die approbierte gedruckte Originalversion dieser Diplomarbeit ist an der TU Wien Bibliothek verfügbar
The approved original version of this thesis is available in print at TU Wien Bibliothek.
TU Bibliothek Your knowledge hub WIEN

However, although it is effective, the use of argon poses challenges due to its higher cost and greater volatility in our testing setup, making it difficult to maintain very low oxygen levels [121]. This confirms that the use of inert dry nitrogen was the best option to investigate the behavior in oxygen depleted atmospheres. Therefore, we limited our argon experiments to two tungsten samples as a representative test case.

4.3 Tungsten Ditelluride

Prior attempts by colleagues of our group to synthesize TMDs through tribochemical reactions with Te instead of Se in air atmospheres were unsuccessful. To explore the possibility of forming TMD layers when oxygen levels are reduced, we conducted experiments with tungsten and tellurium under nitrogen atmospheres. As shown in Figure 4.10, the absence of oxygen in a nitrogen atmosphere did not enable the formation of TMD layers within the tribofilm. The COF remained steady at around 0.15, showing no significant tribological enhancement over the reference tungsten measurements, apart from a minor reduction possibly due to particle shearing or rolling [11].

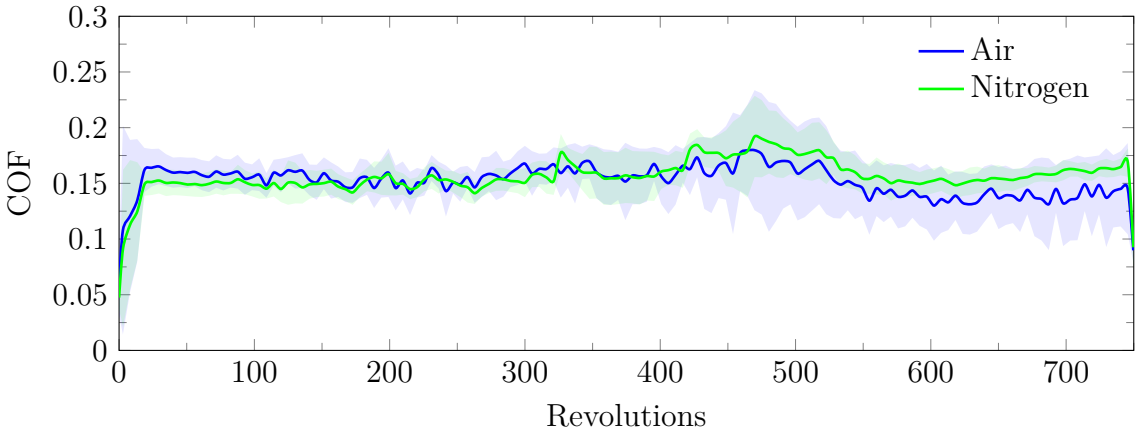

Figure 4.10: COF performance for W with Te powder addition under a 1 N load and a linear speed of 1000 $^{mm}/_{\text{min}}$, conducted in air with 30 % RH (blue curve) and in nitrogen atmosphere with 8 % RH (green curve).

The failure of W and Te to form a TMD via tribochemical reactions can be attributed to several factors. Firstly, the electronegativity difference between W and Te is relatively low, at 0.25 eV, indicating weak atomic bonding. Molybdenum and tellurium have an even smaller difference of 0.06 eV, which is a reason for their exclusion from these experiments. However, future research may explore conditions that could enable their synthesis, such as adjusting speed, force, or temperature.

Die approbierte gedruckte Originalversion dieser Diplomarbeit ist an der TU Wien Bibliothek verfügbar
The approved original version of this thesis is available in print at TU Wien Bibliothek.
TU Bibliothek Your knowledge hub WIEN

Secondly, the formation energy of WTe_2 is $\Delta E = -0.66\,^{eV}/_{atom}$, compared to more negative values for WSe_2 ($\Delta E = -1.09\,^{eV}/_{atom}$) and $MoSe_2$ ($\Delta E = -1.21\,^{eV}/_{atom}$) [122], suggesting that WTe_2 layers are less likely to form. This is also a possible reason why the $MoSe_2$ tribofilm is more durable due to its more favorable formation energy. Additionally, the higher wear rate of the softer molybdenum contributes to more wear particles that could potentially form TMD layers with selenium [11]. Another point to consider is that tellurides have been reported to exhibit lower thermal and oxidation stability compared to sulfides and selenides, which suggests they oxidize more quickly. This rapid oxidation could be a contributing factor to the difficulties encountered in synthesizing them witht he proposed in operando method [123, 124].

However, even if a TMD layer of WTe_2 would form, its COF is reported to be relatively high at 0.49 [125], which is thought to be related to its orthorhombic crystal structure [126]. This confirms that no successful formation occurred in our experiments, as we did not observe those high friction values.

4.4 Analysis of $MoSe_2$ and WSe_2 Results

With all tests completed and analyzed, the average friction values including their respective standard deviation as error bars for the last 100 cycles of the 750 cycle tests are presented and compared in a detailed overview in Figure 4.11. The COF across different experiments is plotted against the oxygen (O_2) concentration levels, which are 20.9 %, 10 %, and <0.1 %. To enhance visibility and ensure clarity when markers overlap, data points within the same oxygen concentration are slightly shifted left or right.

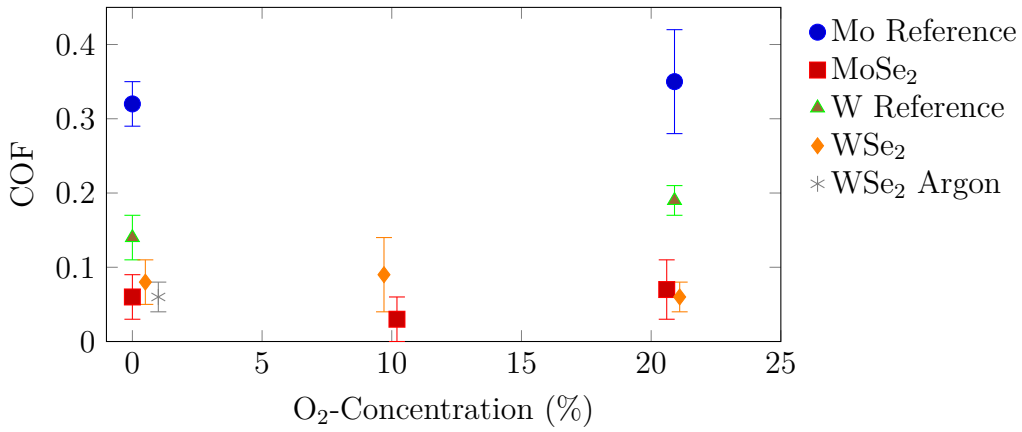

Figure 4.11: Comprehensive overview of the average COF values, along with their standard deviation, for the last 100 cycles of the 750-cycle tests; displayed according to the oxygen concentrations.

Die approbierte gedruckte Originalversion dieser Diplomarbeit ist an der TU Wien Bibliothek verfügbar
The approved original version of this thesis is available in print at TU Wien Bibliothek.
TU Bibliothek Your knowledge hub WIEN

This comparison illustrates the significant lower COF values of the experiments when Se powder was added, compared to reference measurements. The COF values ranged between 0.03 to 0.07 for experiments using a molybdenum substrate with added Se powder, and between 0.06 to 0.09 for those using a tungsten substrate with added Se powder. These ranges indicated the formation of TMD layers, which are known to exhibit such low friction coefficients. Additionally, the minimal difference in friction values between the two types of TMDs layers aligned with reports from Chakrapani [17].

In further analysis, Figure 4.12 presents the average number of revolutions required to reach the COF threshold of 0.2 for each extended test. A clear trend was observed, showing an increase in the number of cycles needed to reach the COF threshold as the oxygen concentration decreased. Specifically, for molybdenum in atmospheric air, the average cycles before failure was 6000, which rose to 8240 cycles in 10 % oxygen, and further to 19 800 cycles in a nitrogen atmosphere. Tungsten, on the other hand, showed a quicker degradation rate, failing after 3550 cycles in air, 5900 cycles in 10 % oxygen, 9150 cycles in nitrogen, and 13 500 cycles in argon.

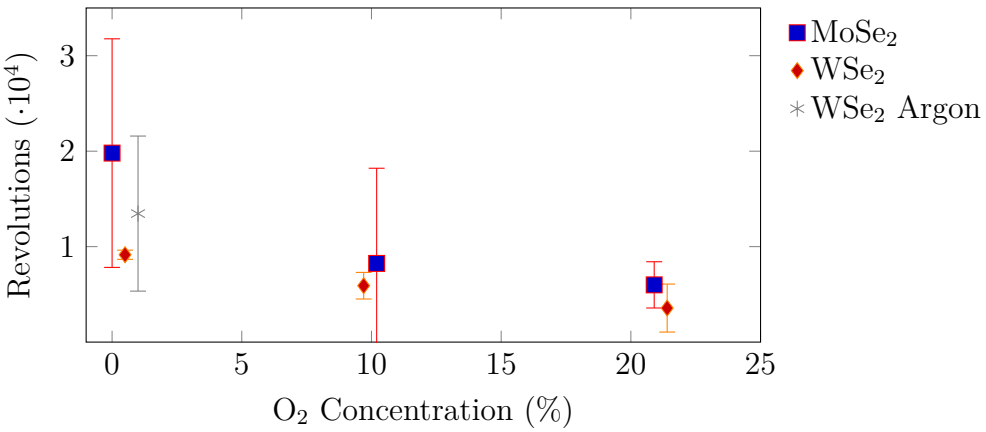

Figure 4.12: Graphical illustration showing the average number of revolutions required to reach a COF of 0.2 in each extended test, plotted against oxygen concentration levels and including the standard deviation.

Although the error bars for the results of molybdenum overlap due to a high variance, the deviation between nitrogen and air atmospheres towards higher cycle counts in environments with less oxygen is particularly notable. Nonetheless, the experiments with tungsten showed reduced variance and a separation between the error bars for air and nitrogen atmospheres, indicating a significant difference. This pattern, suggesting that reduced oxygen levels extend the durability of TMDs, aligned with findings reported in other studies [118].

Die approbierte gedruckte Originalversion dieser Diplomarbeit ist an der TU Wien Bibliothek verfügbar
The approved original version of this thesis is available in print at TU Wien Bibliothek.
TU Bibliothek Your knowledge hub WIEN

It is crucial to note that the experiments conducted in a nitrogen atmosphere contained approximately 8 % humidity, indicating that it was not a purely dry nitrogen environment. Consequently, enough water molecules and oxygen atoms were present, potentially leading to the degradation of the TMD layers. For more accurate analysis and reliable results, it is recommended to use a more sophisticated inert gas chamber that was not available for our experiments and is first evacuated and then filled with dry nitrogen or a noble gas, such as argon. This approach would ensure a high purity atmosphere without oxygen, enabling a more precise test setup [120].

4.5 TEM Analysis of the Tribofilm

The TEM analysis was conducted on the 750-cycle nitrogen Mo and W samples with added Se powder. This analysis aimed to investigate the characteristics of the tribofilm, including its formation, thickness, and elemental composition.

4.5.1 TEM and STEM Images of the Tribofilm

Images of Molybdenum Sample

Using the STEM mode enabled the detailed visualization of the layered structure of the $MoSe_2$ specimen, as depicted in Figure 4.13a. With the tools of DigitalMicrograph by Gatan Inc., the PVD Mo coating could be precisely measured to be 2.44 μm thick. Moreover, Figure 4.13b illustrates the selected trajectory for the EDX line profile analysis across the tribofilm. The results from this analysis are elaborated in Section 4.5.2.

Die approbierte gedruckte Originalversion dieser Diplomarbeit ist an der TU Wien Bibliothek verfügbar
The approved original version of this thesis is available in print at TU Wien Bibliothek.
TU Bibliothek Your knowledge hub WIEN

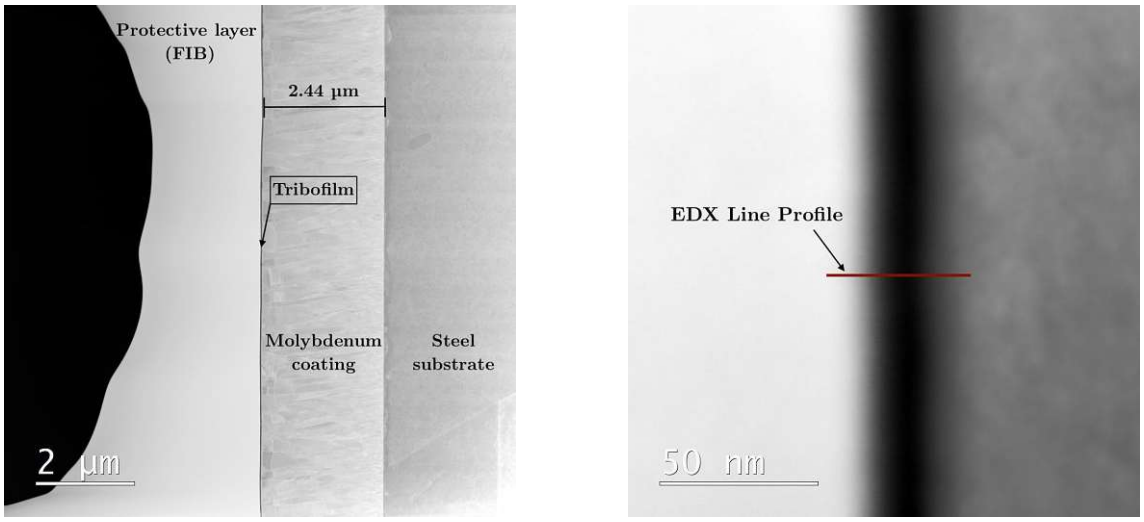

(a) (b)

Figure 4.13: STEM image illustrating a) the layers of the Mo specimen including the steel substrate, PVD coating, tribofilm, and the protective layer and (b) the EDX line measurement location across the tribofilm.

Figure 4.14a shows the tribofilm and its thickness of approximately 17.4 nm at this location. To the left of the tribofilm, the carbon protective layer was visible as a white section, with the tungsten protective layer situated even further to the left. On the right side of the tribofilm, the Mo coating was identified. The lattice structures and amorphous zones within this region were distinctly visible, exhibiting lattice spacings significantly smaller than those characteristic of $MoSe_2$ [11].

In this respect, Figure 4.14b provides a magnified view of the area depicted in Figure 4.14a. This close-up image facilitates the measurement of the interlayer distance, which was approximately 6.46 Å, closely aligning with the (0 0 2) planes of hexagonal $MoSe_2$ as described by Deng et al. [127].

Die approbierte gedruckte Originalversion dieser Diplomarbeit ist an der TU Wien Bibliothek verfügbar
The approved original version of this thesis is available in print at TU Wien Bibliothek.

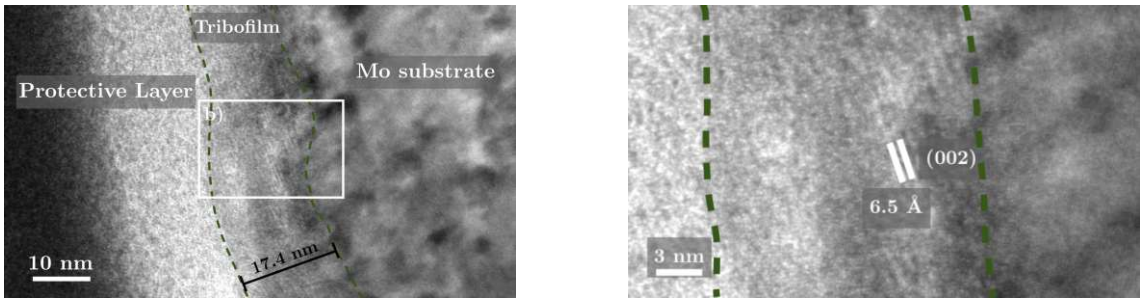

(a) (b)

Figure 4.14: TEM image of (a) tribofilm and its location on the Mo sustrate with a thickness of 17.4 nm and (b) a magnification into the tribofilm, highlighting the $MoSe_2$ layers with a lattice distance of 6.46 Å.

Images of Tungsten Sample

Figure 4.15a presents a detailed TEM view of the specimen's layered composition, which included the steel substrate, the tungsten coating with a thickness of 2.56 µm, the notably thin tribofilm, and the overlying protective layer. In addition, EDX spectroscopy was conducted to analyze the elemental composition across the tribofilm, with the specific line path highlighted in Figure 4.15b. The findings from this EDX analysis are comprehensively discussed in Section 4.5.2.

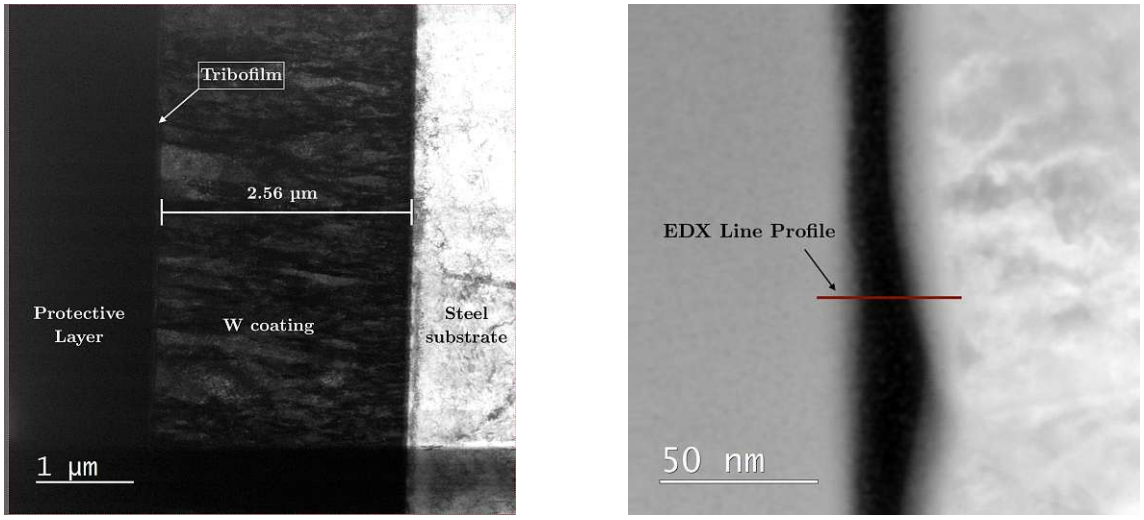

(a) (b)

Figure 4.15: TEM image illustrating a) the layers of the W specimen including the steel substrate, PVD coating, tribofilm, and the protective layer and (b) a STEM image of the EDX line measurement location across the tribofilm.

In Figure 4.16a, the tribofilm was identified and its thickness measured to 13 nm, confirming the findings of Grützmacher et al. [11] that the tribofilm containing

Die approbierte gedruckte Originalversion dieser Diplomarbeit ist an der TU Wien Bibliothek verfügbar
The approved original version of this thesis is available in print at TU Wien Bibliothek.
TU Bibliothek Your knowledge hub WIEN

WSe_2 layers was thinner than with $MoSe_2$ layers. The higher wear rate of the softer molybdenum metal results in more wear particles, that are essential for the formation of TMD layers with selenium, but also act as third body in the tribofilm, resulting in a thicker tribofilm compared to tungsten [11].Similar to the molybdenum sample, the carbon and tungsten protective layer was positioned to the left of the tribofilm and the tungsten coating to its right.

Further detail is provided in the magnified view of Figure 4.16b, which focused on the interlayer spacing within the tungsten sample. The measured distance was 6.8 Å, closely aligning with the (0 0 2) planes of hexagonal WSe_2, as documented by Li et al. [128].

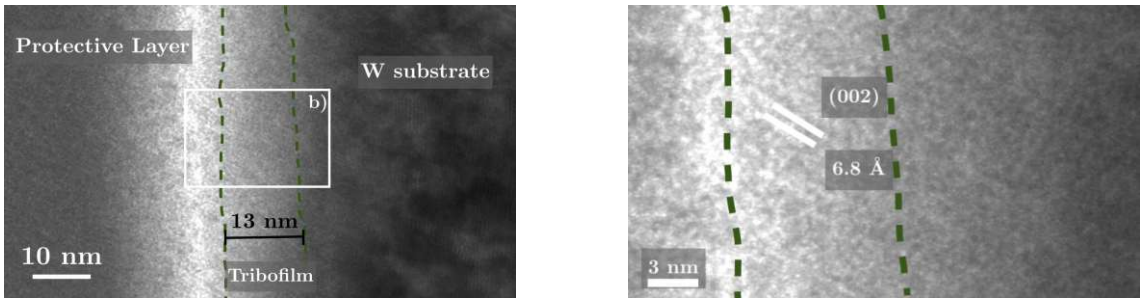

(a) (b)

Figure 4.16: TEM image of (a) tribofilm and its location on the W sustrate with a thickness of 13 nm and (b) a magnification into the tribofilm, highlighting the WSe_2 layers with a lattice distance of 6.8 Å.

4.5.2 Energy Dispersive X-Ray Spectroscopy

The TEM was equipped with an EDX spectrometer, so we investigated the tribofilm of both samples, to gain qualitative information about the elemental composition, distribution and concentration.

EDX Analysis on Molybdenum

The elemental composition along the analyzed line profile on the molybdenum sample is depicted in Figure 4.17. Tungsten was predominantly detected on the left due to its use as a protective layer. Subsequently, there was a notable increase in selenium levels at around the 15 nm mark, where the tribofilm was situated and at about 25 nm molybdenum levels rose significantly. This suggested the coexistence of these elements in a confined area. The analysis confirmed that there is little oxygen within the examined sample, which could be attributed to the metal oxides and oxidized TMD layers.

Die approbierte gedruckte Originalversion dieser Diplomarbeit ist an der TU Wien Bibliothek verfügbar
The approved original version of this thesis is available in print at TU Wien Bibliothek.
TU Bibliothek Your knowledge hub WIEN

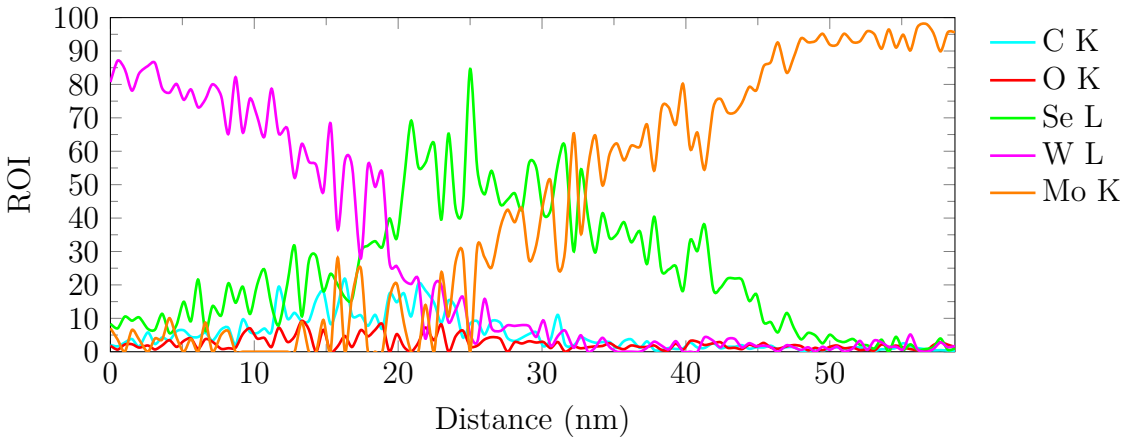

Figure 4.17: ROI values of the EDX line scan across the tribofilm of the molybdenum sample.

Figure 4.18 presents a color-coded visualization of the EDX line profile, emphasizing the transition from tungsten (violet) through carbon (blue) to selenium (green) and molybdenum (orange), effectively illustrating the elemental composition along the profile. Although low, oxygen was present along the whole profile, indicating oxidation.

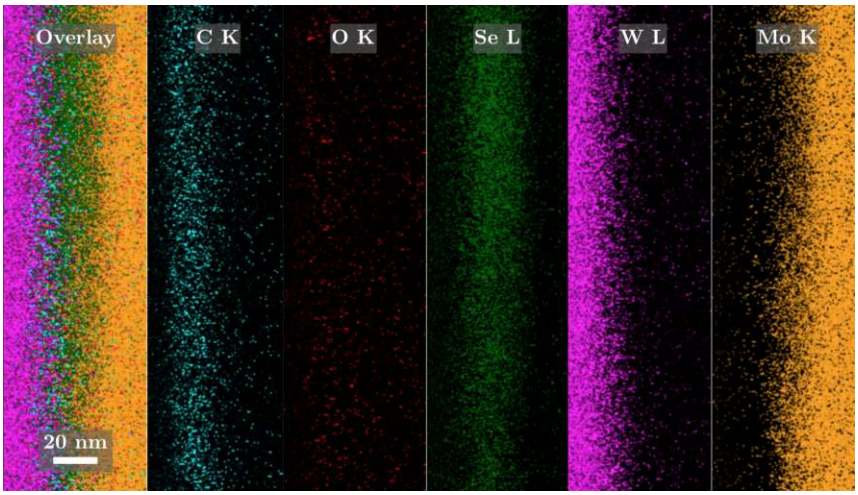

Figure 4.18: Illustration with color coding showing the elemental distribution from the molybdenum EDX analysis, including carbon (blue), oxygen (red), selenium (green), and tungsten (magenta), presented both individually and in an overlay.

EDX Analysis on Tungsten

Figure 4.19 illustrates the elemental distribution along the EDX line scan on the tungsten specimen. Similar to results of the molybdenum sample, the spectrometer detected the tungsten and carbon protective layers on the left, then selenium at

Die approbierte gedruckte Originalversion dieser Diplomarbeit ist an der TU Wien Bibliothek verfügbar
The approved original version of this thesis is available in print at TU Wien Bibliothek.

approximately 30 nm, beyond which the presence of the tungsten coating became predominant. Again, the presence of oxygen indicated the existence of metal oxides and possibly oxidized TMDs.

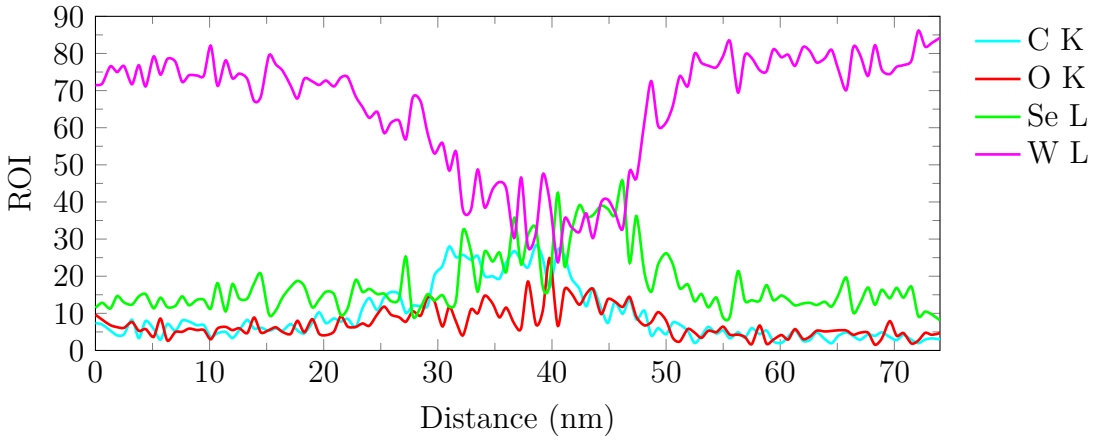

Figure 4.19: ROI values of the EDX line scan across the tribofilm of the tungsten sample.

Figure 4.20 provides a color-coded depiction of the elements near the tribofilm. The overlay highlights the sequence from tungsten (violet) though carbon (blue), then to selenium (green), and back to tungsten (violet). Additionally, an increased presence of oxygen was detectable along the tribofilm, suggesting that the TMD or tungsten coating was partly oxidizing.

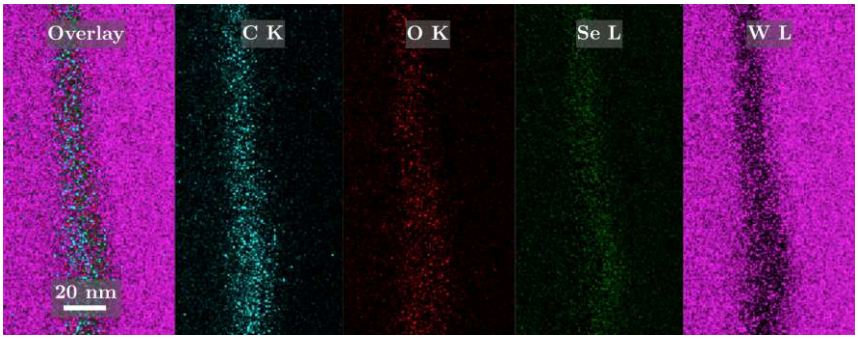

Figure 4.20: Illustration with color coding showing the elemental distribution from the tungsten EDX analysis, including carbon (blue), oxygen (red), selenium (green), and tungsten (magenta), presented both individually and in an overlay.

4.6 Raman Spectroscopy

To characterize the tribofilm further, Raman spectroscopy was performed at the Centre for Electrochemical Surface Technology (CEST) in Wiener Neustadt using a Micro-Raman spectrometer LabRam ARAMIS-UV Vis from Horiba Yvon. This

Die approbierte gedruckte Originalversion dieser Diplomarbeit ist an der TU Wien Bibliothek verfügbar
The approved original version of this thesis is available in print at TU Wien Bibliothek.

analysis utilized green light at a wavelength of 532 nm, with each measurement lasting 75 seconds and conducted three times to minimize background noise. A 50x optical magnification was applied in all instances to enhance the accuracy of the measurements. For both molybdenum and tungsten samples tested under nitrogen, measurements were taken directly on the wear track and on an area next to the tribofilm for reference, as illustrated in Figure 4.21a and 4.21c. Similarly, the molybdenum and tungsten samples exposed to air were analyzed on the wear track, shown in Figure 4.21b and 4.21d. In these images, the tribofilm could be distinctly seen, displaying a bluish, rainbow-like color where the measurements were specifically taken.

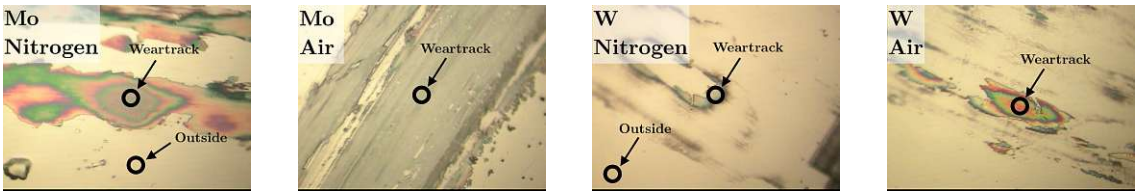

(a) (b) (c) (d)

Figure 4.21: Optical images of the locations for the Raman spectroscopy on the molybdenum test under (a) nitrogen and (b) air, and on the tungsten test under (c) nitrogen and (d) air.

The results are presented in Figure 4.22, where the Raman shift in cm^{-1} is plotted against the intensity, with each line adjusted vertically for clarity. The raw data was processed using the Asymmetric Least Squares (ALS) method [129], resulting in smoother and more accurate visual representations. Drawing on the research of Grützmacher et al. [11], we identified the same peaks of $MoSe_2$ (star), MoO_2 (circle), and MoO_3 (diamond) for both molybdenum samples, in nitrogen (blue line) and air (green line) atmosphere, within the tribofilms. Notably, a distinct peak at 242 cm^{-1} signaled the presence of $MoSe_2$ and MoO_3, aligning closely with literature values found at 240 cm^{-1} [130] and 247 cm^{-1} [131], respectively. The intensity of these peaks is higher in the nitrogen sample, which could be attributed to a high laser power that damages the tribofilm. Overly high power can even lead to the formation of diamond-like carbon, as demonstrated by Li et al. [132]. Additionally, the presence of these compounds was again observed at 290 cm^{-1}, matching reported values of 287 cm^{-1} [130] and 292 cm^{-1} [131]. For both MoO_2 and MoO_3, peaks were identified at 460 cm^{-1}, with MoO_2 also appearing at 591 cm^{-1} and MoO3 at 150 cm^{-1}, as verified against existing studies [131, 133, 134]. On the reference measurement nothing was detected.

Die approbierte gedruckte Originalversion dieser Diplomarbeit ist an der TU Wien Bibliothek verfügbar
The approved original version of this thesis is available in print at TU Wien Bibliothek.
TU Bibliothek Your knowledge hub WIEN

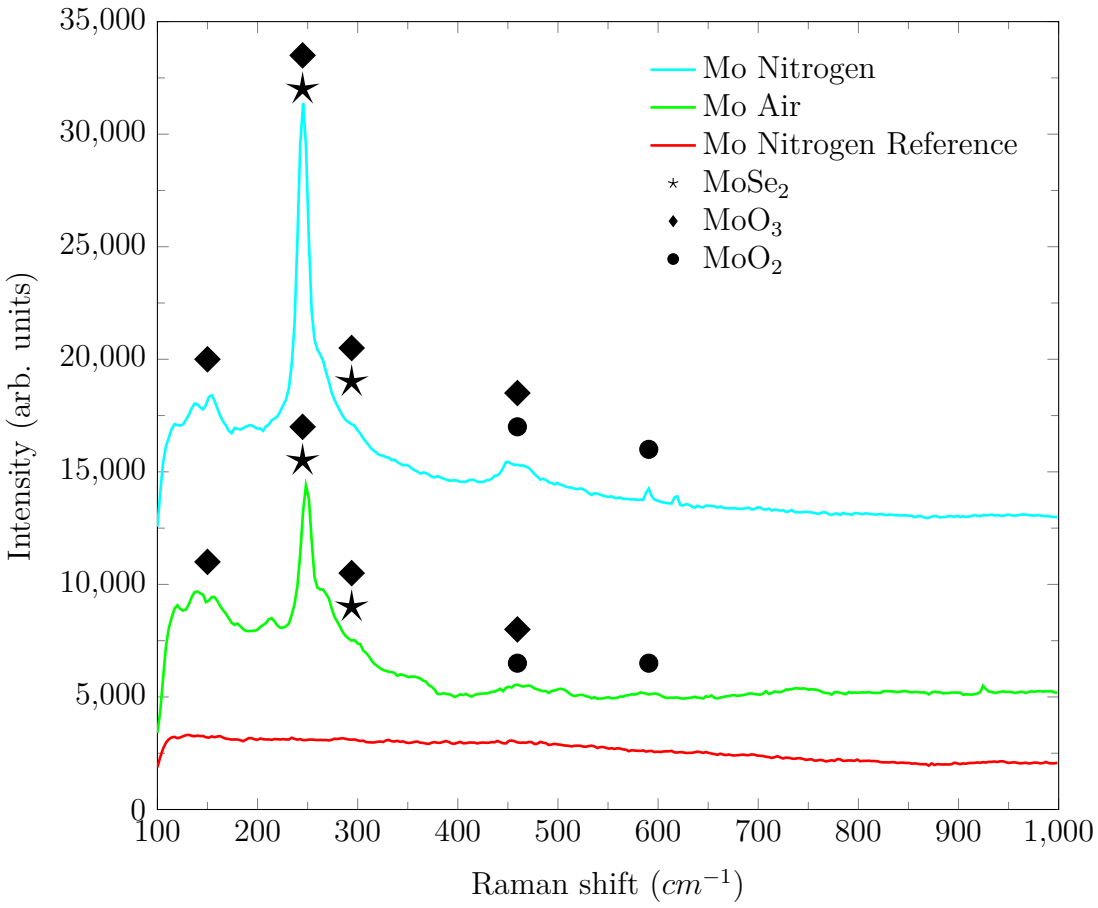

Figure 4.22: Raman spectra displaying characteristic peaks of metal oxides and $MoSe_2$ on a molybdenum sample, evidencing the effects of mechanical stress on the tribofilm. Reference measurements are also included for comparison.

Die approbierte gedruckte Originalversion dieser Diplomarbeit ist an der TU Wien Bibliothek verfügbar
The approved original version of this thesis is available in print at TU Wien Bibliothek.

The Raman spectroscopy findings for the tungsten samples, illustrated in Figure 4.23, revealed almost the same peaks for both investigated samples. There were two peaks attributable to WSe_2 (star) at 250 cm^{-1} and 525 cm^{-1}, consistent with literature references. However, WSe_2 is reported to be detectable at both 250 cm^{-1} and 260 cm^{-1}, indicating a possible overlap [11, 130]. This peak is more pronounced for the sample under nitrogen, similar to the molybdenum sample, possibly due to the use of high laser power. WO_3 (diamond) was detected at 134 cm^{-1} and 260 cm^{-1} under nitrogen and air conditions, overlapping with the WSe_2 peak. An additional minor peak is potentially linked to WO_3 at 390 cm^{-1} in air atmosphere [135, 136]. The reference measurements did not show any peaks for a substance. These observations aligned with those of Grützmacher et al. [11], affirming the formation of $MoSe_2$ and WSe_2.

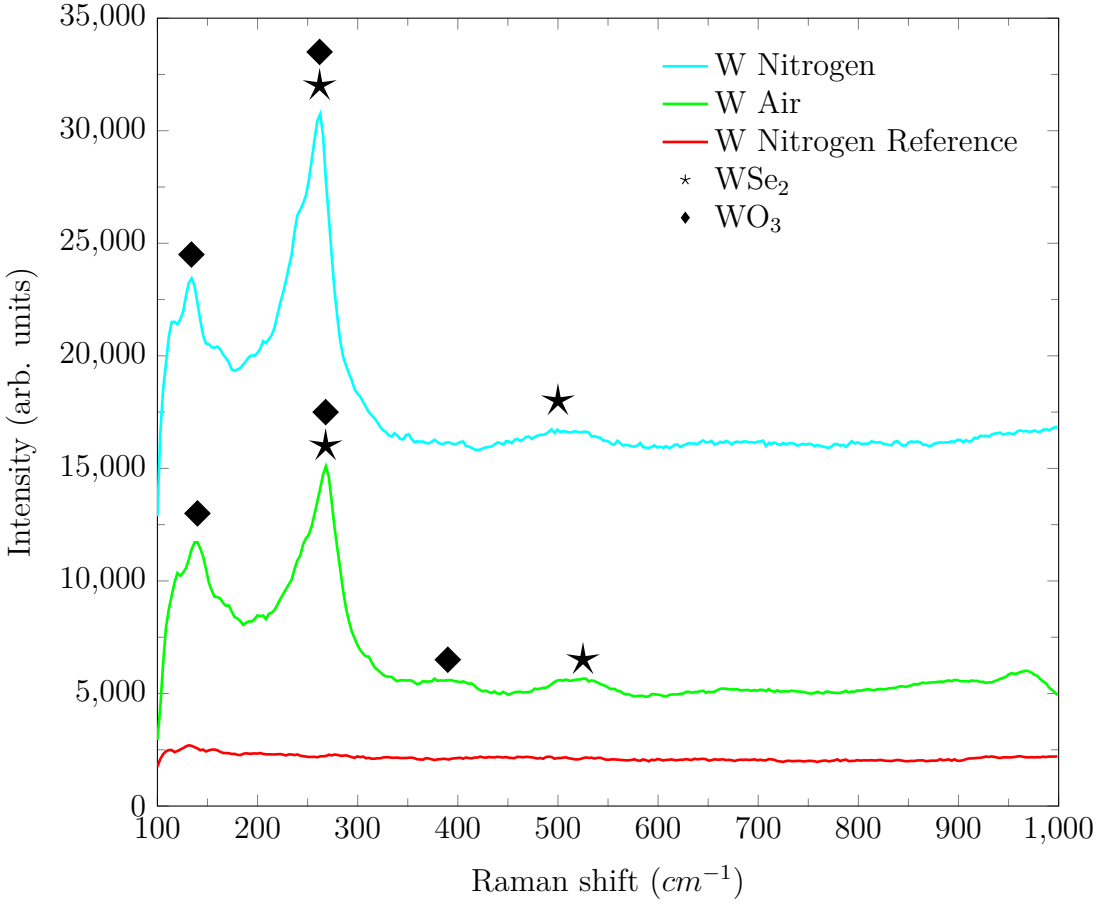

Figure 4.23: Raman spectra displaying characteristic peaks of metal oxides and WSe_2 on a tungsten sample, evidencing the effects of mechanical stress on the tribofilm. Reference measurements are also included for comparison.

Die approbierte gedruckte Originalversion dieser Diplomarbeit ist an der TU Wien Bibliothek verfügbar
The approved original version of this thesis is available in print at TU Wien Bibliothek.
TU Bibliothek Your knowledge hub WIEN

4.7 Tribological Investigation of the Wear Scar

After the detailed investigation into the elemental composition of the tribofilm, we analyzed the wear tracks using the VK-X1000 laser scanning microscope by Keyence. This tool enabled precise measurements of the tracks' width, length, roughness, and depth. Building on the findings of Grützmacher et al. [11], which highlighted the significant reduction in wear due to the tribochemical formation of TMD layers, this thesis further examines the influence of varying oxygen and humidity levels on TMD layer wear. Previous research, has documented that for MoS_2, the best studied alternative TMD lubricant, wear increases significantly under higher humidity and oxygen conditions [17, 20]. In contrast, $MoSe_2$ layers exhibit higher temperature stability and reduced sensitivity to humidity, despite a lower activation energy for oxidation compared to MoS_2. Notably, MoS_2 begins to oxidize at a lower temperature than $MoSe_2$. However, the specific effects of humidity on the oxidation of selenides, such as $MoSe_2$, require further investigation [137]. Although TMDs are generally resistant to oxidation when perfectly layered, the presence of defects in real-world applications makes them more susceptible to rapid oxidation [138].

4.7.1 Tribofilm Formation

After conducting the experiments, optical images of the wear scars on various samples were captured, which are illustrated in Figure 4.24 with 20x magnification. The images of the molybdenum samples subjected to 750 cycles in both air and nitrogen atmospheres (Figure 4.24a and 4.24b) revealed a distinctive bluish, rainbow-like glace indicative of the tribofilm. This coloration suggested a nearly continuous layer, signaling the successful formation of a tribofilm that incorporated third-body particles. Upon comparing these molybdenum samples, which exhibited a fully formed tribofilm, to those after failure (shown in Figure 4.24c and 4.24d), a difference was evident. After failure, the tribofilm became barely recognizable, with only isolated patches remaining visible in both environments. Similarly, the tungsten samples after 750 cycles demonstrated a tribofilm formation that was quite continuous, showing more interruptions than molybdenum samples across both atmospheres (Figure 4.24e and 4.24f). However, when the experiments were extended to the point of failure, the tribofilm significantly deteriorated, showing signs of delamination, and the wear grooves became more pronounced in both size and depth (Figure 4.24g and 4.24h). Figure 4.24i depicts the Al_2O_3 ball after 750 cycles in contact with the tungsten sample under a nitrogen atmosphere. Here, the wear scar was visible, yet its depth was minimal, and no adhesion of third body particles

Die approbierte gedruckte Originalversion dieser Diplomarbeit ist an der TU Wien Bibliothek verfügbar
The approved original version of this thesis is available in print at TU Wien Bibliothek.
TU Bibliothek Your knowledge hub WIEN

was noticeable, leading to the conclusion that abrasive wear was the dominant wear mechanism in this scenario.

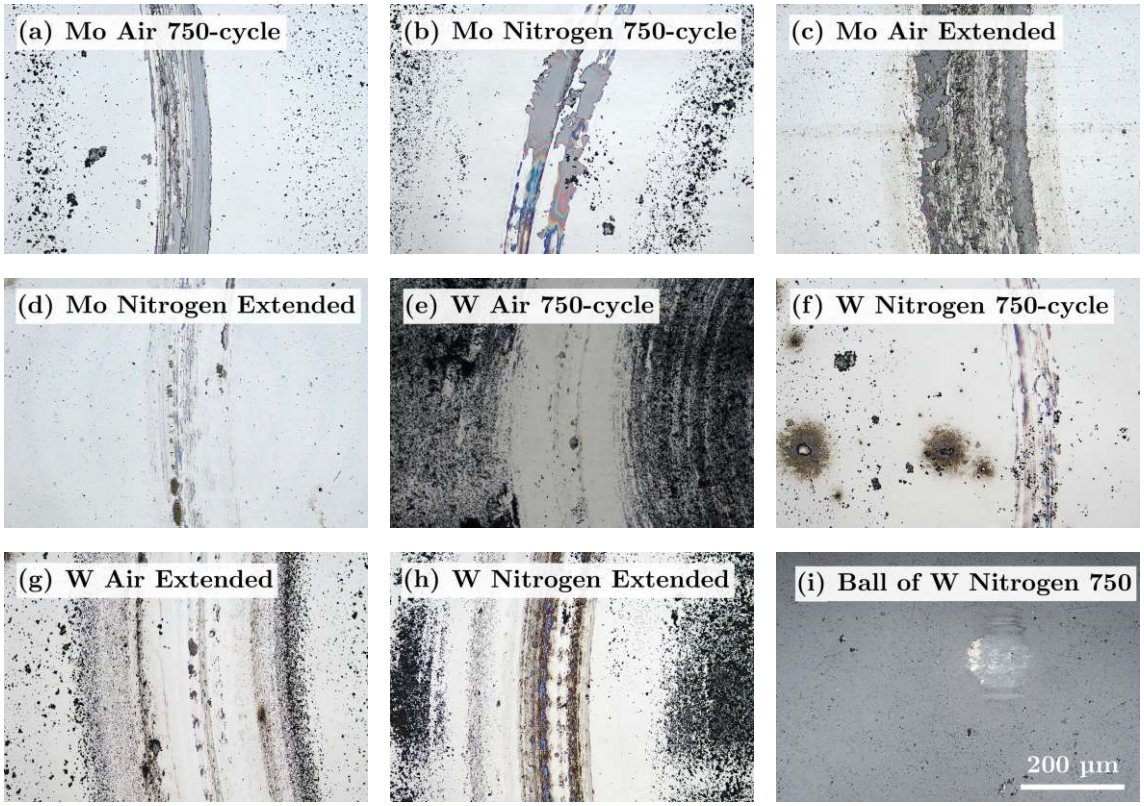

Figure 4.24: Optical images at 20x magnification showcasing the tribofilm on molybdenum samples: (a) exposed to air and (b) nitrogen atmosphere after 750 cycles, and once the COF exceeded 0.2 in (c) air and (d) nitrogen. For tungsten samples: images after 750 cycles in (e) air and (f) nitrogen atmosphere, and after the friction coefficient reached 0.2 in (g) air and (h) nitrogen atmosphere. Additionally, (i) illustrates the wear scar on the counterbody from the nitrogen atmosphere test with tungsten after 750 cycles.

4.7.2 Wear Scar Analysis

In a next step, the surface roughness using the S_z parameter was measured across the entire tribofilm of the CLSM image, which quantifies the height difference between the highest peak and the lowest valley within a specified area [139]. However, our analysis did not reveal any consistent trend in surface roughness under varying oxygen levels, as illustrated in Figure 4.25. Especially the values for the short tests are almost identical. The reference values for surface roughness were obtained next to to the tribofilm, on the unaffected plane surface. Consequently, an increase in surface roughness across all experimental conditions was observed. Despite giving a general tendency of surface texture, the S_z parameter is not reliable in all cases. For

Die approbierte gedruckte Originalversion dieser Diplomarbeit ist an der TU Wien Bibliothek verfügbar
The approved original version of this thesis is available in print at TU Wien Bibliothek.
TU Bibliothek Your knowledge hub WIEN

instance, a contaminant, an incidental particle, or a particularly deep scar within the area of measurement can easily alter the value of the surface roughness, underscoring the limitations of using S_z as the sole indicator of surface condition.

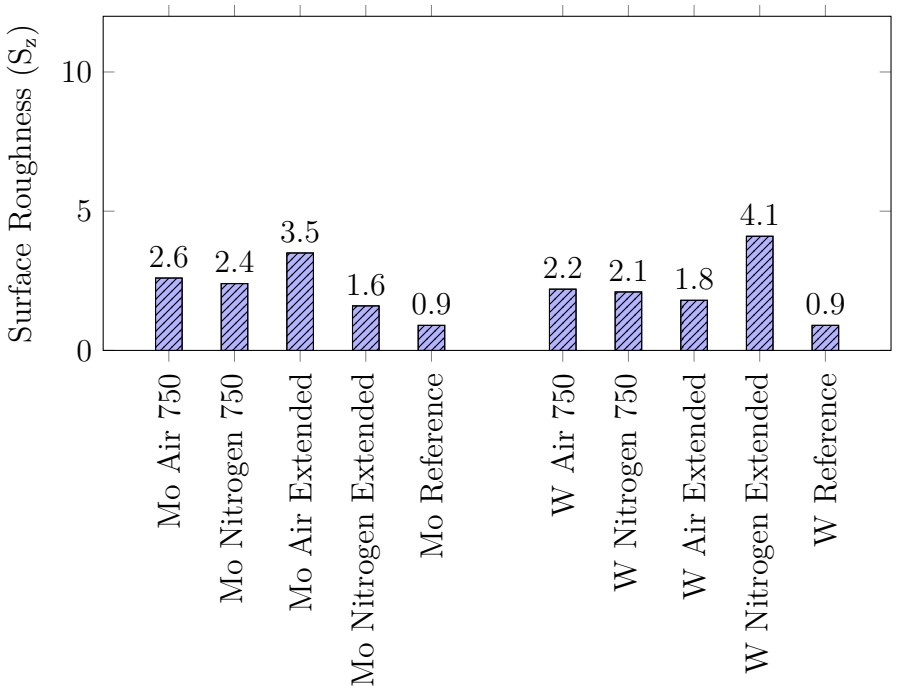

Figure 4.25: Surface Roughness (S_z) on the wear scar for each experiment under nitrogen and air including a reference measurement next to the tribofilm.

To gain a better understanding of the wear scars, detailed 3D images and their respective line profiles were acquired, as presented in Figure 4.26. Images on the molybdenum samples after 750 cycles in both air and nitrogen atmospheres (Figure 4.26a and 4.26b) show the formation of narrow valleys attributed to ploughing and abrasive wear. The accumulation of wear particles next to these valleys emphasized the abrasive nature of the wear process, although no significant differences in wear shape or size were observed between the two atmospheres. The wear profiles from the extended tests up to failure (Figure 4.26c and 4.26d) offer a similar observation, that the depth of wear in the nitrogen atmosphere have been notably deeper due to the longer duration of the tests. Nonetheless, the wear characteristics between atmospheres remained consistent.

Die approbierte gedruckte Originalversion dieser Diplomarbeit ist an der TU Wien Bibliothek verfügbar
The approved original version of this thesis is available in print at TU Wien Bibliothek.
TU Bibliothek Your knowledge hub WIEN

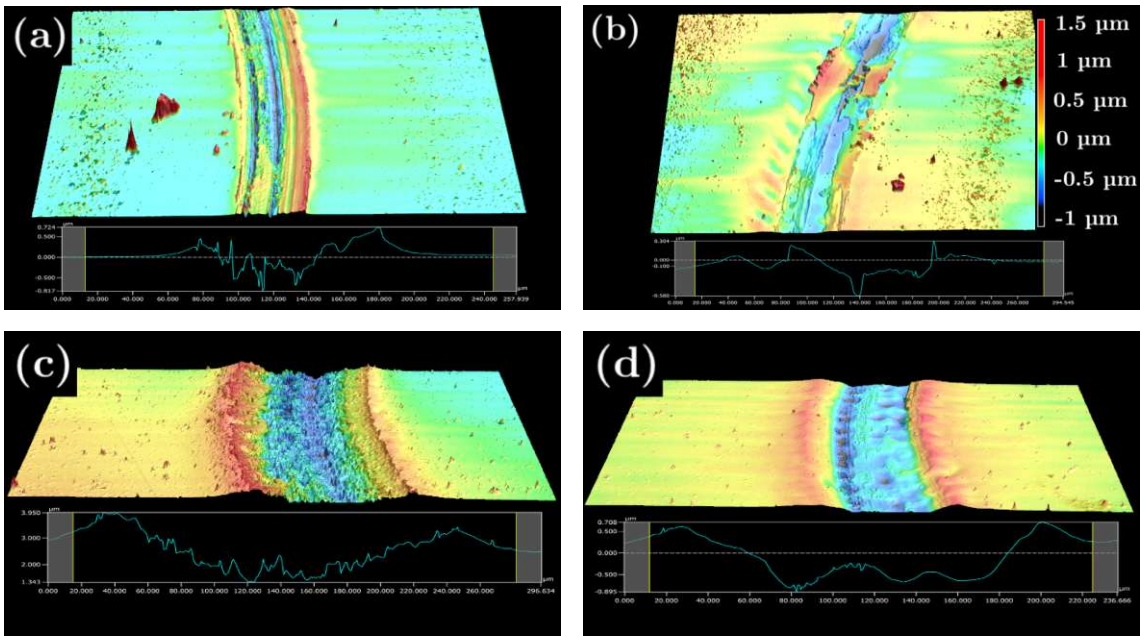

Figure 4.26: Molybdenum 3D profiles and its profile across the tribofilm: (a) exposed to air and (b) nitrogen atmosphere after 750 cycles, and once the COF exceeded 0.2 in (c) air and (d) nitrogen.

Moreover, the tungsten samples, shown in Figure 4.27, did not show noticeable differences in groove shape or size across atmospheric conditions, but demonstrating lower wear than molybdenum. The Young's modulus for both TMD layers was reported to be around 170 GPa [140, 141], thus this difference was attributed to tungsten's higher hardness, reduced contact conformity, smaller contact area, and lower friction [11].

Die approbierte gedruckte Originalversion dieser Diplomarbeit ist an der TU Wien Bibliothek verfügbar
The approved original version of this thesis is available in print at TU Wien Bibliothek.

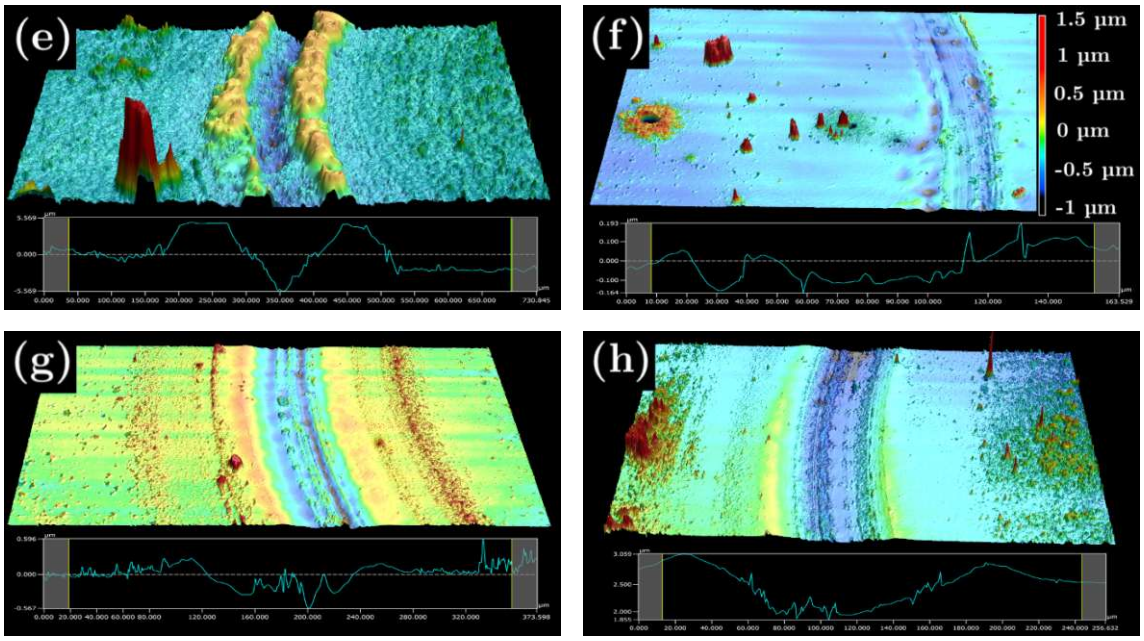

Figure 4.27: Tungsten 3D profiles and its profile across the tribofilm: Profile after 750 cycles in (a) air and (b) nitrogen atmosphere, and after the friction coefficient reached 0.2 in (c) air and (d) nitrogen atmosphere.

According to Fischer-Cripps [34], to avoid the influence of a substrate on coating measurements, such as those for our PVD-coated samples, the penetration depth during testing must not exceed 10 % of the coating's thickness. The extended test on the molybdenum sample in a nitrogen atmosphere resulted in a wear-induced valley with a depth of up to $-1.005\,\mu$m, thus reducing the effective coating thickness to about 1.44 µm. Given that the calculated penetration depth of $0.179\,\mu$m surpassed 10 % of the coating's thickness, it implies the steel substrate could have potentially affected the measurements in the latter stages. Despite this, observations from Section 4.1.3 did not explicitly show such influence. Future research should consider employing thicker coatings, especially in conditions expected to prolong wear resistance, such as vacuum, to avoid the potential influence of the steel substrate on the accuracy of the measurement. To quantify the wear experienced in different experiments, wear rates were calculated for the 750-cycle experiments, as they are most comparable. Table 4.1 lists the wear rates for an exemplary sample from each short experiment.

Die approbierte gedruckte Originalversion dieser Diplomarbeit ist an der TU Wien Bibliothek verfügbar
The approved original version of this thesis is available in print at TU Wien Bibliothek.
TU Bibliothek Your knowledge hub WIEN

Table 4.1: Average wear rates for the 750-cycle experiments under air and nitrogen atmosphere.

Experiment	Cross section	Wear vol.	Distance	Wear rate
Molybdenum Air	8.9×10^{-6}	9.8×10^{-5}	8.3	1.2×10^{-5}
Molybdenum Nitrogen	2.8×10^{-5}	3.1×10^{-4}	8.3	3.7×10^{-5}
Tungsten Air	2.1×10^{-6}	2.3×10^{-5}	8.3	2.8×10^{-6}
Tungsten Nitrogen	5.6×10^{-6}	6.1×10^{-5}	8.3	7.4×10^{-6}

It was observed that the wear rates for molybdenum samples were higher by approximately an order of magnitude than those for tungsten, attributed to the higher hardness of tungsten resulting in reduced wear. These findings were consistent with the research reported by Grützmacher et al. [11]. For additional clarification, Figure 4.28 illustrates the average COF versus the specific wear rate from the 750-cycle tests. Note that the x-axis is presented on a logarithmic scale. For comparison, the results from Grützmacher et al. [11], that were conducted in an air atmosphere, are included. However, the error bars in these reference values are absent, as they were not provided in their study.

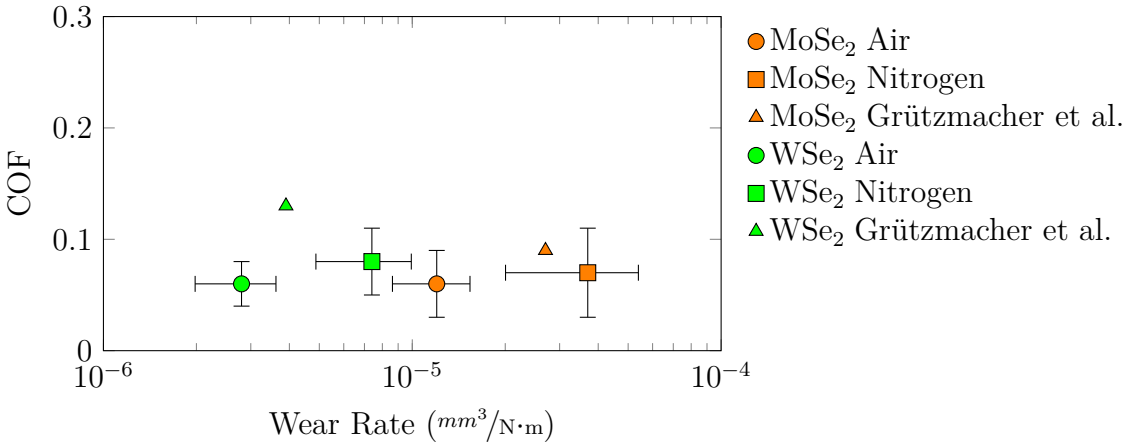

Figure 4.28: Graphical illustration showing the average COF versus the specific wear rate from the 750-cycle experiments including the respective standard deviation and the wear rates from the study of Grützmacher et al. [11] as reference. Note the logarithmic scale on the x-axis.

The reference values of 2.7×10^{-5} mm^3/N·m and 3.9×10^{-6} mm^3/N·m for Mo and W respectively, fall between the results of our study. Interestingly, the wear rate for the molybdenum sample in a nitrogen atmosphere was found to be nearly three times higher than that in an air atmosphere, a result that was not supported by existing literature. According to Kubart et al. [19], the wear rate of $MoSe_2$ is independent of humidity levels, and similarly, Gustavsson et al. [137] observed no significant difference in wear rates between dry nitrogen and humid air atmospheres. This dis-

Die approbierte gedruckte Originalversion dieser Diplomarbeit ist an der TU Wien Bibliothek verfügbar
The approved original version of this thesis is available in print at TU Wien Bibliothek.
TU Bibliothek Your knowledge hub WIEN

crepancy might be explained by the specific locations where the measurements were taken. Additionally, the wear rate for WSe_2 appeared also higher in nitrogen than in air, a finding that also contradicted other reports, as Domínguez-Meister et al. [20] noted no considerable difference in the wear rates of WSe_2 between air and nitrogen atmospheres. Furthermore, literature such as [111] reported that the friction and wear behavior of selenides are not significantly affected by humidity levels, suggesting that other factors may have contributed to these observed discrepancies in wear rates. Nonetheless, the wear rate values of the nitrogen samples showed a significant decrease of about an order of magnitude compared to the reference measurements without the addition of selenium powder conducted by Grützmacher et al. [11].

Die approbierte gedruckte Originalversion dieser Diplomarbeit ist an der TU Wien Bibliothek verfügbar
The approved original version of this thesis is available in print at TU Wien Bibliothek.
TU Bibliothek Your knowledge hub WIEN

5 Conclusion and Outlook

This thesis aimed to explore how oxygen and humidity levels affect the tribological properties of molybdenum and tungsten diselenides, specifically when these compounds are generated through an in operando method. Building upon the research of Grützmacher et al. [11], this study used ball-on-disc tribometer tests across various oxygen and humidity environments: ambient air (20.9 % oxygen), a 10 % oxygen atmosphere, and atmospheres with <0.1 % oxygen achieved using nitrogen and argon gas. To facilitate these experiments, a custom inert gas chamber was designed and constructed, enabling precise control over the atmospheric conditions during the tribometer tests. The experiments involved sprinkling selenium powder onto arc evaporated molybdenum and tungsten coatings on a steel substrate. The subsequent frictional energy induced the tribochemical formation of $MoSe_2$ and WSe_2 layers, respectively, leading to a significant reduction in both friction and wear.

Interestingly, the oxygen and humidity levels did not significantly affect the COF, as similar values were recorded across all tested atmospheres. However, the wear rate varied with atmospheric conditions, though the results were inconclusive and at times contradictory to existing literature. Specifically, molybdenum and tungsten showed higher wear rates in nitrogen than in an air atmosphere.

Notably, extended testing until the failure of the tribofilm revealed a significant impact of oxygen and humidity on the wear life of the tribofilm. This phenomenon is likely due to the rapid oxidation process of TMD layers, which slows down as oxygen and humidity levels decrease.

The characterization methods TEM, EDX, and Raman spectroscopy indicated the successful formation of the TMD layers that are incorporated in the tribofilm. Thus, this novel method poses a great approach for lubrication in extreme conditions where replenishment is of importance.

Drawing from this research, several key recommendations are proposed for future studies:

Die approbierte gedruckte Originalversion dieser Diplomarbeit ist an der TU Wien Bibliothek verfügbar
The approved original version of this thesis is available in print at TU Wien Bibliothek.
TU Bibliothek Your knowledge hub WIEN

- Development of a more advanced inert gas or vacuum chamber to achieve even lower oxygen and humidity levels, enhancing the understanding of the effect of oxidation on the TMD layer's wear life.
- Experiments with different applied loads to determine the activation energy required for the formation of TMD layers and understand their friction behavior. This should include different speeds and temperatures to determine the degradation and longevity of the TMD layers, providing a more comprehensive understanding of their performance under various environmental conditions.
- Improving the reproducibility of the experiments and refining the method for applying the selenium powder.
- Exploration of practical applications, converting these laboratory results into real-world tribological solutions.

Die approbierte gedruckte Originalversion dieser Diplomarbeit ist an der TU Wien Bibliothek verfügbar
The approved original version of this thesis is available in print at TU Wien Bibliothek.
TU Bibliothek Your knowledge hub WIEN

Bibliography

[1] Bharat Bhushan. *Modern tribology handbook. Vol. 1, Principles of tribology.* eng. Vol. 1. Mechanics and materials science series. OCLC: 628203674. Boca Raton: CRC Press, 2001. ISBN: 978-0-8493-8403-5.

[2] Qipeng Huang et al. 'Recent progress on surface texturing and solid lubricants in tribology: Designs, properties, and mechanisms'. In: *Materials Today Communications* 35 (June 2023), p. 105854. ISSN: 2352-4928. DOI: 10.1016/j.mtcomm.2023.105854. URL: https://www.sciencedirect.com/science/article/pii/S2352492823005457 (visited on 20/02/2024).

[3] Kenneth Holmberg and Ali Erdemir. 'Influence of tribology on global energy consumption, costs and emissions'. en. In: *Friction* 5.3 (Sept. 2017), pp. 263–284. ISSN: 2223-7690, 2223-7704. DOI: 10.1007/s40544-017-0183-5. URL: http://link.springer.com/10.1007/s40544-017-0183-5 (visited on 21/03/2024).

[4] Rahul Kumar et al. 'Solid Lubrication at High-Temperatures—A Review'. en. In: *Materials* 15.5 (Jan. 2022). Number: 5 Publisher: Multidisciplinary Digital Publishing Institute, p. 1695. ISSN: 1996-1944. DOI: 10.3390/ma15051695. URL: https://www.mdpi.com/1996-1944/15/5/1695 (visited on 20/02/2024).

[5] Moumita Sarkar and Nilrudra Mandal. 'Solid lubricant materials for high temperature application: A review'. In: *Materials Today: Proceedings*. Symposium on Failure and Preventive Maintenance of Machineries 2022 (FPMM 2022) 66 (Jan. 2022), pp. 3762–3768. ISSN: 2214-7853. DOI: 10.1016/j.matpr.2022.06.030. URL: https://www.sciencedirect.com/science/article/pii/S2214785322039633 (visited on 20/02/2024).

[6] Andreas Rosenkranz et al. 'Synergetic effects of surface texturing and solid lubricants to tailor friction and wear – A review'. In: *Tribology International* 155 (Mar. 2021), p. 106792. ISSN: 0301-679X. DOI: 10.1016/j.triboint.2020.106792. URL: https://www.sciencedirect.com/science/article/pii/S0301679X20306174 (visited on 20/02/2024).

[7] Bo Li et al. 'Microstructure, mechanical and tribological properties of NiAl matrix composites with addition of BaO/TiO2 binary oxides'. In: *Tribology*

Die approbierte gedruckte Originalversion dieser Diplomarbeit ist an der TU Wien Bibliothek verfügbar
The approved original version of this thesis is available in print at TU Wien Bibliothek.

International 144 (Apr. 2020), p. 106108. ISSN: 0301-679X. DOI: 10.1016/j.triboint.2019.106108. URL: https://www.sciencedirect.com/science/article/pii/S0301679X1930622X (visited on 21/02/2024).

[8] Jia-Hu Ouyang et al. 'High-Temperature Solid Lubricants and Self-Lubricating Composites: A Critical Review'. en. In: *Lubricants* 10.8 (Aug. 2022). Number: 8 Publisher: Multidisciplinary Digital Publishing Institute, p. 177. ISSN: 2075-4442. DOI: 10.3390/lubricants10080177. URL: https://www.mdpi.com/2075-4442/10/8/177 (visited on 20/02/2024).

[9] Changqing Miao et al. 'Recent Progress on the Tribological Applications of Solid Lubricants'. In: *Journal of Tribology* 146.020801 (Nov. 2023). ISSN: 0742-4787. DOI: 10.1115/1.4063701. URL: https://doi.org/10.1115/1.4063701 (visited on 20/02/2024).

[10] Yang Li, Zelong Zhou and Yongyong He. 'Solid Lubrication System and Its Plasma Surface Engineering: A Review'. en. In: *Lubricants* 11.11 (Nov. 2023). Number: 11 Publisher: Multidisciplinary Digital Publishing Institute, p. 473. ISSN: 2075-4442. DOI: 10.3390/lubricants11110473. URL: https://www.mdpi.com/2075-4442/11/11/473 (visited on 20/02/2024).

[11] Philipp G. Grützmacher et al. 'Se Nanopowder Conversion into Lubricious 2D Selenide Layers by Tribochemical Reactions'. en. In: *Advanced Materials* 35.42 (2023). _eprint: https://onlinelibrary.wiley.com/doi/pdf/10.1002/adma.202302076, p. 2302076. ISSN: 1521-4095. DOI: 10.1002/adma.202302076. URL: https://onlinelibrary.wiley.com/doi/abs/10.1002/adma.202302076 (visited on 19/10/2023).

[12] Anupama B. Kaul. 'Two-dimensional layered materials: Structure, properties, and prospects for device applications'. en. In: *Journal of Materials Research* 29.3 (Feb. 2014), pp. 348–361. ISSN: 2044-5326. DOI: 10.1557/jmr.2014.6. URL: https://doi.org/10.1557/jmr.2014.6 (visited on 18/01/2024).

[13] Holger Büch et al. 'Superlubricity of epitaxial monolayer WS2 on graphene'. en. In: *Nano Research* 11.11 (Nov. 2018), pp. 5946–5956. ISSN: 1998-0000. DOI: 10.1007/s12274-018-2108-7. URL: https://doi.org/10.1007/s12274-018-2108-7 (visited on 14/03/2024).

[14] Yu Kobayashi et al. 'Slidable atomic layers in van der Waals heterostructures'. en. In: *Applied Physics Express* 10.4 (Mar. 2017). Publisher: IOP Publishing, p. 045201. ISSN: 1882-0786. DOI: 10.7567/APEX.10.045201. URL: https://iopscience.iop.org/article/10.7567/APEX.10.045201/meta (visited on 14/03/2024).

[15] Shuai Zhang et al. 'Tribology of two-dimensional materials: From mechanisms to modulating strategies'. In: *Materials Today* 26 (June 2019), pp. 67–

Die approbierte gedruckte Originalversion dieser Diplomarbeit ist an der TU Wien Bibliothek verfügbar
The approved original version of this thesis is available in print at TU Wien Bibliothek.
TU Bibliothek Your knowledge hub WIEN

86. ISSN: 1369-7021. DOI: 10.1016/j.mattod.2018.12.002. URL: https://www.sciencedirect.com/science/article/pii/S1369702118309039 (visited on 11/01/2024).

[16] Sajedeh Manzeli et al. '2D transition metal dichalcogenides'. en. In: *Nature Reviews Materials* 2.8 (June 2017). Number: 8 Publisher: Nature Publishing Group, pp. 1–15. ISSN: 2058-8437. DOI: 10.1038/natrevmats.2017.33. URL: https://www.nature.com/articles/natrevmats201733 (visited on 08/01/2024).

[17] Vidhya Chakrapani. 'Correlative trends between tribological and electronic properties of dry lubricants: Influence of humidity and dopants'. In: *Tribology International* 177 (Jan. 2023), p. 107951. ISSN: 0301-679X. DOI: 10.1016/j.triboint.2022.107951. URL: https://www.sciencedirect.com/science/article/pii/S0301679X22005229 (visited on 22/02/2024).

[18] Mohammad R. Vazirisereshk et al. 'Nanoscale friction behavior of transition-metal dichalcogenides: Role of the chalcogenide'. English (US). In: *ACS Nano* 14.11 (Nov. 2020). Publisher: American Chemical Society, pp. 16013–16021. ISSN: 1936-0851. DOI: 10.1021/acsnano.0c07558. URL: https://researchwith.njit.edu/en/publications/nanoscale-friction-behavior-of-transition-metal-dichalcogenides-r (visited on 22/02/2024).

[19] T. Kubart et al. 'Temperature dependence of tribological properties of MoS2 and MoSe2 coatings'. In: *Surface and Coatings Technology*. Asian-European International Conference on Plasma Surface Engineering 2003 193.1 (Apr. 2005), pp. 230–233. ISSN: 0257-8972. DOI: 10.1016/j.surfcoat.2004.08.146. URL: https://www.sciencedirect.com/science/article/pii/S0257897204008205 (visited on 22/02/2024).

[20] Santiago Domínguez-Meister et al. 'Solid lubricant behavior of MoS2 and WSe2-based nanocomposite coatings'. In: *Science and Technology of Advanced Materials* 18.1 (Dec. 2017). Publisher: Taylor & Francis _eprint: https://doi.org/10.1080/14686996.2016.1275784, pp. 122–133. ISSN: 1468-6996. DOI: 10.1080/14686996.2016.1275784. URL: https://doi.org/10.1080/14686996.2016.1275784 (visited on 22/02/2024).

[21] B. Kohlhauser et al. 'How to get noWear? – A new take on the design of in-situ formed high performing low-friction tribofilms'. In: *Materials & Design* 190 (May 2020), p. 108519. ISSN: 0264-1275. DOI: 10.1016/j.matdes.2020.108519. URL: https://www.sciencedirect.com/science/article/pii/S0264127520300526 (visited on 30/03/2024).

[22] Bernhard Kohlhauser et al. 'Reactive in-situ formation and self-assembly of MoS2 nanoflakes in carbon tribofilms for low friction'. In: *Materials &*

Die approbierte gedruckte Originalversion dieser Diplomarbeit ist an der TU Wien Bibliothek verfügbar
The approved original version of this thesis is available in print at TU Wien Bibliothek.
TU Bibliothek Your knowledge hub WIEN

Design 199 (Feb. 2021), p. 109427. ISSN: 0264-1275. DOI: 10.1016/j.matdes.2020.109427. URL: https://www.sciencedirect.com/science/article/pii/S0264127520309631 (visited on 30/03/2024).

[23] Vladimir Totolin et al. 'Enhanced tribological performance of tungsten carbide functionalized surfaces via in-situ formation of low-friction tribofilms'. In: *Tribology International* 94 (Feb. 2016), pp. 269–278. ISSN: 0301-679X. DOI: 10.1016/j.triboint.2015.08.017. URL: https://www.sciencedirect.com/science/article/pii/S0301679X1500359X (visited on 30/03/2024).

[24] Diana Berman and Ali Erdemir. 'Achieving Ultralow Friction and Wear by Tribocatalysis: Enabled by In-Operando Formation of Nanocarbon Films'. In: *ACS Nano* 15.12 (Dec. 2021). Publisher: American Chemical Society, pp. 18865–18879. ISSN: 1936-0851. DOI: 10.1021/acsnano.1c08170. URL: https://doi.org/10.1021/acsnano.1c08170 (visited on 30/03/2024).

[25] G. Amontons. 'De la resistance cause'e dans les machines (About resistance and force in machines)'. In: Mem. l'Acedemie R. A, 1699, pp. 257–282.

[26] Charles Augustin Coulomb. *Théorie des machines simples, en ayant égard au frottement de leurs parties, et a la roideur des cordages: piece qui a remporté le prix double de l'Académie des sciences pour l'année 1781.* fr. Google-Books-ID: kmBozQEACAAJ. De l'Imprimerie Royale, 1785.

[27] Ian Hutchings and Philip Shipway. 'Tribology Friction and Wear of Engineering Materials'. en. In: *Tribology Friction and Wear of Engineering Materials*. 2nd. Butterworth-Heinemann, Jan. 2017, pp. i–ii. ISBN: 978-0-08-100910-9. DOI: 10.1016/B978-0-08-100910-9.09983-9. URL: https://www.sciencedirect.com/science/article/pii/B9780081009109099839 (visited on 12/07/2023).

[28] F. P. Bowden and D. Tabor. 'Mechanism of Metallic Friction'. en. In: *Nature* 150.3798 (Aug. 1942). Number: 3798 Publisher: Nature Publishing Group, pp. 197–199. ISSN: 1476-4687. DOI: 10.1038/150197a0. URL: https://www.nature.com/articles/150197a0 (visited on 05/03/2024).

[29] David Tabor. 'Friction—The Present State of Our Understanding'. In: *Journal of Lubrication Technology* 103.2 (Apr. 1981), pp. 169–179. ISSN: 0022-2305. DOI: 10.1115/1.3251622. URL: https://doi.org/10.1115/1.3251622 (visited on 06/03/2024).

[30] Koji Kato and Koshi Adachi. 'Wear mechanisms'. English. In: *Modern Tribology Handbook: Volume One: Principles of Tribology*. CRC Press, Jan. 2000, pp. 273–300. URL: https://tohoku.elsevierpure.com/en/publications/wear-mechanisms (visited on 06/03/2024).

[31] J. F. Archard. 'Contact and Rubbing of Flat Surfaces'. en. In: *Journal of Applied Physics* 24.8 (Aug. 1953), pp. 981–988. ISSN: 0021-8979, 1089-7550.

Die approbierte gedruckte Originalversion dieser Diplomarbeit ist an der TU Wien Bibliothek verfügbar
The approved original version of this thesis is available in print at TU Wien Bibliothek.
TU Bibliothek Your knowledge hub WIEN

doi: 10.1063/1.1721448. url: https://pubs.aip.org/jap/article/24/8/981/160178/Contact-and-Rubbing-of-Flat-Surfaces (visited on 04/04/2024).

[32] Horst Czichos and Karl-Heinz Habig, eds. *Tribologie-Handbuch: Tribometrie, Tribomaterialien, Tribotechnik*. de. Wiesbaden: Springer Fachmedien, 2020. isbn: 978-3-658-29484-7. doi: 10.1007/978-3-658-29484-7. url: http://link.springer.com/10.1007/978-3-658-29484-7 (visited on 11/07/2023).

[33] Heinrich Hertz. 'The contact of elastic solids'. In: *J Reine Angew, Math* 92 (1881), pp. 156–171. url: https://home.uni-leipzig.de/pwm/web/download/Hertz1881.pdf.

[34] Anthony C. Fischer-Cripps. *Nanoindentation*. en. Google-Books-ID: D23TpyBM_EcC. Springer Science & Business Media, Aug. 2011. isbn: 978-1-4419-9872-9.

[35] Kenneth C Ludema. *Friction, Wear, Lubrication: A Textbook in Tribology*. English. Vol. 1. Boca Raton: CRC Press, 1996. isbn: 978-0-8493-2685-1. url: https://www.lehmanns.de/shop/technik/184815-9780849326851-friction-wear-lubrication (visited on 11/07/2023).

[36] 'Engineering Tribology'. en. In: *Engineering Tribology (Fourth Edition)*. Ed. by Gwidon W. Stachowiak and Andrew W. Batchelor. Boston: Butterworth-Heinemann, Jan. 2013, p. i. isbn: 978-0-12-397047-3. doi: 10.1016/B978-0-12-397047-3.00018-7. url: https://www.sciencedirect.com/science/article/pii/B9780123970473000187 (visited on 12/07/2023).

[37] R. Stribeck. *Kugellager für beliebige Belastungen*. de. Google-Books-ID: zEbbMAAACAAJ. Springer, 1901.

[38] R. I. Taylor and I. Sherrington. 'A simplified approach to the prediction of mixed and boundary friction'. In: *Tribology International* 175 (Nov. 2022), p. 107836. issn: 0301-679X. doi: 10.1016/j.triboint.2022.107836. url: https://www.sciencedirect.com/science/article/pii/S0301679X2200408X (visited on 04/04/2024).

[39] B. J. Hamrock and D. Dowson. 'Isothermal Elastohydrodynamic Lubrication of Point Contacts: Part 1—Theoretical Formulation'. en. In: *Journal of Lubrication Technology* 98.2 (Apr. 1976), pp. 223–228. issn: 0022-2305. doi: 10.1115/1.3452801. url: https://asmedigitalcollection.asme.org/tribology/article/98/2/223/419780/Isothermal-Elastohydrodynamic-Lubrication-of-Point (visited on 01/03/2024).

[40] Meirong Cai et al. 'Ionic liquid lubricants: when chemistry meets tribology'. en. In: *Chemical Society Reviews* 49.21 (2020). Publisher: Royal Society of Chemistry, pp. 7753–7818. doi: 10.1039/D0CS00126K. url: https://pubs.rsc.org/en/content/articlelanding/2020/cs/d0cs00126k (visited on 02/03/2024).

Die approbierte gedruckte Originalversion dieser Diplomarbeit ist an der TU Wien Bibliothek verfügbar
The approved original version of this thesis is available in print at TU Wien Bibliothek.
TU Bibliothek Your knowledge hub WIEN

[41] Qiang Ma et al. 'Achieving macroscale liquid superlubricity using glycerol aqueous solutions'. In: *Tribology International* 160 (Aug. 2021), p. 107006. ISSN: 0301-679X. DOI: 10.1016/j.triboint.2021.107006. URL: https://www.sciencedirect.com/science/article/pii/S0301679X21001547 (visited on 02/03/2024).

[42] Md Hafizur Rahman et al. 'Water-Based Lubricants: Development, Properties, and Performances'. en. In: *Lubricants* 9.8 (Aug. 2021). Number: 8 Publisher: Multidisciplinary Digital Publishing Institute, p. 73. ISSN: 2075-4442. DOI: 10.3390/lubricants9080073. URL: https://www.mdpi.com/2075-4442/9/8/73 (visited on 02/03/2024).

[43] Wilfried Dresel. 'Lubricating Greases'. en. In: *Encyclopedia of Lubricants and Lubrication*. Ed. by Theo Mang. Berlin, Heidelberg: Springer Berlin Heidelberg, 2014, pp. 1076–1096. ISBN: 978-3-642-22647-2. DOI: 10.1007/978-3-642-22647-2_16. URL: http://link.springer.com/10.1007/978-3-642-22647-2_16 (visited on 31/03/2024).

[44] T. W. Scharf and S. V. Prasad. 'Solid lubricants: a review'. en. In: *Journal of Materials Science* 48.2 (Jan. 2013), pp. 511–531. ISSN: 1573-4803. DOI: 10.1007/s10853-012-7038-2. URL: https://doi.org/10.1007/s10853-012-7038-2 (visited on 04/03/2024).

[45] Donald H. Buckley. *Surface effects in adhesion, friction, wear, and lubrication*. Tribology series 5. Amsterdam ; New York : New York: Elsevier Scientific Pub. Co. ; Distributors for the U.S. and Canada, Elsevier North-Holland, 1981. ISBN: 978-0-444-41966-8.

[46] The Materials Project. *Materials Data on Se by Materials Project*. en. 2020. DOI: 10.17188/1189869. URL: https://www.osti.gov/servlets/purl/1189869/ (visited on 19/12/2023).

[47] Koichi Momma and Fujio Izumi. '*VESTA 3* for three-dimensional visualization of crystal, volumetric and morphology data'. In: *Journal of Applied Crystallography* 44.6 (Dec. 2011), pp. 1272–1276. ISSN: 0021-8898. DOI: 10.1107/S0021889811038970. URL: https://scripts.iucr.org/cgi-bin/paper?S0021889811038970 (visited on 03/04/2024).

[48] Chandan Kumar, Santanu Das and Satyabrata Jit. '7 - Device physics and device integration of two-dimensional heterostructures'. In: *2D Nanoscale Heterostructured Materials*. Ed. by Satyabrata Jit and Santanu Das. Micro and Nano Technologies. Elsevier, Jan. 2020, pp. 195–214. ISBN: 978-0-12-817678-8. DOI: 10.1016/B978-0-12-817678-8.00007-5. URL: https://www.sciencedirect.com/science/article/pii/B9780128176788000075 (visited on 05/04/2024).

Die approbierte gedruckte Originalversion dieser Diplomarbeit ist an der TU Wien Bibliothek verfügbar
The approved original version of this thesis is available in print at TU Wien Bibliothek.
TU Bibliothek Your knowledge hub WIEN

[49] Martin Dienwiebel et al. 'Superlubricity of Graphite'. en. In: *Physical Review Letters* 92.12 (Mar. 2004), p. 126101. ISSN: 0031-9007, 1079-7114. DOI: 10.1103/PhysRevLett.92.126101. URL: https://link.aps.org/doi/10.1103/PhysRevLett.92.126101 (visited on 03/04/2024).

[50] Yabing Qi et al. 'Electronic contribution to friction on GaAs: An atomic force microscope study'. In: *Physical Review B* 77.18 (May 2008). Publisher: American Physical Society, p. 184105. DOI: 10.1103/PhysRevB.77.184105. URL: https://link.aps.org/doi/10.1103/PhysRevB.77.184105 (visited on 05/03/2024).

[51] Jeong Young Park et al. 'Electronic Control of Friction in Silicon pn Junctions'. In: *Science* 313.5784 (July 2006). Publisher: American Association for the Advancement of Science, pp. 186–186. DOI: 10.1126/science.1125017. URL: https://www.science.org/doi/10.1126/science.1125017 (visited on 05/03/2024).

[52] Michael Naguib et al. 'Two-Dimensional Nanocrystals Produced by Exfoliation of Ti3AlC2'. In: *Advanced Materials* 23.37 (2011), pp. 4248–4253. ISSN: 1521-4095. DOI: 10.1002/adma.201102306. URL: https://onlinelibrary.wiley.com/doi/abs/10.1002/adma.201102306 (visited on 23/02/2024).

[53] Xiaonan Miao et al. 'MXenes in tribology: Current status and perspectives'. In: *Advanced Powder Materials* 2.2 (Apr. 2023), p. 100092. ISSN: 2772-834X. DOI: 10.1016/j.apmate.2022.100092. URL: https://www.sciencedirect.com/science/article/pii/S2772834X22000756 (visited on 20/02/2024).

[54] Kang Rui Garrick Lim et al. 'Fundamentals of MXene synthesis'. en. In: *Nature Synthesis* 1.8 (Aug. 2022). Number: 8 Publisher: Nature Publishing Group, pp. 601–614. ISSN: 2731-0582. DOI: 10.1038/s44160-022-00104-6. URL: https://www.nature.com/articles/s44160-022-00104-6 (visited on 26/02/2024).

[55] Philipp G. Grützmacher et al. 'Combining Tailored Ionic Liquids with Ti3C2Tx MXenes for an Enhanced Load-Carrying Capacity Under Boundary Lubrication'. en. In: *Advanced Engineering Materials* n/a.n/a (June 2023). _eprint: https://onlinelibrary.wiley.com/doi/pdf/10.1002/adem.202300721, p. 2300721. ISSN: 1527-2648. DOI: 10.1002/adem.202300721. URL: https://onlinelibrary.wiley.com/doi/abs/10.1002/adem.202300721 (visited on 23/02/2024).

[56] Philipp G. Grützmacher et al. 'Superior Wear-Resistance of Ti3C2Tx Multilayer Coatings'. In: *ACS Nano* 15.5 (May 2021). Publisher: American Chemical Society, pp. 8216–8224. ISSN: 1936-0851. DOI: 10.1021/acsnano.1c01555. URL: https://doi.org/10.1021/acsnano.1c01555 (visited on 23/02/2024).

Die approbierte gedruckte Originalversion dieser Diplomarbeit ist an der TU Wien Bibliothek verfügbar
The approved original version of this thesis is available in print at TU Wien Bibliothek.
TU Bibliothek Your knowledge hub WIEN

[57] A. Rodriguez et al. 'The potential of Ti3C2TX nano-sheets (MXenes) for nanoscale solid lubrication revealed by friction force microscopy'. In: *Applied Surface Science* 535 (Jan. 2021), p. 147664. ISSN: 0169-4332. DOI: 10.1016/j.apsusc.2020.147664. URL: https://www.sciencedirect.com/science/article/pii/S0169433220324211 (visited on 23/02/2024).

[58] Qingjuan Wang et al. 'Tribological behavior of black phosphorus nanosheets as water-based lubrication additives'. en. In: *Friction* 10.3 (Mar. 2022), pp. 374–387. ISSN: 2223-7704. DOI: 10.1007/s40544-020-0465-1. URL: https://doi.org/10.1007/s40544-020-0465-1 (visited on 23/02/2024).

[59] Gongbin Tang et al. '2D black phosphorus dotted with silver nanoparticles: An excellent lubricant additive for tribological applications'. In: *Chemical Engineering Journal* 392 (July 2020), p. 123631. ISSN: 1385-8947. DOI: 10.1016/j.cej.2019.123631. URL: https://www.sciencedirect.com/science/article/pii/S1385894719330463 (visited on 23/02/2024).

[60] Yu Yu Illarionov et al. 'Highly-stable black phosphorus field-effect transistors with low density of oxide traps'. en. In: *npj 2D Materials and Applications* 1.1 (July 2017). Number: 1 Publisher: Nature Publishing Group, pp. 1–7. ISSN: 2397-7132. DOI: 10.1038/s41699-017-0025-3. URL: https://www.nature.com/articles/s41699-017-0025-3 (visited on 26/02/2024).

[61] Shuangqing Fan et al. 'Black phosphorus-based nanohybrids for energy storage, catalysis, sensors, electronic/photonic devices, and tribological applications'. en. In: *Journal of Materials Chemistry C* 10.38 (Oct. 2022). Publisher: The Royal Society of Chemistry, pp. 14053–14079. ISSN: 2050-7534. DOI: 10.1039/D2TC02355E. URL: https://pubs.rsc.org/en/content/articlelanding/2022/tc/d2tc02355e (visited on 23/02/2024).

[62] Ahmad Majed et al. 'Transition Metal Carbo-Chalcogenide "TMCC:" A New Family of 2D Materials'. en. In: *Advanced Materials* 34.26 (2022). _eprint: https://onlinelibrary.wiley.com/doi/pdf/10.1002/adma.202200574, p. 2200574. ISSN: 1521-4095. DOI: 10.1002/adma.202200574. URL: https://onlinelibrary.wiley.com/doi/abs/10.1002/adma.202200574 (visited on 09/10/2023).

[63] Roscoe G. Dickinson and Linus Pauling. 'THE CRYSTAL STRUCTURE OF MOLYBDENITE'. In: *Journal of the American Chemical Society* 45.6 (June 1923). Publisher: American Chemical Society, pp. 1466–1471. ISSN: 0002-7863. DOI: 10.1021/ja01659a020. URL: https://doi.org/10.1021/ja01659a020 (visited on 11/01/2024).

[64] R. F. Frindt, A. D. Yoffe and Frank Philip Bowden. 'Physical properties of layer structures : optical properties and photoconductivity of thin crystals of molybdenum disulphide'. In: *Proceedings of the Royal Society of London.*

Die approbierte gedruckte Originalversion dieser Diplomarbeit ist an der TU Wien Bibliothek verfügbar
The approved original version of this thesis is available in print at TU Wien Bibliothek.
TU Bibliothek Your knowledge hub WIEN

Series A. Mathematical and Physical Sciences 273.1352 (1963). Publisher: Royal Society, pp. 69–83. DOI: 10.1098/rspa.1963.0075. URL: https://royalsocietypublishing.org/doi/abs/10.1098/rspa.1963.0075 (visited on 07/03/2024).

[65] Per Joensen, R. F. Frindt and S. Roy Morrison. 'Single-layer MoS2'. In: *Materials Research Bulletin* 21.4 (Apr. 1986), pp. 457–461. ISSN: 0025-5408. DOI: 10.1016/0025-5408(86)90011-5. URL: https://www.sciencedirect.com/science/article/pii/0025540886900115 (visited on 11/01/2024).

[66] K. S. Novoselov et al. 'Electric Field Effect in Atomically Thin Carbon Films'. In: *Science* 306.5696 (Oct. 2004). Publisher: American Association for the Advancement of Science, pp. 666–669. DOI: 10.1126/science.1102896. URL: https://www.science.org/doi/10.1126/science.1102896 (visited on 07/03/2024).

[67] Kin Fai Mak et al. 'Atomically Thin ${\mathrm{MoS}}_{2}$: A New Direct-Gap Semiconductor'. In: *Physical Review Letters* 105.13 (Sept. 2010). Publisher: American Physical Society, p. 136805. DOI: 10.1103/PhysRevLett.105.136805. URL: https://link.aps.org/doi/10.1103/PhysRevLett.105.136805 (visited on 07/03/2024).

[68] Andrea Splendiani et al. 'Emerging Photoluminescence in Monolayer MoS2'. In: *Nano Letters* 10.4 (Apr. 2010). Publisher: American Chemical Society, pp. 1271–1275. ISSN: 1530-6984. DOI: 10.1021/nl903868w. URL: https://doi.org/10.1021/nl903868w (visited on 07/03/2024).

[69] B. Radisavljevic et al. 'Single-layer MoS2 transistors'. en. In: *Nature Nanotechnology* 6.3 (Mar. 2011). Number: 3 Publisher: Nature Publishing Group, pp. 147–150. ISSN: 1748-3395. DOI: 10.1038/nnano.2010.279. URL: https://www.nature.com/articles/nnano.2010.279 (visited on 07/03/2024).

[70] Thomas Prohaska et al. 'Standard atomic weights of the elements 2021 (IUPAC Technical Report)'. en. In: *Pure and Applied Chemistry* 94.5 (May 2022). Publisher: De Gruyter, pp. 573–600. ISSN: 1365-3075. DOI: 10.1515/pac-2019-0603. URL: https://www.degruyter.com/document/doi/10.1515/pac-2019-0603/html (visited on 11/01/2024).

[71] Janosh Riebesell and Stefan Bringuier. *Collection of standalone TikZ images*. Aug. 2020. DOI: 10.5281/zenodo.7486911. URL: https://github.com/janosh/tikz (visited on 04/04/2024).

[72] The Materials Project. *Materials Data on MoSe2 by Materials Project*. en. 2020. DOI: 10.17188/1191826. URL: https://www.osti.gov/servlets/purl/1191826/ (visited on 05/12/2023).

[73] Saju Joseph et al. 'A review of the synthesis, properties, and applications of 2D transition metal dichalcogenides and their heterostructures'. In: *Materials*

Die approbierte gedruckte Originalversion dieser Diplomarbeit ist an der TU Wien Bibliothek verfügbar
The approved original version of this thesis is available in print at TU Wien Bibliothek.
TU Bibliothek Your knowledge hub WIEN

Chemistry and Physics 297 (Mar. 2023), p. 127332. ISSN: 0254-0584. DOI: 10.1016/j.matchemphys.2023.127332. URL: https://www.sciencedirect.com/science/article/pii/S0254058423000408 (visited on 08/03/2024).

[74] Qing Hua Wang et al. 'Electronics and optoelectronics of two-dimensional transition metal dichalcogenides'. en. In: *Nature Nanotechnology* 7.11 (Nov. 2012). Publisher: Nature Publishing Group, pp. 699–712. ISSN: 1748-3395. DOI: 10.1038/nnano.2012.193. URL: https://www.nature.com/articles/nnano.2012.193 (visited on 08/03/2024).

[75] Hai Li et al. 'Preparation and Applications of Mechanically Exfoliated Single-Layer and Multilayer MoS2 and WSe2 Nanosheets'. In: *Accounts of Chemical Research* 47.4 (Apr. 2014). Publisher: American Chemical Society, pp. 1067–1075. ISSN: 0001-4842. DOI: 10.1021/ar4002312. URL: https://doi.org/10.1021/ar4002312 (visited on 09/03/2024).

[76] Jian Zheng et al. 'High yield exfoliation of two-dimensional chalcogenides using sodium naphthalenide'. en. In: *Nature Communications* 5.1 (Jan. 2014). Publisher: Nature Publishing Group, p. 2995. ISSN: 2041-1723. DOI: 10.1038/ncomms3995. URL: https://www.nature.com/articles/ncomms3995 (visited on 09/03/2024).

[77] Goki Eda et al. 'Photoluminescence from Chemically Exfoliated MoS2'. In: *Nano Letters* 11.12 (Dec. 2011), pp. 5111–5116. ISSN: 1530-6984. DOI: 10.1021/nl201874w. URL: https://doi.org/10.1021/nl201874w (visited on 09/03/2024).

[78] Zhiyuan Zeng et al. 'An Effective Method for the Fabrication of Few-Layer-Thick Inorganic Nanosheets<a/>'. English. In: *Angewandte Chemie International Edition* 36.51 (Aug. 2012), pp. 9052–9056. ISSN: 1433-7851, 1521-3773. DOI: 10.1002/anie.201204208. URL: https://www.infona.pl//resource/bwmeta1.element.wiley-anie-v-51-i-36-anie201204208 (visited on 09/03/2024).

[79] Zhiyuan Zeng et al. 'Single-Layer Semiconducting Nanosheets: High-Yield Preparation and Device Fabrication<a/>'. English. In: *Angewandte Chemie International Edition* 47.50 (Nov. 2011), pp. 11093–11097. ISSN: 1433-7851, 1521-3773. DOI: 10.1002/anie.201106004. URL: https://www.infona.pl//resource/bwmeta1.element.wiley-anie-v-50-i-47-anie201106004 (visited on 09/03/2024).

[80] Wonbong Choi et al. 'Recent development of two-dimensional transition metal dichalcogenides and their applications'. In: *Materials Today* 20.3 (Apr. 2017), pp. 116–130. ISSN: 1369-7021. DOI: 10.1016/j.mattod.2016.10.002. URL: https://www.sciencedirect.com/science/article/pii/S1369702116302917 (visited on 14/03/2024).

Die approbierte gedruckte Originalversion dieser Diplomarbeit ist an der TU Wien Bibliothek verfügbar
The approved original version of this thesis is available in print at TU Wien Bibliothek.
TU Bibliothek Your knowledge hub WIEN

[81] Yongjie Zhan et al. 'Large Area Vapor Phase Growth and Characterization of MoS2 Atomic Layers on SiO2 Substrate'. In: (2011). Publisher: [object Object] Version Number: 1. DOI: 10.48550/ARXIV.1111.5072. URL: https://arxiv.org/abs/1111.5072 (visited on 13/03/2024).

[82] Arend M. van der Zande et al. 'Grains and grain boundaries in highly crystalline monolayer molybdenum disulphide'. en. In: *Nature Materials* 12.6 (June 2013). Publisher: Nature Publishing Group, pp. 554–561. ISSN: 1476-4660. DOI: 10.1038/nmat3633. URL: https://www.nature.com/articles/nmat3633 (visited on 13/03/2024).

[83] Sina Najmaei et al. 'Vapour phase growth and grain boundary structure of molybdenum disulphide atomic layers'. en. In: *Nature Materials* 12.8 (Aug. 2013). Publisher: Nature Publishing Group, pp. 754–759. ISSN: 1476-4660. DOI: 10.1038/nmat3673. URL: https://www.nature.com/articles/nmat3673 (visited on 13/03/2024).

[84] Jeong-Gyu Song et al. 'Layer-Controlled, Wafer-Scale, and Conformal Synthesis of Tungsten Disulfide Nanosheets Using Atomic Layer Deposition'. In: *ACS Nano* 7.12 (Dec. 2013). Publisher: American Chemical Society, pp. 11333–11340. ISSN: 1936-0851. DOI: 10.1021/nn405194e. URL: https://doi.org/10.1021/nn405194e (visited on 10/03/2024).

[85] Bodhi R. Manu, Anju Gupta and Ahalapitiya H. Jayatissa. 'Tribological Properties of 2D Materials and Composites—A Review of Recent Advances'. en. In: *Materials* 14.7 (Jan. 2021). Number: 7 Publisher: Multidisciplinary Digital Publishing Institute, p. 1630. ISSN: 1996-1944. DOI: 10.3390/ma14071630. URL: https://www.mdpi.com/1996-1944/14/7/1630 (visited on 14/03/2024).

[86] Tomáš Hudec et al. 'Titanium doped MoSe2 coatings – Synthesis, structure, mechanical and tribological properties investigation'. In: *Applied Surface Science* 568 (Dec. 2021), p. 150990. ISSN: 0169-4332. DOI: 10.1016/j.apsusc.2021.150990. URL: https://www.sciencedirect.com/science/article/pii/S0169433221020481 (visited on 26/03/2024).

[87] ASTM G99-17. *Standard Test Method for Wear Testing with a Pin-on-Disk Apparatus*. en. 2017. DOI: 10.1520/G0099-17. URL: https://www.astm.org/g0099-17.html (visited on 04/10/2023).

[88] Autodesk. *Autodesk Inventor 2024*. San Rafael, CA, 2023. URL: https://www.autodesk.de/products/inventor/ (visited on 01/09/2023).

[89] Caroline A. Schneider, Wayne S. Rasband and Kevin W. Eliceiri. 'NIH Image to ImageJ: 25 years of image analysis'. en. In: *Nature Methods* 9.7 (July 2012). Publisher: Nature Publishing Group, pp. 671–675. ISSN: 1548-7105. DOI: 10.

Die approbierte gedruckte Originalversion dieser Diplomarbeit ist an der TU Wien Bibliothek verfügbar
The approved original version of this thesis is available in print at TU Wien Bibliothek.
TU Bibliothek Your knowledge hub WIEN

1038/nmeth.2089. URL: https://www.nature.com/articles/nmeth.2089 (visited on 20/03/2024).

[90] Nicolas Schoeni and Gervais Chapuis. *ReciprOgraph*. Lausanne, Switzerland. URL: https://www.epfl.ch/schools/sb/research/iphys/teaching/crystallography/reciprograph/ (visited on 19/03/2024).

[91] David B. Williams and C. Barry Carter. *Transmission Electron Microscopy: A Textbook for Materials Science*. en. Google-Books-ID: dXdrG39VtUoC. Springer Science & Business Media, Aug. 2009. ISBN: 978-0-387-76500-6.

[92] Gwidon W. Stachowiak, Andrew W. Batchelor and Grazyna B. Stachowiak. '8 - Surface Micrography and Analysis'. In: *Tribology Series*. Ed. by Gwidon W. Stachowiak, Andrew W. Batchelor and Grazyna B. Stachowiak. Vol. 44. Experimental Methods in Tribology. Elsevier, Jan. 2004, pp. 165–220. DOI: 10.1016/S0167-8922(04)80024-5. URL: https://www.sciencedirect.com/science/article/pii/S0167892204800245 (visited on 16/02/2024).

[93] G. Binnig et al. 'Surface Studies by Scanning Tunneling Microscopy'. en. In: *Physical Review Letters* 49.1 (July 1982), pp. 57–61. ISSN: 0031-9007. DOI: 10.1103/PhysRevLett.49.57. URL: https://link.aps.org/doi/10.1103/PhysRevLett.49.57 (visited on 18/03/2024).

[94] Joseph I. Goldstein et al. 'Energy Dispersive X-ray Spectrometry: Physical Principles and User-Selected Parameters'. en. In: *Scanning Electron Microscopy and X-Ray Microanalysis*. Ed. by Joseph I. Goldstein et al. New York, NY: Springer, 2018, pp. 209–234. ISBN: 978-1-4939-6676-9. DOI: 10.1007/978-1-4939-6676-9_16. URL: https://doi.org/10.1007/978-1-4939-6676-9_16 (visited on 16/02/2024).

[95] Daisuke Shindo and Tetsuo Oikawa. 'Energy Dispersive X-ray Spectroscopy'. en. In: *Analytical Electron Microscopy for Materials Science*. Ed. by Daisuke Shindo and Tetsuo Oikawa. Tokyo: Springer Japan, 2002, pp. 81–102. ISBN: 978-4-431-66988-3. DOI: 10.1007/978-4-431-66988-3_4. URL: https://doi.org/10.1007/978-4-431-66988-3_4 (visited on 16/02/2024).

[96] Deena Titus, E. James Jebaseelan Samuel and Selvaraj Mohana Roopan. 'Chapter 12 - Nanoparticle characterization techniques'. In: *Green Synthesis, Characterization and Applications of Nanoparticles*. Ed. by Ashutosh Kumar Shukla and Siavash Iravani. Micro and Nano Technologies. Elsevier, Jan. 2019, pp. 303–319. ISBN: 978-0-08-102579-6. DOI: 10.1016/B978-0-08-102579-6.00012-5. URL: https://www.sciencedirect.com/science/article/pii/B9780081025796000125 (visited on 18/02/2024).

[97] Stephen W. Paddock and Kevin W. Eliceiri. 'Laser Scanning Confocal Microscopy: History, Applications, and Related Optical Sectioning Techniques'.

Die approbierte gedruckte Originalversion dieser Diplomarbeit ist an der TU Wien Bibliothek verfügbar
The approved original version of this thesis is available in print at TU Wien Bibliothek.
TU Bibliothek Your knowledge hub WIEN

en. In: *Confocal Microscopy: Methods and Protocols*. Ed. by Stephen W. Paddock. Methods in Molecular Biology. New York, NY: Springer, 2014, pp. 9–47. ISBN: 978-1-60761-847-8. DOI: 10.1007/978-1-60761-847-8_2. URL: https://doi.org/10.1007/978-1-60761-847-8_2 (visited on 17/02/2024).

[98] B. V. R. Tata and Baldev Raj. 'Confocal laser scanning microscopy: Applications in material science and technology'. en. In: *Bulletin of Materials Science* 21.4 (Aug. 1998), pp. 263–278. ISSN: 0973-7669. DOI: 10.1007/BF02744951. URL: https://doi.org/10.1007/BF02744951 (visited on 17/02/2024).

[99] Amicia D. Elliott. 'Confocal Microscopy: Principles and Modern Practices'. In: *Current protocols in cytometry* 92.1 (Mar. 2020), e68. ISSN: 1934-9297. DOI: 10.1002/cpcy.68. URL: https://www.ncbi.nlm.nih.gov/pmc/articles/PMC6961134/ (visited on 17/02/2024).

[100] Ewen Smith and Geoffrey Dent. *Modern Raman Spectroscopy: A Practical Approach*. en. Google-Books-ID: WsqFDwAAQBAJ. John Wiley & Sons, Apr. 2019. ISBN: 978-1-119-44055-0.

[101] Peter Vandenabeele. *Practical Raman Spectroscopy – An Introduction*. en. 1st ed. Wiley, July 2013. ISBN: 978-1-119-96128-4. DOI: 10.1002/9781119961284. URL: https://onlinelibrary.wiley.com/doi/book/10.1002/9781119961284 (visited on 19/02/2024).

[102] John R. Ferraro. *Introductory Raman Spectroscopy*. en. Elsevier, Jan. 2003. ISBN: 978-0-08-050912-9.

[103] Tania Dey. 'Microplastic pollutant detection by Surface Enhanced Raman Spectroscopy (SERS): a mini-review'. en. In: *Nanotechnology for Environmental Engineering* 8.1 (Mar. 2023), pp. 41–48. ISSN: 2365-6387. DOI: 10.1007/s41204-022-00223-7. URL: https://doi.org/10.1007/s41204-022-00223-7 (visited on 19/02/2024).

[104] NANOSHEL UK Ltd. *Nanoshel a Nanotechnology Company - Nanoshel*. en. URL: https://www.nanoshel.com/product/selenium-nanoparticle (visited on 14/03/2024).

[105] Mohsen Safaei et al. 'Optimization of Green Synthesis of Selenium Nanoparticles and Evaluation of Their Antifungal Activity against Oral Candida albicans Infection'. In: *Advances in Materials Science and Engineering* 2022 (Apr. 2022), p. 1376998. DOI: 10.1155/2022/1376998.

[106] Roberto Avendaño et al. 'Production of selenium nanoparticles in Pseudomonas putida KT2440'. en. In: *Scientific Reports* 6.1 (Nov. 2016). Publisher: Nature Publishing Group, p. 37155. ISSN: 2045-2322. DOI: 10.1038/srep37155. URL: https://www.nature.com/articles/srep37155 (visited on 19/03/2024).

Die approbierte gedruckte Originalversion dieser Diplomarbeit ist an der TU Wien Bibliothek verfügbar
The approved original version of this thesis is available in print at TU Wien Bibliothek.
TU Bibliothek Your knowledge hub WIEN

[107] Peter Blau. 'On the nature of running-in'. In: *Tribology International - TRIBOL INT* 38 (Nov. 2005), pp. 1007–1012. DOI: 10.1016/j.triboint.2005.07.020.

[108] Tomasz Suszko, Witold Gulbiński and Jacek Jagielski. 'The role of surface oxidation in friction processes on molybdenum nitride thin films'. In: *Surface and Coatings Technology* 194.2 (May 2005), pp. 319–324. ISSN: 0257-8972. DOI: 10.1016/j.surfcoat.2004.07.119. URL: https://www.sciencedirect.com/science/article/pii/S0257897204007145 (visited on 20/03/2024).

[109] Jianhui Yan et al. 'Microstructure and Wear Resistance of Plasma-Sprayed Molybdenum Coating Reinforced by MoSi2 Particles'. en. In: *Journal of Thermal Spray Technology* 25.7 (Oct. 2016), pp. 1322–1329. ISSN: 1544-1016. DOI: 10.1007/s11666-016-0440-6. URL: https://doi.org/10.1007/s11666-016-0440-6 (visited on 20/03/2024).

[110] L. Păduraru et al. 'Investigations on Dry Sliding Wear and Corrosion Resistance of Thermal Sprayed Molybdenum Coatings'. en. In: *IOP Conference Series: Materials Science and Engineering* 416.1 (Sept. 2018). Publisher: IOP Publishing, p. 012027. ISSN: 1757-899X. DOI: 10.1088/1757-899X/416/1/012027. URL: https://dx.doi.org/10.1088/1757-899X/416/1/012027 (visited on 20/03/2024).

[111] Zhe Chen et al. 'Effect of Humidity on Friction and Wear—A Critical Review'. en. In: *Lubricants* 6.3 (Sept. 2018). Number: 3 Publisher: Multidisciplinary Digital Publishing Institute, p. 74. ISSN: 2075-4442. DOI: 10.3390/lubricants6030074. URL: https://www.mdpi.com/2075-4442/6/3/74 (visited on 20/03/2024).

[112] Donald H. Buckley. *Friction, Wear, and Lubrication in Vacuum*. en. Google-Books-ID: mt8_AQAAMAAJ. National Aeronautics and Space Administration, 1971.

[113] Ulick R. Evans. 'The mechanism of the so-called "dry corrosion" of metals'. en. In: *Trans. Faraday Soc.* 19.July (1923), pp. 201–212. ISSN: 0014-7672. DOI: 10.1039/TF9231900201. URL: http://xlink.rsc.org/?DOI=TF9231900201 (visited on 21/03/2024).

[114] Alexander V. Kolobov and Junji Tominaga. *Two-Dimensional Transition-Metal Dichalcogenides*. Vol. 239. Springer Series in Materials Science. Cham: Springer International Publishing, 2016. ISBN: 978-3-319-31450-1. DOI: 10.1007/978-3-319-31450-1. URL: http://link.springer.com/10.1007/978-3-319-31450-1 (visited on 21/03/2024).

[115] D. Javdošňák et al. 'Tribological properties and oxidation resistance of tungsten and tungsten nitride films at temperatures up to 500 °C'. In: *Tribology*

Die approbierte gedruckte Originalversion dieser Diplomarbeit ist an der TU Wien Bibliothek verfügbar
The approved original version of this thesis is available in print at TU Wien Bibliothek.
TU Bibliothek Your knowledge hub WIEN

International 132 (Apr. 2019), pp. 211–220. ISSN: 0301-679X. DOI: 10.1016/j.triboint.2018.12.019. URL: https://www.sciencedirect.com/science/article/pii/S0301679X18305899 (visited on 22/03/2024).

[116] J. A. R. Wesmann and N. Espallargas. 'Effect of atmosphere, temperature and carbide size on the sliding friction of self-mated HVOF WC–CoCr contacts'. In: *Tribology International* 101 (Sept. 2016), pp. 301–313. ISSN: 0301-679X. DOI: 10.1016/j.triboint.2016.04.032. URL: https://www.sciencedirect.com/science/article/pii/S0301679X1630086X (visited on 22/03/2024).

[117] A. J. W. Moore, W. J. Mcg. Tegart and Frank Philip Bowden. 'Relation between friction and hardness'. In: *Proceedings of the Royal Society of London. Series A. Mathematical and Physical Sciences* 212.1111 (Jan. 1997). Publisher: Royal Society, pp. 452–458. DOI: 10.1098/rspa.1952.0234. URL: https://royalsocietypublishing.org/doi/10.1098/rspa.1952.0234 (visited on 22/03/2024).

[118] S. V. Prasad, J. S. Zabinski and N. T. McDevitt. 'Friction Behavior of Pulsed Laser Deposited Tungsten Disulfide Films'. In: *Tribology Transactions* 38.1 (Jan. 1995). Publisher: Taylor & Francis _eprint: https://doi.org/10.1080/10402009508983380 pp. 57–62. ISSN: 1040-2004. DOI: 10.1080/10402009508983380. URL: https://doi.org/10.1080/10402009508983380 (visited on 22/03/2024).

[119] J. G. Calvert. 'Glossary of atmospheric chemistry terms (Recommendations 1990)'. en. In: *Pure and Applied Chemistry* 62.11 (Jan. 1990), pp. 2167–2219. ISSN: 1365-3075, 0033-4545. DOI: 10.1351/pac199062112167. URL: https://www.degruyter.com/document/doi/10.1351/pac199062112167/html (visited on 23/03/2024).

[120] Manfred Nitsche. *Abluft-Fibel: Reinigung lösemittelhaltiger Abgase*. de. Berlin, Heidelberg: Springer Berlin Heidelberg, 2015. ISBN: 978-3-662-45310-0. DOI: 10.1007/978-3-662-45310-0. URL: https://link.springer.com/10.1007/978-3-662-45310-0 (visited on 23/03/2024).

[121] Heinz-Wolfgang Häring, ed. *Industrial gases processing*. eng. OCLC: ocn189413516. Weinheim: Wiley-VCH Verlag GmbH & Co. KGaA, 2008. ISBN: 978-3-527-31685-4.

[122] Yi Ding et al. 'First principles study of structural, vibrational and electronic properties of graphene-like MX2 (M=Mo, Nb, W, Ta; X=S, Se, Te) monolayers'. In: *Physica B: Condensed Matter* 406.11 (May 2011), pp. 2254–2260. ISSN: 0921-4526. DOI: 10.1016/j.physb.2011.03.044. URL: https://www.sciencedirect.com/science/article/pii/S0921452611002651 (visited on 23/03/2024).

Die approbierte gedruckte Originalversion dieser Diplomarbeit ist an der TU Wien Bibliothek verfügbar
The approved original version of this thesis is available in print at TU Wien Bibliothek.
TU Bibliothek Your knowledge hub WIEN

[123] Conor P. Cullen et al. 'Synthesis and thermal stability of TMD thin films: A comprehensive XPS and Raman study'. In: (2021). Publisher: [object Object] Version Number: 1. DOI: 10.48550/ARXIV.2106.07366. URL: https://arxiv.org/abs/2106.07366 (visited on 03/04/2024).

[124] Gioele Mirabelli et al. 'Air sensitivity of MoS2, MoSe2, MoTe2, HfS2, and HfSe2'. en. In: *Journal of Applied Physics* 120.12 (Sept. 2016), p. 125102. ISSN: 0021-8979, 1089-7550. DOI: 10.1063/1.4963290. URL: https://pubs.aip.org/jap/article/120/12/125102/345824/Air-sensitivity-of-MoS2-MoSe2-MoTe2-HfS2-and-HfSe2 (visited on 03/04/2024).

[125] Carl Zerbe, ed. *Mineralöle und verwandte Produkte*. de. Berlin, Heidelberg: Springer Berlin Heidelberg, 1969. ISBN: 978-3-642-87509-0. DOI: 10.1007/978-3-642-87509-0. URL: http://link.springer.com/10.1007/978-3-642-87509-0 (visited on 23/03/2024).

[126] David J. Boes. 'New Solid Lubricants: Their Preparations, Properties and Potential for Aerospace Applications'. In: *IEEE Transactions on Aerospace* 2.2 (1964), pp. 457–466. ISSN: 0536-1516. DOI: 10.1109/TA.1964.4319624. URL: http://ieeexplore.ieee.org/document/4319624/ (visited on 23/03/2024).

[127] Shengjue Deng et al. 'Directional Construction of Vertical Nitrogen-Doped 1T-2H MoSe2/Graphene Shell/Core Nanoflake Arrays for Efficient Hydrogen Evolution Reaction'. en. In: *Advanced Materials* 29.21 (2017). _eprint: https://onlinelibrary.wiley.com/doi/pdf/10.1002/adma.201700748, p. 1700748. ISSN: 1521-4095. DOI: 10.1002/adma.201700748. URL: https://onlinelibrary.wiley.com/doi/abs/10.1002/adma.201700748 (visited on 01/02/2024).

[128] Wenjing Li et al. 'Synthesis and tribological properties of Mo-doped WSe2 Nanolamellars'. en. In: *Crystal Research and Technology* 47.8 (2012). _eprint: https://onlinelibrary.wiley.com/doi/pdf/10.1002/crat.201200131, pp. 876–881. ISSN: 1521-4079. DOI: 10.1002/crat.201200131. URL: https://onlinelibrary.wiley.com/doi/abs/10.1002/crat.201200131 (visited on 13/02/2024).

[129] Paul H. C. Eilers. 'A Perfect Smoother'. en. In: *Analytical Chemistry* 75.14 (July 2003), pp. 3631–3636. ISSN: 0003-2700, 1520-6882. DOI: 10.1021/ac034173t. URL: https://pubs.acs.org/doi/10.1021/ac034173t (visited on 25/03/2024).

[130] Philipp Tonndorf et al. 'Photoluminescence emission and Raman response of monolayer MoS_2, MoSe_2, and WSe_2'. en. In: *Optics Express* 21.4 (Feb. 2013), p. 4908. ISSN: 1094-4087. DOI: 10.1364/OE.21.004908. URL: https://opg.optica.org/oe/abstract.cfm?uri=oe-21-4-4908 (visited on 12/03/2024).

[131] M. Dieterle and G. Mestl. 'Raman spectroscopy of molybdenum oxides'. In: *Physical Chemistry Chemical Physics* 4.5 (Feb. 2002), pp. 822–826. ISSN:

Die approbierte gedruckte Originalversion dieser Diplomarbeit ist an der TU Wien Bibliothek verfügbar
The approved original version of this thesis is available in print at TU Wien Bibliothek.
TU Bibliothek Your knowledge hub WIEN

14639076, 14639084. DOI: 10.1039/b107046k. URL: http://xlink.rsc.org/?DOI=b107046k (visited on 12/03/2024).

[132] Yu-Sheng Li et al. *Do DLC-like features in Raman spectra of tribofilms really mean they are DLC formed by friction?* Oct. 2022. DOI: 10.21203/rs.3.rs-2114549/v1. URL: https://www.researchsquare.com/article/rs-2114549/v1 (visited on 04/04/2024).

[133] M. R. Joya, J. E. Alfonso and L. C. Moreno. 'Photoluminescence and Raman Studies of α-MoO_3 Doped with Erbium and Neodymium'. In: *Current Science* 116.10 (May 2019), p. 1690. ISSN: 0011-3891. DOI: 10.18520/cs/v116/i10/1690-1695. URL: https://www.currentscience.ac.in/Volumes/116/10/1690.pdf (visited on 12/03/2024).

[134] Perry A. Spevack and N. S. McIntyre. 'A Raman and XPS investigation of supported molybdenum oxide thin films. 1. Calcination and reduction studies'. en. In: *The Journal of Physical Chemistry* 97.42 (Oct. 1993), pp. 11020–11030. ISSN: 0022-3654, 1541-5740. DOI: 10.1021/j100144a020. URL: https://pubs.acs.org/doi/abs/10.1021/j100144a020 (visited on 12/03/2024).

[135] M. F. Daniel et al. 'Infrared and Raman study of WO3 tungsten trioxides and WO3, *x*H2O tungsten trioxide tydrates'. In: *Journal of Solid State Chemistry* 67.2 (Apr. 1987), pp. 235–247. ISSN: 0022-4596. DOI: 10.1016/0022-4596(87)90359-8. URL: https://www.sciencedirect.com/science/article/pii/0022459687903598 (visited on 12/03/2024).

[136] Elizabeth I. Ross-Medgaarden and Israel E. Wachs. 'Structural Determination of Bulk and Surface Tungsten Oxides with UV−vis Diffuse Reflectance Spectroscopy and Raman Spectroscopy'. en. In: *The Journal of Physical Chemistry C* 111.41 (Oct. 2007), pp. 15089–15099. ISSN: 1932-7447, 1932-7455. DOI: 10.1021/jp074219c. URL: https://pubs.acs.org/doi/10.1021/jp074219c (visited on 12/03/2024).

[137] F. Gustavsson et al. 'Frictional behavior of self-adaptive nanostructural Mo–Se–C coatings in different sliding conditions'. In: *Wear* 303.1 (June 2013), pp. 286–296. ISSN: 0043-1648. DOI: 10.1016/j.wear.2013.03.032. URL: https://www.sciencedirect.com/science/article/pii/S0043164813002214 (visited on 26/03/2024).

[138] Yu Guo, Si Zhou and Jijun Zhao. 'Oxidation Behaviors of Two-dimensional Metal Chalcogenides'. en. In: *ChemNanoMat* 6.6 (2020). _eprint: https://onlinelibrary.wiley.com/doi/pdf/10.1002/cnma.201900492, pp. 838–849. ISSN: 2199-692X. DOI: 10.1002/cnma.201900492. URL: https://onlinelibrary.wiley.com/doi/abs/10.1002/cnma.201900492 (visited on 27/03/2024).

Die approbierte gedruckte Originalversion dieser Diplomarbeit ist an der TU Wien Bibliothek verfügbar
The approved original version of this thesis is available in print at TU Wien Bibliothek.
TU Bibliothek Your knowledge hub WIEN

[139] *DIN EN ISO 21920-2:2022-12, Geometrische Produktspezifikation_(GPS)_-Oberflächenbeschaffenheit: Profile_- Teil_2: Begriffe und Kenngrößen für die Oberflächenbeschaffenheit (ISO_21920-2:2021, korrigierte Fassung 2022-06); Deutsche Fassung EN_ISO_21920-2:2022*. DOI: 10.31030/3294017. URL: https://www.beuth.de/de/-/-/344762428 (visited on 27/03/2024).

[140] Yingchao Yang et al. 'Brittle Fracture of 2D $MoSe_2$'. eng. In: *Advanced materials (Deerfield Beach, Fla.)* 29.2 (Jan. 2017). ISSN: 1521-4095. DOI: 10.1002/adma.201604201. URL: https://doi.org/10.1002/adma.201604201 (visited on 27/03/2024).

[141] Rui Zhang, Vasileios Koutsos and Rebecca Cheung. 'Elastic properties of suspended multilayer WSe2'. In: *Applied Physics Letters* 108.4 (Jan. 2016), p. 042104. ISSN: 0003-6951. DOI: 10.1063/1.4940982. URL: https://doi.org/10.1063/1.4940982 (visited on 27/03/2024).

Die approbierte gedruckte Originalversion dieser Diplomarbeit ist an der TU Wien Bibliothek verfügbar
The approved original version of this thesis is available in print at TU Wien Bibliothek.
TU Bibliothek Your knowledge hub WIEN

A Technical Drawing

Die approbierte gedruckte Originalversion dieser Diplomarbeit ist an der TU Wien Bibliothek verfügbar
The approved original version of this thesis is available in print at TU Wien Bibliothek.

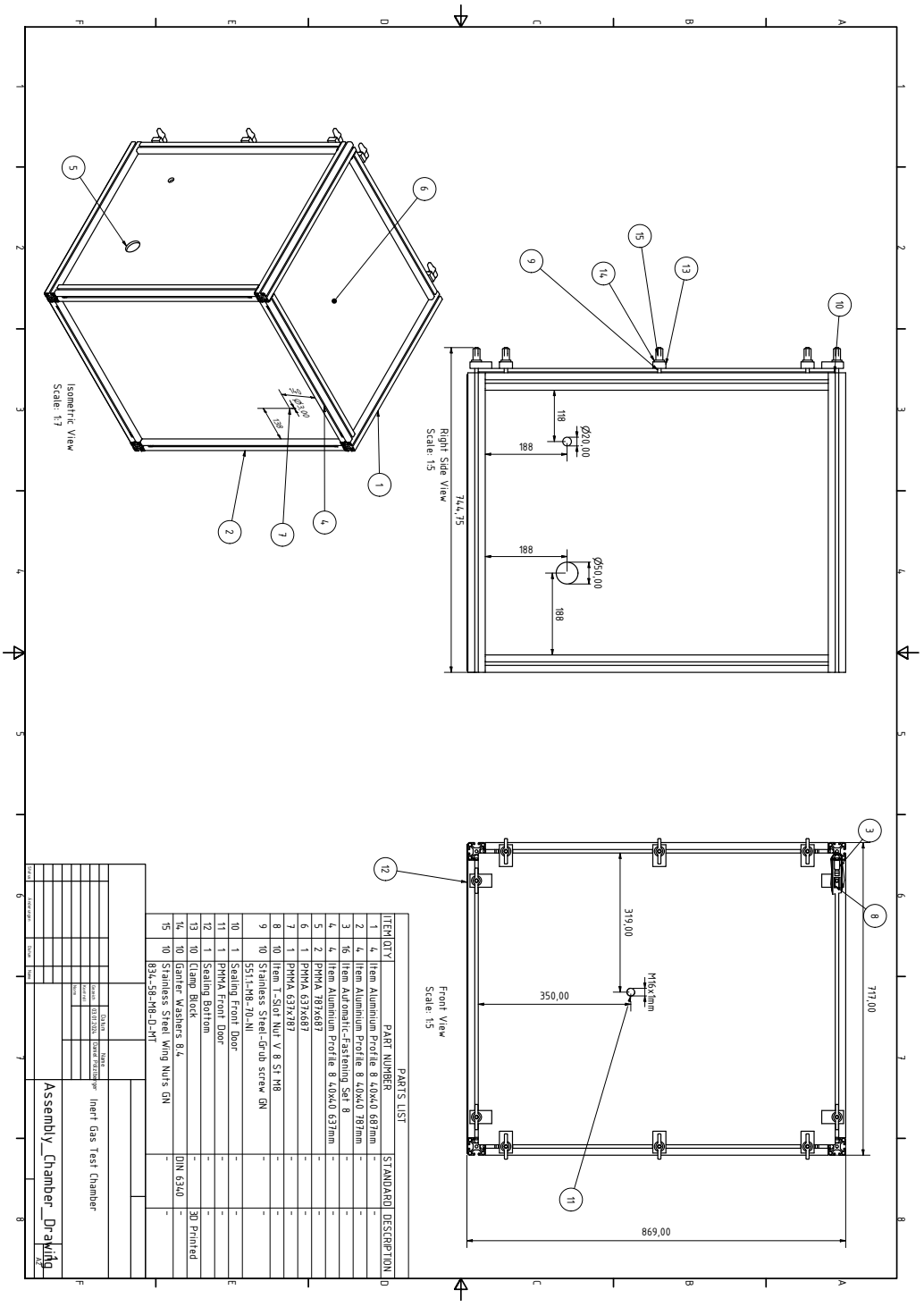

Figure A.1: Technical drawing of the inert gas chamber

Die approbierte gedruckte Originalversion dieser Diplomarbeit ist an der TU Wien Bibliothek verfügbar
The approved original version of this thesis is available in print at TU Wien Bibliothek.
TU Bibliothek Your knowledge hub WIEN